CURVATURE INSTABILITY OF LOCALIZED STRUCTURES

Tesis

entregada a la

Universidad de Chile

en cumplimiento parcial de los requisitos

para optar al grado de

Magíster en Ciencias con Mención en Física

Facultad de Ciencias

Por

IGNACIO ANTONIO BORDEU WELDT

Mayo, 2015

Director de Tesis:

Dr. Marcel Gabriel Clerc Gavilán

FACULTAD DE CIENCIAS

UNIVERSIDAD DE CHILE

INFORME DE APROBACIÓN

TESIS DE MAGÍSTER

Se informa a la Escuela de Postgrado de la Facultad de Ciencias que la Tesis de Magíster presentada por el candidato

IGNACIO ANTONIO BORDEU WELDT

Ha sido aprobada por la comisión de Evaluación de la tesis como requisito para optar al grado de Magíster en Ciencias con Mención en Física, en el examen de Defensa Privada de Tesis rendido el día .....

Director de Tesis:

Dr. Marcel Gabriel Clerc Gavilán _____

Comisión de Evaluación de la Tesis

Dr. Enrique Cerda. _____

Dr. Sergio Rica. _____

Dr. Mustapha Tlidi. _____

Dr. Juan A. Valdivia, Presidente de la Comisíon. _____

TO MY MOTHER.

Biography

I was born in Concepción, Chile on the 4th of June, 1989. I am son of Luz María Weldt Suazo and Jorge Bordeu Urrejola, and brother of 6. I studied Physics at Universidad de Concepción. As a scientist I am deeply interested in understanding macroscopic phenomena in nature, specially, where Physics, Chemistry and Biology merge.

Aknowledgements

I would like to thank Professor Marcel Clerc for the passion for knowledge he transmits during his lectures, his research and life in general. His guidance and support have been essential in my formation as a scientist. I thank also Professor Mustapha Tlidi, for receiving me at the Uiversité Libre de Bruxelles, and for sharing his knowledge with me.

I must thank my future wife Constanza for her support, patience and sacrifice. I thank also my family and friends for their company and for helping me enjoy this years.

I thank the financing from CONICYT, Beca de Magíster Nacional number 22130947, and thank the Departamento de Postgrado y Postítulo of the Vicerrectoría de Asuntos Académicos, Universidad de Chile for financing my visit to the Université Libre de Bruxelles.

Contents

1 Introduction **1**

1.1 Motivation 1

1.2 Objectives 4

1.2.1 Structure of the thesis 4

2 Theoretical background **6**

2.1 Structure formation 7

2.2 Swift-Hohenberg equation 8

2.2.1 Imperfect pitchfork bifurcation 10

2.2.2 Spatial instability 11

2.2.3 Variational and nonvariational systems 12

2.2.4 Defects and pinning phenomena 15

3 Curvature instability and labyrinthine patterns **16**

3.1 Preliminary observations 17

3.2 Stability of localized spots 19

3.3 Transversal instability 24

3.3.1 Stability analysis of a regular pattern 25

3.4 Non-variational model 27

3.5 Chapter summary 29

4 Rodlike localized structure **30**

4.1 Preliminary observations 31

4.2 New localized solution 32

4.3 One-dimensional interpretation 35

4.4 Instabilities and bifurcation diagrams 37

4.5 Interaction properties of the rod structure: dimer approach 41

4.5.1 Localized spots interaction 42

4.5.2 Dimer approach 43

4.6 Non-variational stabilization 46

4.7 Chapter summary 47

5 Universality of the curvature mechanism **48**

5.1 Interaction-redistribution model 49

5.2 Gray-Scott model 53

5.3 Labyrinth connectivities 57

5.4 Chapter summary 59

6 Self-replication in vegetation dynamics **60**

6.1 Preliminary observations 60

6.2 Field observations 63

6.2.1 Location 63

6.2.2 Spatial distribution analysis 65

6.2.3 Nearest neighbor distance and structure properties 66

6.2.4 Fourier analysis 67

6.2.5 Voronoi cells characterization 69

6.3 Model equation for vegetation dynamics 70

6.4 Field observations vs model 73

6.5 Chapter summary 76

7 Conclusions and perspectives **77**

References **82**

Appendix A **93**

Appendix B **100**

Appendix C **109**

Appendix D **120**

List of Figures

1.1 Natural pattern formation examples. 2

1.2 Dissipative localized structure and extended labyrinth pattern. 3

2.1 Collective behaviour of Blue Mackerel. 6

2.2 Imperfect pitchfork bifurcation. 10

2.3 Bifurcation diagram of the generalized Swift-Hohenberg equation. . . 12

2.4 Classification of defects in 2D systems. 15

3.1 Temporal evolution of the growth of the Cholesteric phase in a liquid crystal. 17

3.2 Transition from localized spot to an elongated structure. 19

3.3 Transition from a single localized spot to invaginated pattern. 20

3.4 Bifurcation diagram including labyrinth transition zone. 22

3.5 Growth rate λ_m of the most unstable perturbation mode for localized structures. 23

3.6 Transversal instability of a single infinite stripe. 25

3.7 Stripe pattern and its profile. 26

3.8 Spatial instability of a stripe pattern. 27

3.9 Transition from a single peak LS to labyrinthine pattern in the non-variational Swift-Hohenberg equation. 28

4.1 Triangular localized structure. 31
4.2 Stationary rod localized structure. 32
4.3 Bifurcation diagram of the 2D generalized Swift-Hohenberg including the stability zone of the rod localized structure. 34
4.4 One-dimensional projections of the 2D rod structure. 36
4.5 Bifurcation diagrams of rod structures. 38
4.6 Decay rate from a rod structure into a circular localized structure. . . 39
4.7 Zoomed phase diagram of rod structure. 40
4.8 Saddle-node bifurcations for the splitting of a rod structure. 41
4.9 Dimer approach to rod structure. 43
4.10 Tailored crystal-type configurations of rod structures. 45
4.11 Nonvariational stationary rod localized structure. 46

5.1 Natural vegetation patterns. 49
5.2 Bifurcation diagram of homogeneous plant population states. 51
5.3 Curvature instability mechanism for the generation of a labyrinth from a localized patch. 53
5.4 Belousov-Zhabotinsky chemical reaction. 53
5.5 Bifurcation diagram for the Gray-Scott model. 56
5.6 Curvature instability mechanism in the Gray-Scott model. 57
5.7 Alternative mechanism for the generation of a labyrinth from a localized concentration peak. 58

6.1 Localized patch instability. 61
6.2 Study site in the Catamarca region. 63
6.3 Histograms for nearest neighbour distance. 67
6.4 Spatial Fourier transform. 68

6.5 Voronoi cell tessellation. 69
6.6 Bifurcation diagram of homogeneous plant population states. 72
6.7 Localized patch self-replication of the vegetation model. 74
6.8 Numerical simulations of non-variational phytomass model. 75

Abstract

Curvature instability of localized structures

Ignacio Antonio Bordeu Weldt

The main objective of this thesis was to study the stability of two-dimensional localized structures, and to investigate how the destabilization due to the curvature could lead to the formation of extended patterns. This, in the context of macroscopic physics.

Localized structures are nonlinear peaks or holes in spatially extended systems. They belong to the general class of dissipative structures found far from equilibrium. Spatial structures that are not localized and occupy the whole system are called extended patterns, these patterns posses some characteristic wavelength and usually emerge from the destabilization of an homogeneous state. One particular extended pattern in the Labyrinth, this type of pattern is characterized by its spatial disorder. In this thesis we focused on the study of the mechanisms by which a localized structure can turn into an extended pattern.

Considering a variation of the most simple model known to exhibit extended patterns, the Swift-Hohenberg equation. We were able to observe how a two-dimensional circular localized structure is affected by a curvature instability, which deforms its

circular shape into an elliptical and later elongated structure. This elongated structure suffers from a transversal instability, the subsequent pattern formed is also unstable, thus, generating a complex extended pattern, namely, a labyrinth. This mechanism occurs far from any pattern forming instability and requires coexistence of homogeneous state.

In the context of the modified Swift-Hohenberg equation, a special parameter region was found where labyrinths coexisted with stable localized structures. In this zone of coexistence another type of localized structures were found to engender labyrinths. These new localized structures were called Rodlike localized structure. These, are non-azimuthally symmetric, and exist both in two and three-dimensions. A complete numerical characterization of their stability, phase diagram and interaction was made. It was shown that this type of structures also develop labyrinths by the curvature mechanism described before.

The curvature instability mechanism of the destabilization of a localized structure leading to the formation of extended labyrinthine patterns exist in a wide range of physical systems. In this thesis we have shown the existence of this mechanism in the context of vegetation dynamics described by a generic interaction-redistribution model. It was also observed in autocatalytic chemical reactions described by the Gray-Scott reaction-diffusion model. This opens the possibility for future interdisciplinary theoretical and experimental work.

Depending on the context and model considered, different classes of labyrinthine structures were shown to emerge from an initial localized structure. The parameters considered in the simulations also affects the type of pattern generated. By this observations we were able to classify the labyrinths based on the difference between the initial and final connectivity of their structures.

In the context of vegetation dynamics described by a generic interaction-redistribution

model, we described the process by which a localized spot destabilizes, elongating and splitting into two new localized spots, this process is called self-replications. Field observations of semi-arid ecosystems show that a certain specie of plant exhibits self-replications. Comparison between numerical and field observations show an underlying process by which self-replication mediates the self-organization of localized structures leading to extended pattern formation. We consider that this is a mechanism by which vegetation extends to cover the landscape, and also helps to explain the emergence of characteristic quantities observed in the statistical analysis of field observations.

Resumen

Inestabilidad de curvatura en estructuras localizadas

Ignacio Antonio Bordeu Weldt

El objetivo principal de esta tesis consistió en el estudio de estabilidad de estructuras localizadas bidimensionales, en particular se investigó cómo la desestabilización debido a la curvatura puede dar lugar a la formación de patrones extendidos. Esto, en el contexto de la física macroscópica.

Las estructuras localizadas son picos o agujeros en los sistemas nolineales espacialmente extendidos. Estas, son parte de la clase general de estructuras disipativas que es posible encontrar lejos del equilibrio termodinámico. Las estructuras que no están espacialmente localizados y abarcan al sistema completo son llamados patrones extendidos. Dichos patrones poseen cierta longitud de onda característica y suelen surgir de la desestabilización de un estado homogéneo. Un patrón extendido particular es el Laberinto, este tipo de patrón se caracteriza por su desorden espacial. En esta tesis nos hemos centrado en el estudio de los mecanismos por los cuales una estructura localizada se desestabiliza para formar un patrón extendido.

Considerando una ecuación tipo Swift-Hohenberg, ecuación prototipo que exhibe

coexistencia de estados homogéneos, patrones extendidos y estructuras localizadas, hemos sido capaces de observar cómo una estructura localizada circular bidimensional se ve afectada por una inestabilidad debido a su curvatura. Esta inestabilidad se ve reflejada en un tansición de la forma de la estructura, de circular a elíptica, luego, alargada. La estructura alargada sufre de una inestabilidad transversal. El patrón formado posteriormente también es inestable, por lo tanto, se genera un patrón extendido complejo, a saber, un laberinto. Este mecanismo ocurre lejos de cualquier inestabilidad formadora de patrones (inestabilidad de Turing) y requiere coexistencia de estados homogéneos.

En el contexto de la ecuación de Swift-Hohenberg generalizada, una región especial de parámetros fue encontrada, donde, los laberintos coexisten con estructuras localizadas estables. En esta zona de coexistencia se encontró un nuevo tipo de estructura localizada, llamada estructura localizada tipo Vara. Este objeto, no posee simetrá azimutal y existe tanto en dos como en tres dimensiones espaciales. Se realizó una caracterización numérica completa de su estabilidad, diagrama de fase e interacción. Se mostró que este tipo de estructuras también desarrollan laberintos a través del mecanismo de curvatura descrito anteriormente.

El mecanismo de inestabilidad de curvatura para la desestabilización de una estructura localizada que conduce a la formación de patrones laberínticos extendidos existe en una amplia gama de sistemas físicos. En esta tesis se mostró la existencia de dicho mecanismo en el contexto de la dinámica de vegetación descritas por un modelo de interacción-redistribución genérico. Además, se observó teóricamente en reacciones químicas autocatalíticas descritas por el modelo de reacción-difusión Gray-Scott. Esto abre la posibilidad de futuras investigaciones interdisciplinarias tanto teóricas como experimentales.

Dependiendo del contexto y el modelo considerado, diferentes estructuras laberínticas

pueden emerger de una estructura localizada inicial. Los parámetros considerados en las simulaciones también influyen en el tipo de patrón resultante. A través de estas observaciones se logró construir una clasificación de los laberintos basados en la diferencia entre la conectividad inicial y final de las estructuras que lo componen.

Finalmente, en el contexto de la dinámica de vegetación descritas por un modelo de interacción-redistribución genérico, se describió el proceso por el cual una estructura localizada se desestabiliza, alargándose y dividiéndose en dos nuevas estructuras localizadas. Este proceso, se denomina auto-replicación. Las observaciones de campo de ecosistemas semiáridos realizadas con el uso de imágenes satelitales, mostraron que una determinada especie de planta exhibe auto-replicación. La comparación entre las observaciones numéricas y de campo muestran un proceso subyacente por el cual la auto-replicación media la auto-organización de las estructuras localizadas que conducen a la formación de patrones extendidos. Consideramos que este es uno de los mecanismos por medio de los cuales la vegetación se extiende para cubrir áreas extensas en ambientes áridos o semi-áridos. Esto permite además explicar la aparición de cantidades características extraídas del análisis estadístico de las observaciones de campo relacionadas a las tamaños y distancias entre las plantas.

Chapter 1

Introduction

1.1 Motivation

Physics, is the branch of science concerned with the properties of matter and energy, and the interaction between them. In other words, Physics is everywhere around us, from the microscopic, in the formation of atoms and molecules, to the macroscopic world, in the movement of falling apples or the creation of galaxies, even our daily life develops in this context. Using the language of mathematics, Physics has been able through the past centuries to not only describe, but to predict the existence and behaviour of natural phenomena in different contexts, ranging from classical mechanics, and electrodynamics to quantum physics and general relativity. In particular, Nonlinear Physics—which studies the nature of macroscopic and complex systems—has achieved the description of collective behaviour, such as, self-organization in which the different components of a macroscopic system interact, organizing itself under the conditions of injection and dissipation of energy, matter and momentum, to create astonishing natural patterns (see Fig. 1.1).

Natural patterns can be observed everywhere around us, fingerprints, and cowlicks

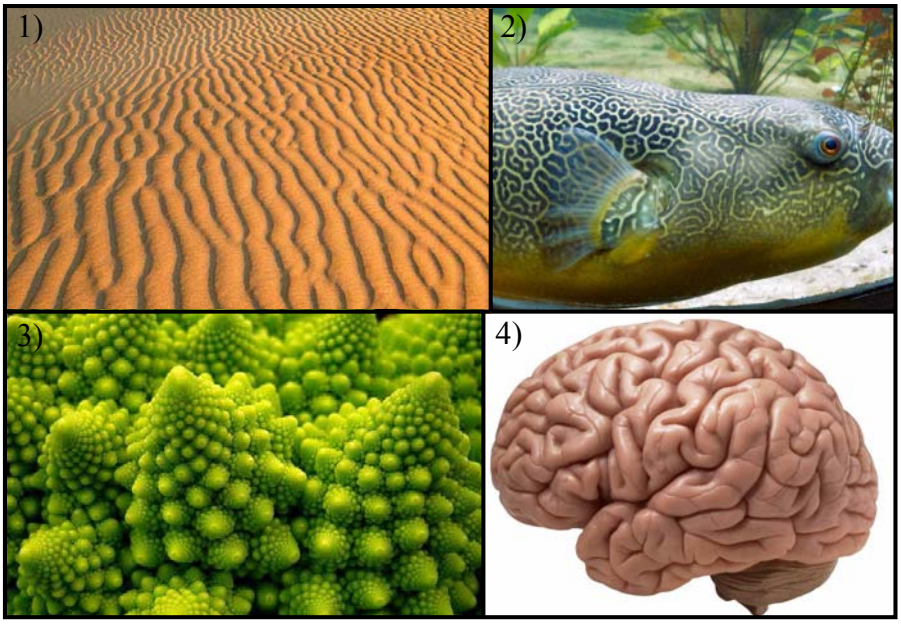

Figure 1.1: Natural pattern formation. 1) Wind induced patterns in sand dunes [1], 2) skin pattern of Giant Freshwater Puffer fish [2], 3) fractal patterns in Romanesque cauliflower [3], and 4) labyrinthine pattern in brain structure [4].

are examples of spatial patterns observed in our bodies, while, the heartbeat and circadian cycle are temporal patterns governed by electrical and chemical signals sent by our brains. These organizational and synchronization properties of macroscopic systems emerge from the idea coming from Statistical Physics where *the dynamic of a single particle is not the same as the dynamic of the whole*. Interaction between elements in the context of dissipative systems (i.e with injection and dissipation of energy) gives rise to emergent physical properties and opens the door to a complete new perspective regarding the possible equilibriums of a system. Chaotic behaviours, stationary patterns, intermittency, synchronisation, turbulence or spatiotemporal chaos are phenomena exhibited by dissipative systems, and its the role of Nonlinear Physics to unveil their mysteries.

Localized structures and extended patterns

When sand is vibrated, clusters of grains behave as oscillators, interaction between grains allow the appearance of interesting spatial structures. In the nineties Paul Umbanohwar, Fransisco Melo and Harry Swinney [5] observed that under certain conditions, vibrated grains exhibited a particular type of structure where only a portion of the gains oscillated with a greater amplitude than the rest of them (see Fig. 1.2.1), this structure called *Oscillon* is a particular case of dissipative localized structures. This type of structure has been observed in a wide variety of physical systems. Spatial structures that are not localized and occupy the whole system are called extended patterns [6, 7, 8]. This patterns posses some characteristic wavelength and usually emerge from the destabilization of an homogeneous state.

One particular extended pattern are Labyrinths, this type pattern are characterized by their spatial disorder (see Fig. 1.2.2). These structures, have been observed

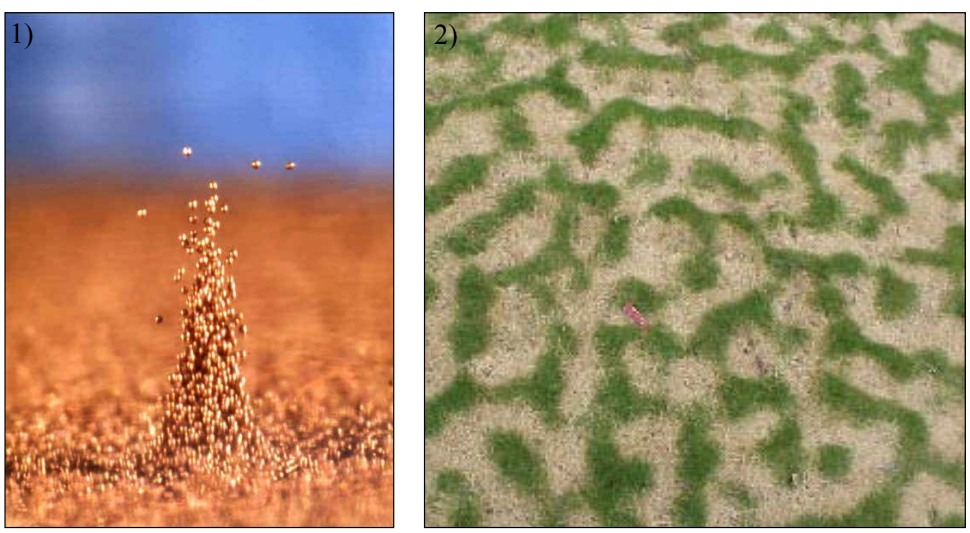

Figure 1.2: 1) *Oscillon*, dissipative localized structure in a vibrated granular system [5], and 2) Vegetation labyrinth formed in semi-arid environment [9, 10].

in various natural systems, from ferromagnetic [11, 12] fluids to Langmuir monolayers [13, 14] and biological systems [15, 16]. In vegetation, for instance, labyrinthine

structures appear when aridity increases and the competition for water resources becomes important [17, 10]. Also in nonlinear cavity optics this structures appear naturally as an effect of the external forcing field [18, 19, 20].

1.2 Objectives

The main objective of this thesis is to study the stability of two-dimensional localized structures, and how the destabilization due to the curvature can lead to extended patterns. To accomplish this objective, this thesis will fulfil the following specific objectives:

- Using a canonical model, characterize the process of destabilization by which a localized structure generates an extended labyrinthine pattern. Extend the results to several physical contexts.
- To shown that the curvature of the localized structures, inherent to the two-dimensional system under study favours the existence of a new type of localized structure.
- Study the self-replication of localized structures in the context of vegetation dynamics. Compare the results with field observations.

1.2.1 Structure of the thesis

This thesis is organized as follow:

- In Chapter 2: Theoretical Background, the general theoretical concepts that will be used along this thesis are presented.

The results of this thesis are presented in Chapters 3, 4, 5 and 6.

- In Chapter 3: Curvature instability and labyrinthine patterns, the mechanism by which localized structures generate labyrinthine structures is presented.
- In Chapter 4: Rodlike localized structure, a complete characterization of the rod localized structure solution is made.
- In Chapter 5: Universality of the curvature mechanism, the curvature mechanism for labyrinth generation is exposed in various physical contexts.
- In Chapter 6: Self-replication in vegetation dynamics, a curvature induced bifurcation of a localized structure is presented where a localized structure splits in two new localized structures.
- In Chapter 7: Conclusions, specific and general conclusions are presented.

Chapter 2

Theoretical background

Macroscopic phenomena emerge from the collective behaviour of a high number of underlying constituents. However, the description of macroscopic phenomena starting from the physics of the individual components of a system is thus extremely complex and in most cases impossible to solve due to the high number of degrees of freedom that emerge naturally from many-body physics. To describe these type

Figure 2.1: Collective behaviour of Blue Mackerel forming a defensive swarm [21].

of problems mean field theory arises, originally, to describe phase transitions. This theory considers the average of microscopic quantities and the approximation of variables through scale analysis, reducing the system to a simpler dynamical equation, thus, describing the whole system through one (or more) order parameter whose evolution is usually described by a nonlinear partial differential equations [22]. This thesis will study dissipative macroscopic phenomena through nonlinear partial differential equations.

2.1 Structure formation

Macroscopic systems under the influence of injection and dissipation of energy and momenta often lead to the formation of spatial structures o patterns [6, 8]. These patterns can be extended, this is, they involve the whole spatial physical system, or localized, which are patterns that exist only on a portion of the spatial system [7, 23, 24].

Localized structures (LSs) are nonlinear peaks or holes in spatially extended systems. They belong to the general class of dissipative structures found far from equilibrium [6]. Experimentally most of these localized states are two-dimensional objects with circular shape as a result of isotropy. In dynamical system theory, one dimensional localized structures are homoclinic connections of the stationary dynamical system involving a stable and an unstable manifold of a given equilibrium [25]. The possibility of coexistence with different equilibria, enriches the variety of possible homoclinic structures. For example, in the case of coexistence between a uniform and a pattern state, the heteroclinic entanglement generates the nucleation of a family of localized structures [26, 27]. In recent decades, localized structures have been observed in different fields, such as, in magnetic materials [28], chemical reac-

tions [29], vertically driven Newtonian fluid [30, 31], granular media [5, 32], liquid crystals [33], liquid crystal light valve [34, 35, 36], colloidal fluids [37], electrical discharges [38], thermal convection [39, 40], non-linear optics [41, 42], chemistry [43, 44], plant ecology [45], fluid dynamics [30], to mention a few.

Localized structures are particle-type solutions for non-linear equations, as they exhibit a series of characteristics often attributed to particles, such as size, position, and velocity defined by the parameters of the system, and an interaction law between them. Localized structures have attracted the interest of the scientific community due to their potential applications for all-optical control of light, optical information storage and processing [46] .

Extended patterns in the other hand emerge typically as the destabilization of an homogeneous state of the system, from which a structure with a characteristic wavelength invades the totality of the system under study.

2.2 Swift-Hohenberg equation

Throughout this thesis Swift-Hohenberg type equations will be deeply studied. Here, some important concepts that will be used along this work will be introduced.

The Swift-Hohenberg equation, named after Jack Swift and Pierre Hohenberg, is the simplest known equation that exhibits pattern formation and it was deduced in the hydrodynamic context to describe the amplitude of the patterns generated by Bénard convection cells in fluids, this equation reads

$$\frac{\partial u}{\partial t} = \epsilon u - u^3 - \nu \nabla^2 u - \nabla^4 u \tag{2.1}$$

By the addition of a constant term, a modified Swift-Hohenberg equation can be written

$$\frac{\partial u}{\partial t} = \eta + \epsilon u - u^3 - \nu \nabla^2 u - \nabla^4 u \tag{2.2}$$

where $u = u(x, y, t)$ is a real scalar field, x and y are spatial coordinates and t is time. The control or the bifurcation parameter ϵ measures the input field amplitude, the aridity parameter, or chemical concentration. This equation will be called ***generalized Swift-Hohenberg equation***, the order parameter $u(x, y, t)$, describes the amplitude of the pattern, ϵ is the bifurcation parameter, which goes along with the linear term. This equation possesses also a cubic nonlinear saturation. Spatial coupling is considered in the diffusive and hyperdiffusive terms, where ν is the diffusion coefficient. The addition of the η term brakes the symmetry $u \to -u$, and accounts for the asymmetry between the homogeneous states. Equation (2.2) has been deduced in various field on nonlinear science such as chemistry [47], plant ecology [48], nonlinear optics [49, 50] and material physics [51]. It is important to note that by the change of variable $u \to u' + q$, where q is a constant, the term η from Eq. (2.2), can be absorbed by the inclusion of a quadratic nonlinearity in the following way

$$\frac{\partial u'}{\partial t} = \epsilon' u' - \alpha u'^2 - u'^3 - \nu \nabla^2 u' - \nabla^4 u' \tag{2.3}$$

where q must satisfy $q^3 - \epsilon q - \eta \equiv 0$ then $\epsilon' = \epsilon - 3q^2$ and $\alpha = 3q$.

Depending on the context in which this equation has been derived, the physical meaning of the field variable $u(x, y, t)$ (or $u'(x, y, t)$) can be the electric field, chemical concentration or phytomass density, to name a few.

2.2.1 Imperfect pitchfork bifurcation

The goal now it to study the stability of stationary homogeneous states of the generalized Swift-Hohenberg equation. The homogeneous states u_0 are solutions of

$$0 = \eta + \epsilon u_0 - u_0^3 \tag{2.4}$$

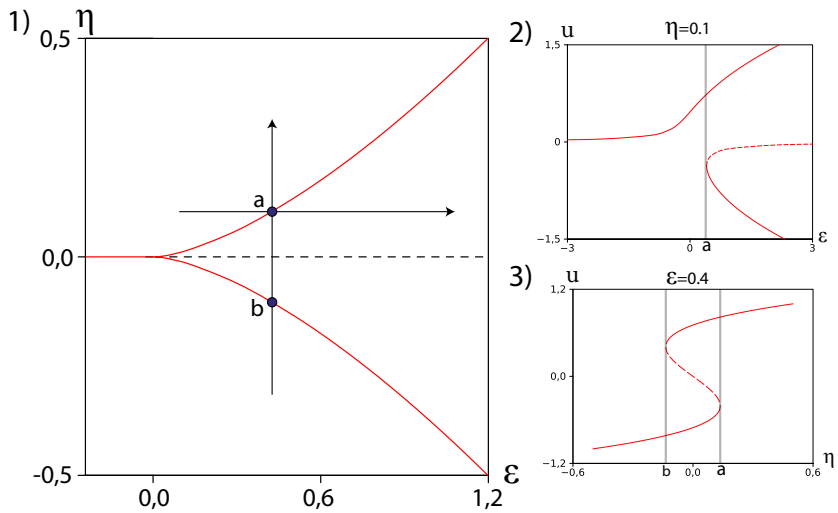

Figure 2.2: Imperfect pitchfork bifurcation in 1) (ϵ, η)-plane. Homogeneous states amplitudes as function of 2) ϵ for $\eta = 0.1$, and 3) η for $\epsilon = 0.4$. Stable states are represented by solid red lines, while unstable states are depicted by dashed lines.

We want to build the—(ϵ, η)—bifurcation diagram for this states, for this, we consider $\eta = \eta(u_0)$, such that $\eta(u_0) = -\epsilon u_0 + u_0^3$, we want to find now the maximum value of η for which this equation holds, in consequence we impose

$$\left.\frac{d\eta}{du_0}\right|_{u_0^*} \equiv 0 \Rightarrow u_0^* = \pm\sqrt{\frac{\epsilon}{3}} \tag{2.5}$$

finally, by replacing (2.5) in (2.4) we obtain an expression for the critical curves (see Fig. 2.2)

$$\eta_\pm(\epsilon) = \pm 2\left(\frac{\epsilon}{3}\right)^{3/2} \tag{2.6}$$

These curves are plotted in Fig. 2.2.1, and represents the birth of an hysteresis cycle through an imperfect pitchfork bifurcation.

2.2.2 Spatial instability

The emergence of periodic patterns in a systems is a consequence of the spatial coupling, the destabilization of an homogeneous state is the simplest mechanism for their appearance. Following this mechanism it will be shown how the generalized Swift-Hohenberg equation exhibits pattern formation.

Lets consider first, a homogeneous state perturbed periodically $u = u_0 + u_p \cos(ikx) exp(\Lambda t)$, where $u_p << 0$ is a small perturbation amplitude, the pattern has been set in the x-direction without loss of generality. By introducing the perturbed solution into Eq. (2.2) and linearizing in u_p, one obtains an equation for $Re(\Lambda) = \lambda(k)$,

$$\lambda(k) = \epsilon - 3u_0^2 + \nu k^2 - k^4 \tag{2.7}$$

this equation indicates that the system will be unstable for wave numbers k such that $\lambda > 0$. We look now for the critical value $k = k_c$ such that $\lambda(k_c) = 0$, this is

$$0 = \epsilon - 3u_0^2 + \nu k_c^2 - k_c^4. \tag{2.8}$$

As the dynamics of the system will be dominated by the larger unstable wave number, one maximizes $\lambda(k)$, obtaining

$$\left.\frac{d\lambda}{dk}\right|_{k_c} \equiv 0 \Rightarrow k_c = 0 \vee k_c = \pm\sqrt{\frac{\nu}{2}} \tag{2.9}$$

evaluating the non trivial value of k_c in Eq. (2.8) we obtain

$$\epsilon - 3u_0^2 = -\frac{\nu^2}{4} \tag{2.10}$$

by replacing in Eq. (2.4) we find the expression for the critical curve

$$\eta_{\pm} = \pm\sqrt{\frac{\nu^2 + 4\epsilon}{3}}\left(\frac{\nu^2 - 8\epsilon}{24}\right) \tag{2.11}$$

which indicates the onset point where the homogeneous state suffers from a Turing (or pattern forming) instability, see Fig. 2.3 Γ_2-curve.

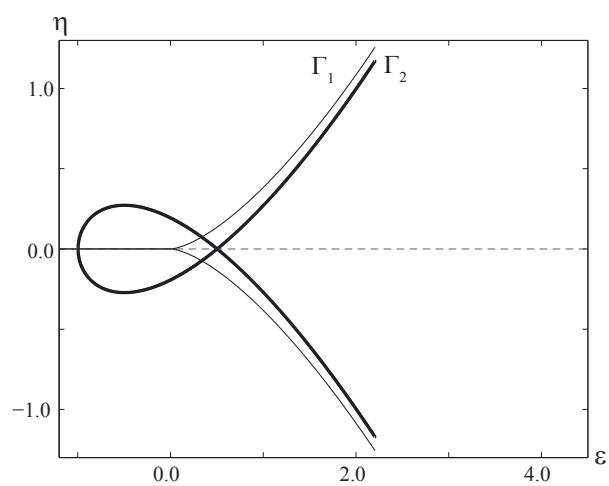

Figure 2.3: Bifurcation diagram of Eq. (2.2). Γ_1-curve corresponds to the imperfect pitchfork bifurcation, Γ_2-curve corresponds to the spatial instability critical curve.

2.2.3 Variational and nonvariational systems

Variational systems

Classical (non dissipative) mechanics is build over the *principle of least action*, this principle states that the dynamics of a system is governed by the minimization of some quantity, namely the *free energy*. These type of systems are called variational,

and their main feature is that they relax to stationary equilibrium states. Though, in dissipative systems, there is no energy conservation and the notion of free energy ceases to exist, however, for a rather large amount of problems it is possible to define a functional—F—such that the evolution of the order parameter is given by the total derivative of a functional

$$\frac{\partial u}{\partial t} = -\frac{1}{2}\frac{\delta F[u, \nabla^2, \nabla^4]}{\delta u} \tag{2.12}$$

where F is often called *Lyapunov functional*, throughout this thesis we will refer to it as the energy of the system.

The generalized Swift-Hohenberg equation (2.2) possesses a gradient form, for this case F reads,

$$F = -\iint \left(\eta u + \epsilon u^2 - \frac{u^4}{2} + \nu(\nabla u)^2 - (\nabla^2 u)^2\right) dxdy. \tag{2.13}$$

Note that this functional satisfies

$$\frac{dF}{dt} = -\iint (\partial_t u)^2 \, dxdy \leq 0, \tag{2.14}$$

so F is a Lyapunov functional that can only decrease in the course of time. This functional guarantees that with temporal evolution, the systems proceeds toward the state for which the functional has the smallest possible value that satisfy the specified boundary conditions. Any initial distribution $u(x, y, t)$ evolves towards a homogeneous or inhomogeneous (periodic or localized) stationary state corresponding to a local or global minimum of F. The analysis of the functional F is provided in Ref. [52].

Nonvariational systems

Nonvariational models can exhibit complex temporal and spatial behaviors as they do not, necessarily, relax to stationary equilibriums. In this sense, nonvariational systems can exhibit permanent dynamics, such as chaotic behaviors, chimera states, intermittency and other states with permanent dynamics.

Near a second order critical point and close to long-wave pattern forming regime, the space-time dynamics of many natural out of equilibrium systems can be described by a single real order parameter equation that includes non-variational effects. This equation is refereed to as *nonvariational generalized Swift-Hohenberg model* or the so called Lifshitz normal form [34, 53].

$$\partial_t u = \eta + \epsilon u - u^3 - \nu \nabla^2 u - \nabla^4 u + c(\nabla u)^2 + b u \nabla^2 u \tag{2.15}$$

This model is a non variational extension of Eq. (2.2).

The model Eq. (2.15) has been derived for numerous far from equilibrium systems such as reaction-diffusion, biological and optical systems [34, 53]. The control or bifurcation parameter measures the input field amplitude or chemical concentration. The terms $c(\nabla u)^2$ and $bu\nabla^2 u$ account for the non-variational dynamic, as they correspond to nonlinear advection and diffusion, respectively. It is important to note that only for the case where $b = 2c$, Eq. (2.15) has a Lyapunov functional (or free energy)

$$\partial_t u = -\frac{1}{2}\frac{\delta F[u, \nabla u, \nabla^2 u]}{\delta u}, \tag{2.16}$$

where

$$F = -\iint \left[\eta u + \epsilon u^2 - \frac{u^4}{2} + \nu(\nabla u)^2 - (\nabla^2 u)^2 - 2cu(\nabla u)^2\right] dxdy. \tag{2.17}$$

When $b \neq 2c$ the Eq. (2.15) is generically non-variational, i.e., there is no Lyapunov functional associated with this equation.

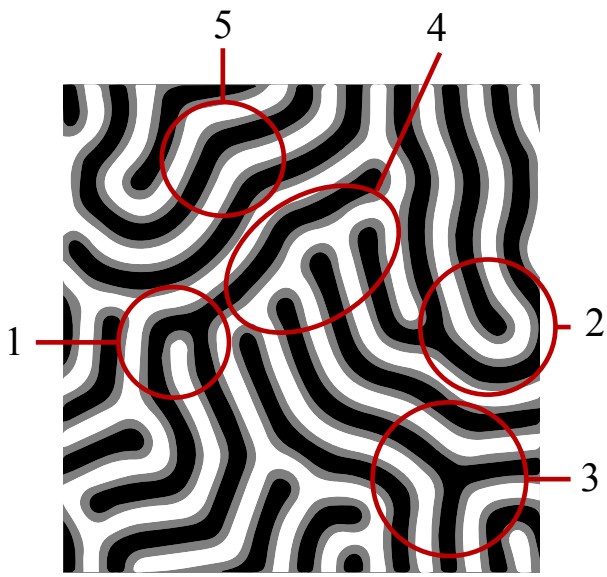

Figure 2.4: Classification of defects in 2D systems, 1) dislocation, 2) concave disclination, 3) convex disclination, 4) amplitude domain wall, 5) phase domain wall.

2.2.4 Defects and pinning phenomena

In the context of pattern formation, defects correspond to the local loss of regularity of the pattern. Defects can turn a rather simple regular pattern into a a complex disordered structure. Labyrinths are in some way defect dominated structures as only local regular structures can be defined and the system as a whole is spatially uncorrelated. Defect are classified according to the type of deformation they introduce to the system (see Fig. 2.4).

Pinning is a phenomenon that occurs to defects in which an effective potential appears around the defect impairing its movement, thus, generating defect pinning. This can be induced by interaction between defects and can favour the existence of defect-dominated patterns as is the case of labyrinths.

Chapter 3

Curvature instability and labyrinthine patterns

In this chapter the two-dimensional generalized Swift-Hohenberg equation (2.2) is considered, in both variational and non-variational forms. Analytical and numerical analysis are preformed concerning the occurrence of the curvature instability that affects the circular shape of two-dimensional localized structures engendering fingering instability. Subsequently, it produces undulations in the finger structure, then, locally forming a pattern, which in turn is also affected by a transversal instability generating labyrinthine patterns.

Numerically, the phase space has been characterized, focusing on regions where the emergence of curvature instabilities are relevant and labyrinths emerge from localized structures. Figure 3.1 illustrates this process in the context of cholesteric liquid crystals, where an initial nematic phase (Fig. 3.1.1) is invaded by a cholesteric phase which is induced by applying an external voltage to the cell. The dynamic of these systems is governed by the minimization of a free energy. These are usually denominated variational or gradient systems.

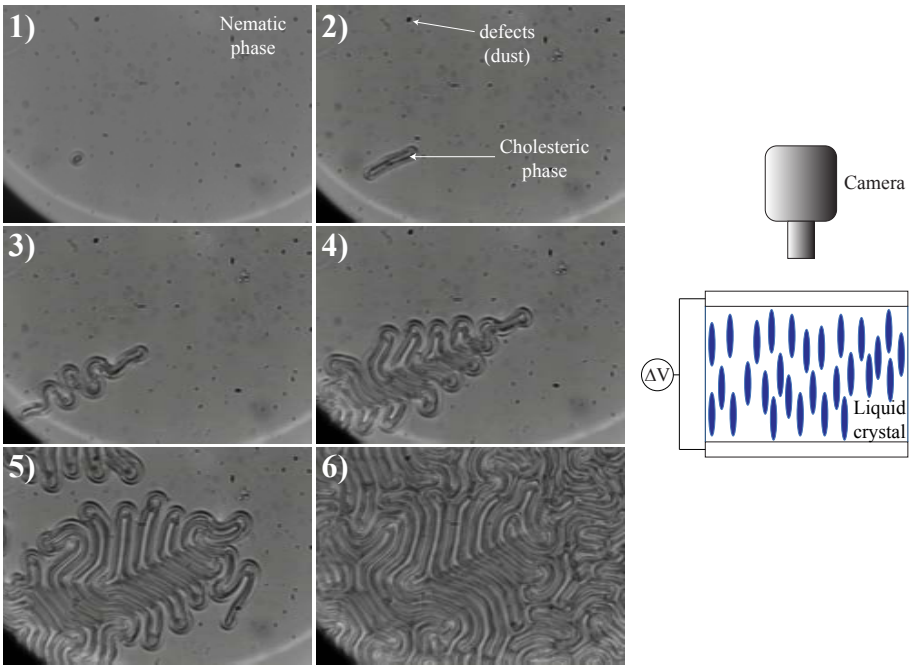

Figure 3.1: Temporal evolution of the growth of the Cholesteric phase in a liquid crystal, where a defect induced localized spot evolves by elongating and produces an extended labyrinth pattern (*Courtesy of R. Barboza, U. Bortolozzo, S. Residori and D. Wei*). On the right side, a schematic of the experimental setup is shown.

3.1 Preliminary observations

Several spatially extended systems that undergo a symmetry breaking instability close to a second-order, codimension two point, can be described by real order parameter equations in the form of Swift-Hohenberg type of models. These models, have been derived in various fields of nonlinear science such as hydrodynamics [54], chemistry [47], plant ecology [48], and nonlinear optics [49, 53, 34].

A complex Swift-Hohenberg equation was deduced in the context of lasers [55, 50, 56] and optical parametric oscillators [57]. Moreover, to describe the nascent optical bistability with transversal effect in nonlinear optical cavities a real approximation has been deduced [58] from laser equations. This approximation allowed the prediction of stable, single and clustered localized structures [58]. A detailed derivation of

this equation from first principles can be found in Ref. [55]. In this chapter, we show that this real modified Swift-Hohenberg equation (2.2) supports a curvature instability over localized structures that leads to an elliptical deformation, producing an elongated unstable structure. With the temporal evolution, the elongated structure exhibits transverse undulations, leading to the formation of invaginated structures. Such a structure is a labyrinthine pattern, characterized by its interconnected structure where the field value is high. The outer region or complement to the invaginated structure corresponds to low field value. This behaviour occurs far from any pattern forming instability and requires a bistable behaviour between homogeneous steady states.

For certain ranges of parameter values, Eq. (2.2) exhibits stable circular localized structures. General properties, such as existence, stability and dynamical evolution of these structures have been well studied (see Refs. [59, 60, 61, 62, 27, 63, 64, 65]). For $\eta < 0$ localized structures emerge as isolated peaks of the field $u(x, y, t)$, instead, for $\eta > 0$ localized structures appear as holes in the field. These localized structures have a fixed stable radius for each parameter value. Curvature instability of localized spot has been experimentally studied or theoretically predicted in magnetic fluids [12], liquid crystals [66, 67], reaction-diffusion systems [68, 29, 69, 70, 43, 44, 71, 72, 73, 74, 69, 75, 76], plant ecology [17], material science [77, 78], in granular and frictional fluids [79, 80], and nonlinear optics [81]. The fingering instability of planar fronts leading to the formation of labyrinth structures has been reported by Hagberg et al. [82]. In this thesis we shall focus on circular localized states. To avoid numerical artifacts and to ensure the stability of our simulations, simulations where performed using both finite differences and pseudo-spectral codes, by carefully choosing the temporal and spatial scales we where able to maintain the stability of the simulation while decreasing the simulation times.

3.2 Stability of localized spots

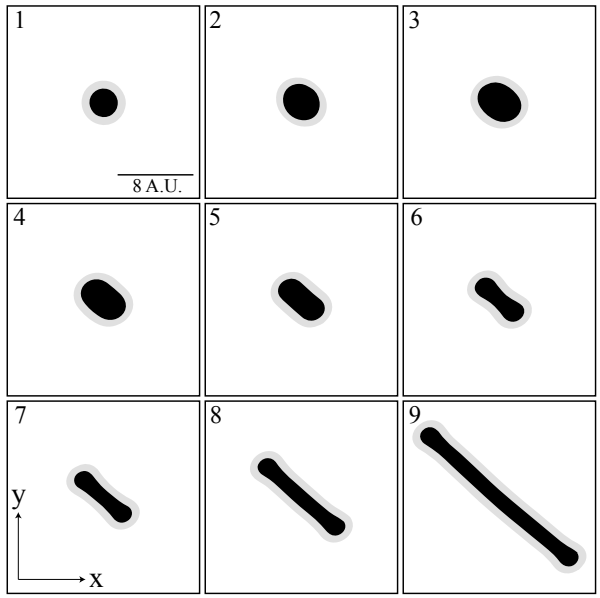

Figure 3.2: Temporal evolution for; 1) $t = 0$; 2) $t = 125$; 3) $t = 175$; 4) $t = 225$; 5) $t = 275$; 6) $t = 340$; 7) $t = 350$; 8) $t = 360$; 9) $t = 400$, of a localized spot through an elliptical deformation into an elongated structure for Eq. (2.2) with: $\eta = -0.065$; $\epsilon = 2.45$; $\nu = 2.0$. Minima are plain white. The image corresponds to a zoom of 16×16 points of a 512×512 point finite-difference simulation, with Neumann boundary conditions.

We consider fixed parameter values, starting with a stationary azimuthally symmetric localized structure. The structure is then perturbed, this perturbation grows radially as shown in Fig. 3.2 The circular shape becomes unstable at some critical radius. The elliptical shape elongates into a stripe structure as shown in Fig. 3.2. This elongation proceeds until a critical size is reached beyond which a transversal instability onset the appearance of fingers near the midsection of the structure (see Fig. 3.3.3). The stripe continue its elongation, and the amplitude of oscillation increases (Figs. 3.3.4 and 3.3.5). The dynamic of the system does not saturate and for a long time evolution, the rod-like structure invades the whole space available in the (x, y)-plane as shown in Fig. 3.3.6. This invaginated structure is stationary solutions

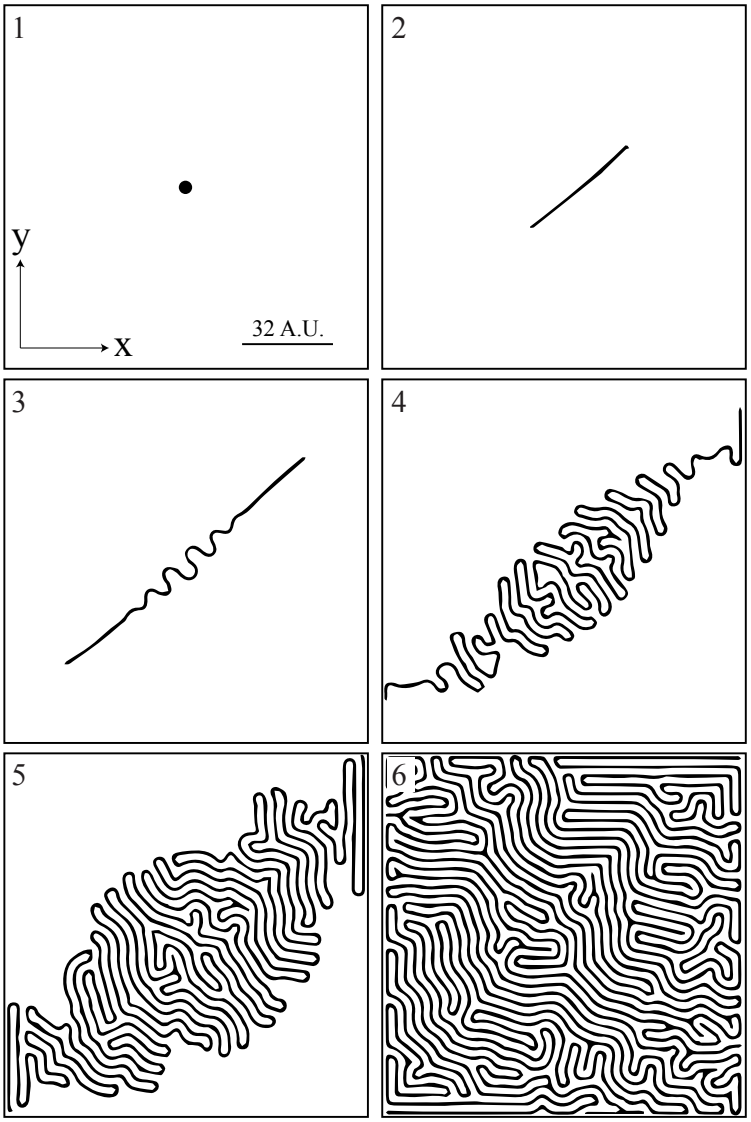

Figure 3.3: Transition from a single localized spot to invaginated pattern. Temporal evolution with Dirichlet boundary conditions and with the same parameters as in Fig. 3.2. 1) $t = 0$, Localized spot, 2) $t = 600$, stripe structure, 3) $t = 1900$, transverse undulation of the stripe structure 4) $t = 2800$, and 5) $t = 3700$, localized transient patterns, and 6) $t > 15000$, stationary invaginated labyrinth pattern. Minima are plain white and the mesh integration is 512×512 points. Simulation done with finite-difference method.

of the SHE. The dynamic described previously has been observed in cholesteric liquid crystals under the presence of an external electric field [66, 67], where an initially circular structure of cholesteric phase suffers from a curvature instability, transversal

oscillations and develops into an extended labyrinthine structure (see Fig. 3.1). The characterization of this dynamic is an open problem.

For $\nu = 2$, the bifurcation diagram of the model Eq. (2.2) in the parameter space (ϵ, η) is shown in Fig. 3.4. For $\epsilon > 0$ the system undergoes a bistable regime between homogeneous steady states. For $\epsilon < 0$, the system possesses only one homogeneous steady state. The curve Γ_1 represents the pitchfork bifurcation, where, the coordinates of the limit points of the bistable curve are given by $\eta_\pm = \pm 2(\epsilon/3)^{3/2}$. The threshold associated with a symmetry breaking or Turing instability is provided by the curve Γ_2. The coordinates of the symmetry breaking instabilities thresholds are $\eta_\pm = \pm\sqrt{(\nu^2 + 4\epsilon)/3}(\nu^2 - 8\epsilon)/24$. The Γ_1 and Γ_2 curves are well known in the literature [83, 84]. We have built numerically the curve Γ_3, which separates the zone of bistability where localized structures are stable, zone II, from the zone where they are unstable, zone I. The transition from localized structures to labyrinthine pattern takes place when crossing from the I-zone to the II-zone, through the Γ_3-curves indicated in Fig. 3.4. This transition occurs via fingering instability at the Γ_3-curves delimiting the parameter domain I and II. In the limit of the classical Swift-Hohenberg equation, $\eta = 0$, there is no observation of fingering instability, instead, at the transition from II-zone to I-zone, localized structures only grow radially. The destabilization of these structures into labyrinthine structures may be observed, as a result of size effect phenomenon due to boundary conditions. In contrast, for $\eta \neq 0$ the transition from the II-zone to the I-zone of a localized spot induces a curvature instability, giving rise to an unstable stripe structure which exhibits transversal oscillations and develops into an extended labyrinthine structure.

In what follows, we first study the stability of a circular localized spot with respect to azimuthal perturbations. This linear analysis allows us to evaluate the threshold above which the transition from a localized spot to a elongated structure

takes place. Then, a linear stability analysis of the stripe structure is performed, to determine the conditions under which the transversal oscillations occur for the SH equation.

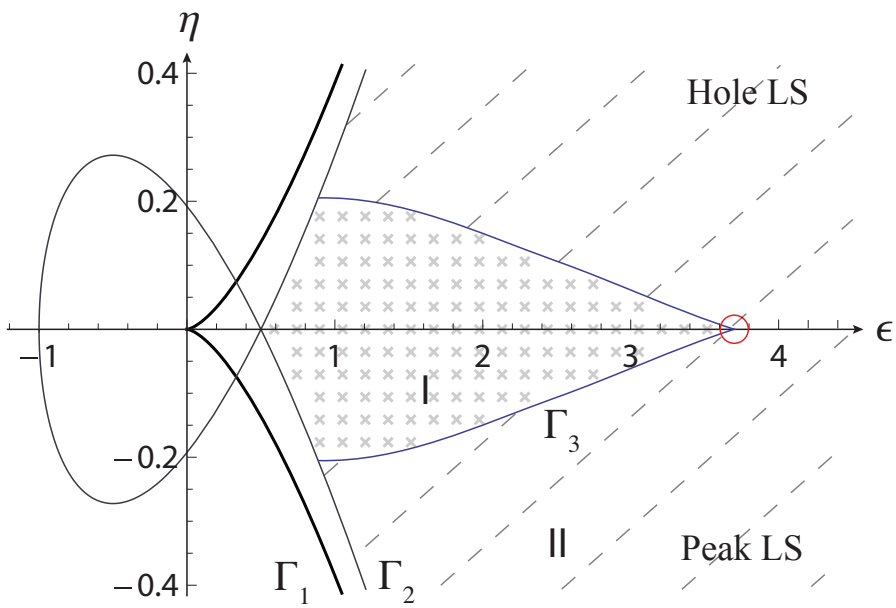

Figure 3.4: Bifurcation diagram of Eq. (2.2) in (ϵ, η) space for $\nu = 2.0$. In II-zone (dashed black), stable circular localized structures are observed. In I-zone (grey crosses) generation of labyrinthine structures are observed from localized structures. Simulations where made using periodic boundary conditions.

Starting from a stationary solution with rotational symmetry (i.e circular localized structure) $u = u_s(r)$ where r is the radial coordinate. Then, the solution is perturbed $u(r, \theta, t) = u_s(r) + \delta u(r) e^{\lambda_m t} \cos(m\theta)$, where θ is the angular coordinate, and $\delta u(r) \ll 1$. It should be noted that the perturbation mode $m = 2$ represents an elongation of the circular structure into an elliptical shape. Using polar representation of Eq. (2.2), considering the above perturbation and parameters in Eq. (2.2) at linear order in W one obtains

$$\frac{\partial W}{\partial t} = \mathcal{L} W \tag{3.1}$$

where the linear operator $\mathcal{L} \equiv \epsilon + 3u_s^2(r) - \nu\nabla^2 - \nabla^4$ is explicitly dependent on the

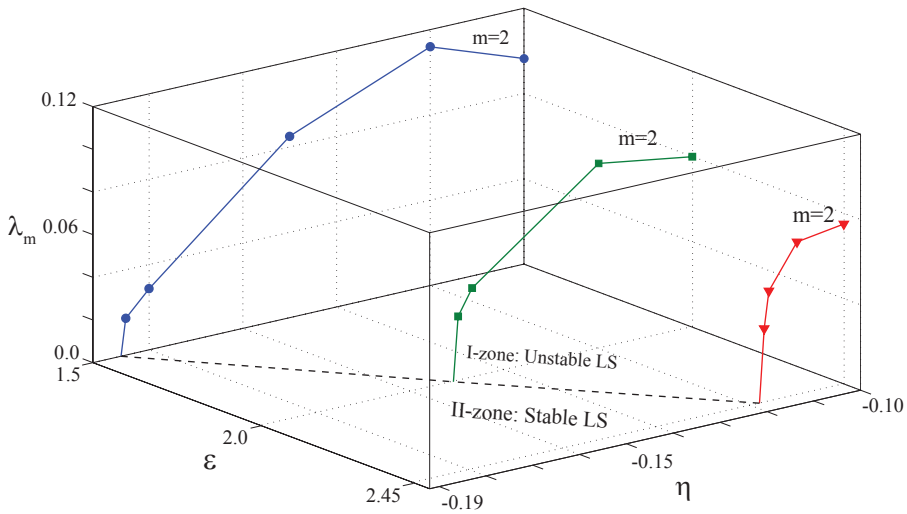

Figure 3.5: Dots show the growth rate λ_m of the most unstable perturbation mode obtained numerically for different values of ϵ. Dashed line separates zones of stable and unstable localized structures. Parameters: $\nu = 2$; $dx = 0.5$; $dt = 0.03$. Periodic boundary conditions were used.

radial coordinate. Analytical calculations are not accessible when the operator is inhomogeneous. However, by direct simulation of Eq. (2.2) with an initially stationary localized structure one can find the growth rate of the most unstable mode. First for fixed values of the parameters $\{\eta, \epsilon, \nu\}$ a stationary localized spot is considered as initial condition. Note that the radius of localized spot is determined by a balance between the interface energy and the energy difference between the homogeneous states which are proportional to ν and η, respectively. The radius of the localized structures r_s is proportional to ν/η [85]. Afterwards, the system is perturbed by homogeneous noise, this type of perturbation can be regarded as a linear combination of all the angular modes m. However, the most unstable mode (the one with largest eigenvalue λ_m) dominates the temporal dynamics and is the the only one observable. By considering the stability of the localized spot for different values of the parameter η under homogeneous noise perturbations we can determine that the most unstable mode ($\lambda_2 > 0$) is $m = 2$ as observed in Figure 3.5. This mode deforms the circular

localized spot into an elliptically shaped structure as shown in Fig, 3.3.2.

3.3 Transversal instability

The SHE Eq. (2.2) admits a single stripe like solution [62, 86]. In order to evaluate the threshold over which transversal oscillations appear, we perform the stability analysis of a stripe structure, by a method similar to the one performed in Ref. [82]. For this purpose we perturb the single stripe solution as $u = u_f(\xi) + W(x, X_0)$ where u_f is the single stripe solution and $\xi = x - X_0(y,t)$ the relative position, X_0 is the field that accounts for the shape and evolution of the stripe, and $W(x, X_0) << 1$ is a non-linear correction of a single stripe. Applying this ansatz in Eq. (2.2) at first order in W and applying the solvability condition [8], the following equation is obtained for the dynamic of X_0

$$\partial_t X_0 = -\Delta' \partial_{yy} X_0 + 6\beta' \partial_y^2 X_0 (\partial_y X_0)^2 - \partial_y^4 X_0, \tag{3.2}$$

where

$$\beta' = \frac{\langle \partial_{\xi\xi} u_f | \partial_{\xi\xi} u_f \rangle}{\langle \partial_\xi u_f | \partial_\xi u_f \rangle}, \text{ and } \Delta' = (\nu - 2\beta'). \tag{3.3}$$

Thus X_0 satisfies a nonlinear diffusion equation. This equation describes the dynamics of an interface between two symmetric states [87, 88]. This model is well known for exhibiting a zigzag instability. Analogously, to the previous section, when $\Delta' < 0$ the single stripe solution is stable, and for $\Delta' > 0$, the solution is unstable as result of the curvature instability. From equation (3.2) one expects to observe the single stripe becomes unstable by the emergence of undulations. Figure 3.6 illustrates the manifestation of this undulations under the consideration of an infinitely long stripe structure, to avoid border effects. The pseudo-spectral code used prevents us from

having discretization effects. Note that similar dynamical behavior is observed in the propagation of cholesteric fingers in liquid crystals [66, 67]. Later, this undulated stripe is replaced by the emergence of facets that form a zig-zag structure. However the higher nonlinear terms control the evolution of the single stripe, then the dynamics of the initial zig-zag is replaced by the growth of undulations without saturation as it is depicted in Fig. 3.3.4. Therefore, the system displays the emergence of a roll-like pattern which is formed in the middle section of the structure and invades the system (see Fig. 3.3.5). To understand the complexity exhibited by these patterns,

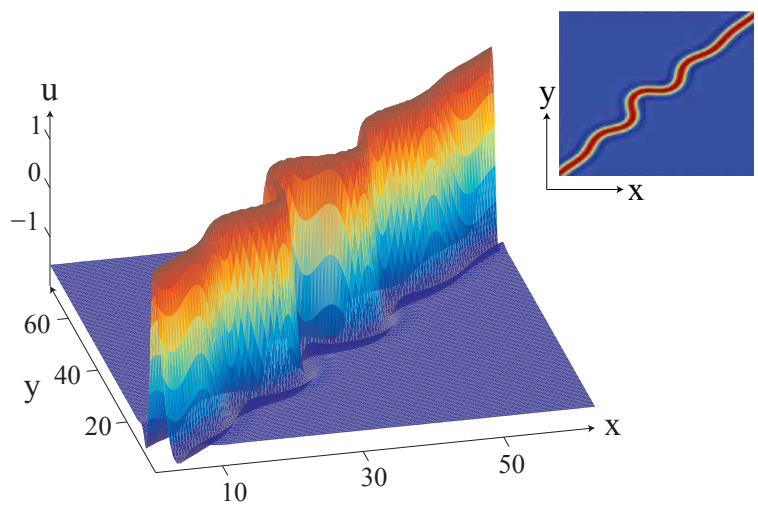

Figure 3.6: Transversal instability of a single infinite stripe of Eq. (2.2). Image shows a section of a 256×256 point simulation with periodic boundary conditions using a pseudo-spectral code. Parameters: $\eta = -0.065$, $\epsilon = 2.45$, $\nu = 2$, $dx = 0.5$, and $dt = 0.03$.

it will be shown how through a pattern instability this roll structure destabilizes generating its own oscillations.

3.3.1 Stability analysis of a regular pattern

In this subsection, we perform a linear stability analysis of an extended periodic pattern. For this purpose, we consider a periodic solution along the x direction

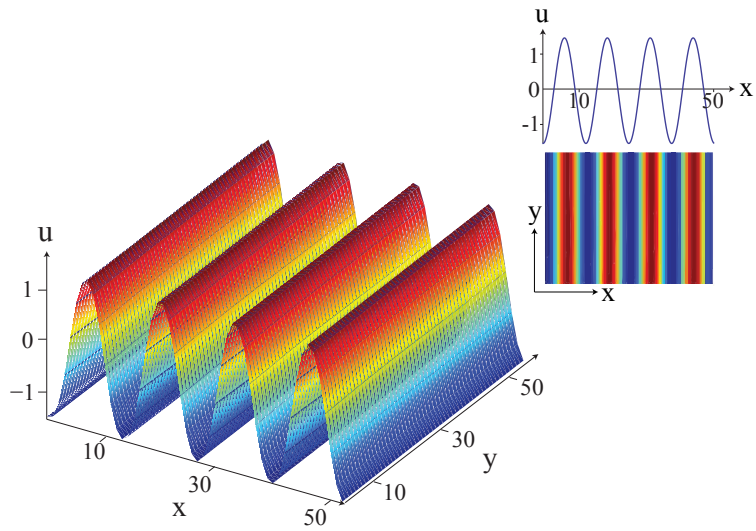

Figure 3.7: Stripe pattern and its profile obtained from the simulation of Eq. (2.2), with periodic boundary conditions and parameters: $\eta = -0.065$; $\epsilon = 2.45$; $\nu = 2.0$; $dx = 0.5$; $dt = 0.03$. The insets depict a profile and colormap plot of the regular pattern.

$u_p = A\exp[iq_0x] + c.c.$, where A is the amplitude, q_0 is the wave number and $c.c.$ initials denote complex conjugate. Due to the spatial isotropy of the Swift-Hohenberg Eq. (2.2) the pattern may be oriented in any specific direction, without loss of generality. For simplicity we have chosen the pattern fo amplitude A, to be in the x-direction. Such stripe solution is plotted in Fig. 3.7. We consider a small perturbation around this periodic solutions as $u(\boldsymbol{r}, t) = u_p(\boldsymbol{r}) + \delta u(\boldsymbol{r}, t)$ such that $\delta u = \delta_0 e^{(\sigma_{q_0} t)}[\exp(iq_0x + \boldsymbol{K}\cdot\boldsymbol{r}) + c.c.]$ and $\delta_0 \ll 1$, where, $\boldsymbol{K} = k_x\hat{x} + k_y\hat{y}$ and $\boldsymbol{r} = x\hat{x} + y\hat{y}$ represent the perturbation wave vector and the position, respectively. σ_{q_0} stands for the temporal growth rate. Substituting this finite wavelength perturbation in Eq. (2.2), after straightforward calculations we obtain the growth rate relation

$$\sigma_{q_0}(\boldsymbol{K}) = \epsilon - 3A^2 + \nu\left[(q_0 + k_x)^2 + k_y^2\right] - [(q_0 + k_x)^4 + (q_0 + k_x)^2 k_y^2 + k_y^4]. \quad (3.4)$$

Hence, the stripe patterns exhibits a spatial instability when $\sigma_{q_0}(\boldsymbol{K}) > 0$, generating

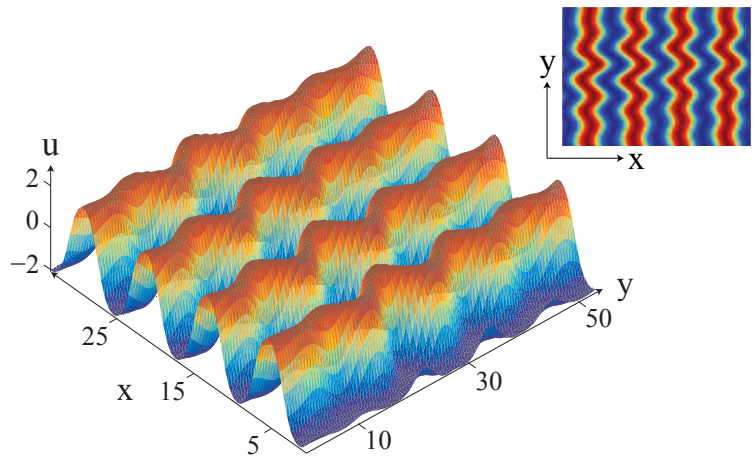

Figure 3.8: Spatial instability of a stripe pattern of the Swift-Hohenberg Eq. (2.2) with periodic boundary conditions and parameters: $\eta = -0.065$; $\epsilon = 2.45$; $\nu = 2.0$; $dx = 0.5$; $dt = 0.03$. The image shows in a given time, the appearance of undulations on the stripes pattern. The inset shows a colormap plot of the undulated stripe pattern.

oscillations along the y-axis. Figure 3.8 shows at a given time, the emergence of undulations in the stripe pattern.

The amplitude of the undulations continued to grow until finally the system finds as equilibrium a labyrinthine pattern [89]. Note that one can derive a nonlinear equation for the phase of the stripe which have the same form as Eq. (3.2) [90]. Therefore, the dynamics exhibited by a single stripe is similar to those exhibits by a stripe pattern.

3.4 Non-variational model

Localized structures are persistent in the presence of non-variational extra terms. As a result of these non variational terms LSs may be exhibit permanent dynamics as oscillation or chaotic dynamical behavior, among others [34, 91]. The dynamics of spots deformation, accompanied by the emergence of unstable fingers with the

final appearance of labyrinthine patterns we also observed in the non variational Swift-Hohenberg model, Eq. (2.15). Figure 3.9 illustrates the process of emergence of labyrinthine patterns from a localized structure

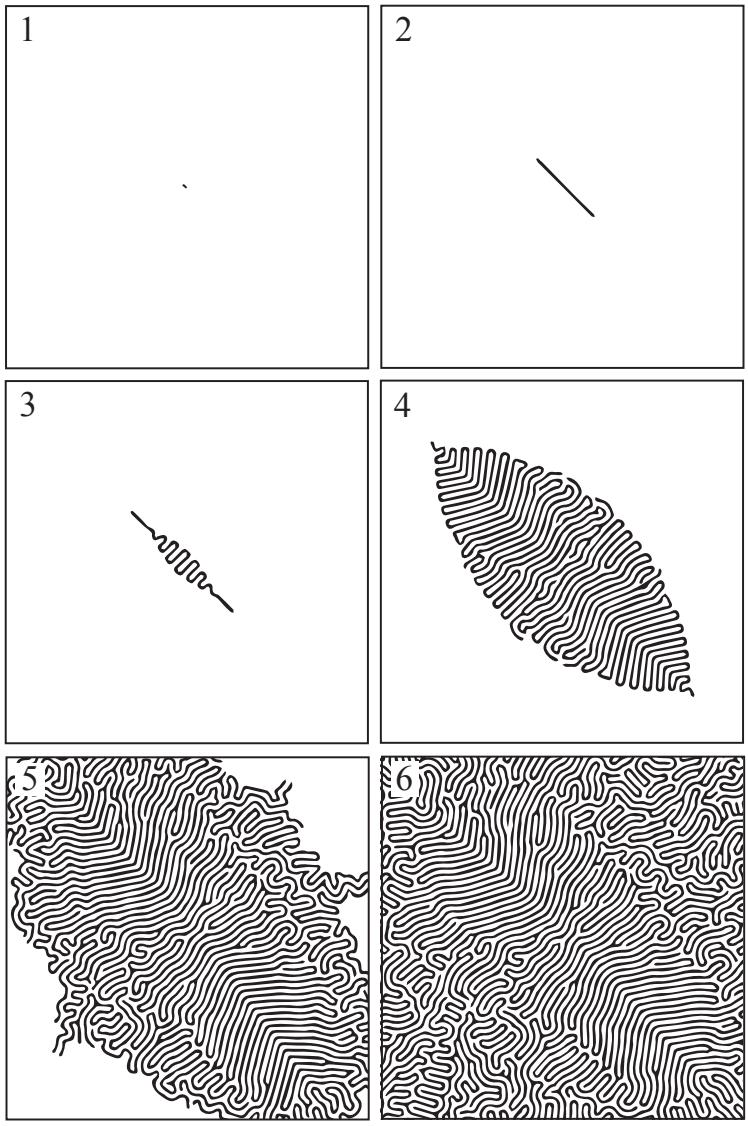

Figure 3.9: Transition from a single peak LS to labyrinthine pattern in the non-variational Swift-Hohenberg Eq. (2.15). Different images sequentially illustrate the temporal evolution of the structure, with parameters: $\eta = -0.225$; $\epsilon = 1.0$; $\nu = 2.0$; $dx = 0.5$; $dt = 0.03$ $c = 0.1$ and $b = -0.1$. 1) Localized structure, 2) stripe structure, 3) undulations in the elongated structure, 4) and 5) localized transient patterns, and 6) stationary labyrinthine pattern.

3.5 Chapter summary

In this chapter we have described the stability of a localized spot in a modified Swift-Hohenberg equation. First, the bifurcation diagram was constructed, showing the possible solutions that appear in different parameter regimes. Afterwards, it was shown that the angular index $m = 2$ becomes unstable as consequence of curvature instability. Such instability leads to an elliptical deformation of the localized spot.

The elliptical deformation leads to the generation of an elongated structure. Subsequently, it causes undulations in the central portion of the stripe structure. The spatiotemporal evolution leads to the formation of invaginated labyrinthine structures. To understand this dynamics, we have performed the analytical stability analysis of a single stripe localized structure.

It should be noted that by an offset transformation, $u \to u + u_0$, where u_0 is a constant, Eq. (2.2) can be rewritten in such a way that the constant parameter η is removed and a quadratic nonlinearity appears, Eq. (2.3). This quadratic model is equivalent to Eq. (2.2). The model with a quadratic nonlinearity has been well studied (see the textbook [8] and the references therein). This equivalence implies that the results presented in this chapter are also valid for physical systems described by the quadratic model.

The results presented in this chapter have been published, a copy of the article can be found in Appendix A.

Chapter 4

Rodlike localized structure

In the previous chapter it was shown how a localized structure suffers from a curvature instability leading to the formation of an extended labyrinthine pattern. However it was observed that for certain—(η, ϵ)—parameter values of 2.2, labyrinths can coexist with localized structures. This favoured the discovery of a new type of localized structure from which labyrinths can develop. This structure is different from the already known circular LS.

In this chapter, we show the existence, stability properties, dynamical evolution and bifurcation diagram of a stationary elongated localized structure, non azimuthally symmetric, in the prototype isotropic two-dimensional Swift-Hohenberg equation (2.2). This structure will be called Rod structure, because of its elongated—rodlike—shape. Figure 4.2 illustrates the typically observed stable rod structure. Based on a dimer approximation, interaction properties of rod structures is characterized. Complex network of equilibria are shown, this allows us to configure different crystallike structures. Numerical simulations show a fair agreement with these predictions.

4.1 Preliminary observations

Isotropic dissipative systems usually exhibit localized structures which are azimuthally symmetric, that is, the localized states have circular symmetry. Spatial breaking of symmetry tends to deform the localized structures and even can generate propagation of them, this is the case of the worm structures observed in binary liquids [39, 92] and electro-convection cells [93]. In the liquid crystal light valve experiment triangular localized structures have been observed by controlling the optical feedback (see Fig. 4.1).

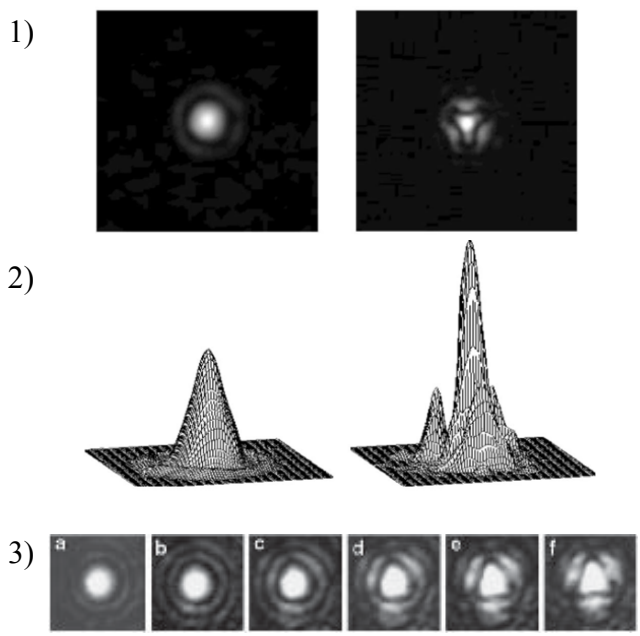

Figure 4.1: Triangular localized structure found in the liquid crystal light valve experiment. 1) and 2) correspond to numerical simulations [35]. 3) Experimental observations [94].

Numerical simulations of the model describing this system also exhibits this type of intrigued localized state. These triangular structures are inherently two-dimensional due to the spontaneous breaking of symmetry of rotation. There is not a global geometric theory to explain the origin of this structure and a characterization

of the different possible localized structures without rotational symmetry.

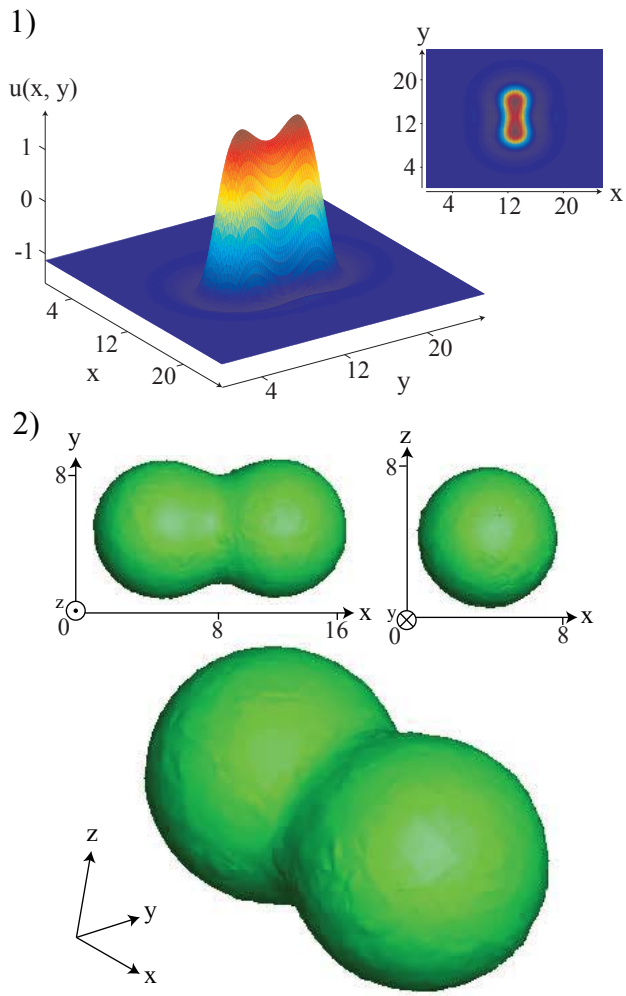

Figure 4.2: Stationary rod localized structure for the Swift-Hohenberg model, Eq. (2.2). 1) In 2D, with $\nu = 2.0$, $\eta = -0.355$, $\epsilon = 1.2$, inset is a colormap of the rod localized structure, and 2) in 3D, with $\nu = 2.0$, $\eta = -0.065$, $\epsilon = 2.45$

4.2 New localized solution

Considering the generalized Swift-Hohenberg equation (2.2), which exhibits both localized and extended patterns. This equation generically applies to systems that undergo a symmetry breaking instability—often called Turing instability [6, 7]—close

to a second-order critical point marking the onset of a hysteresis loop, which corresponds to a Lifshitz point [7, 22, 95] hence, this equation accounts for a bifurcation of codimension three.

The generalized Swift-Hohenberg equation exhibits coexistence between homogeneous and pattern states, thus allowing the stability of localized structures. These are localized structures in the sense of integral boundedness

$$\iint_{\mathbb{R}^2} |u_{ls}(x,y)|^2 dxdy < +\infty, \tag{4.1}$$

where, $u_{ls} \equiv u(x,y) - u_0$ is the relative field of the localized structure with respect to the homogeneous state u_0 which sustains the localized structure. This homogeneous state is a stable solution to the cubic equation $\eta + \epsilon u_0 - u_0^3 = 0$. For a certain range of parameters $\{\eta, \epsilon\}$ two different localized structures are stable, the first, is the well known circular (azimuthally symmetric) localized structure [58]. Notwithstanding, we have found a second type of localized structure corresponds to a novel class of localized structures at least in two and three-dimensional isotropic systems. This structure is a rodlike stable localized structure, it break the azimuthal symmetry, remaining invariant only with respect to a rotation of π around any axis on the (x, y)-plane which contains the center of the localized structure. Figure 4.2 shows the typical rodlike stable localized structures exhibited by both the 2D and 3D Swift-Hohenberg Eq. (2.2). These structures do not correspond to bound states of two independent circular localized structures. In order to figure out the conditions under which the rod structure emerges, the analysis of the bifurcation diagram must be done for the model under study.

For a fixed value of the diffusion coefficient $\nu = 2.0$, typical bifurcation diagram of the model Eq. (2.2) in the parameter space (ϵ, η) is shown in Fig. 4.3. The

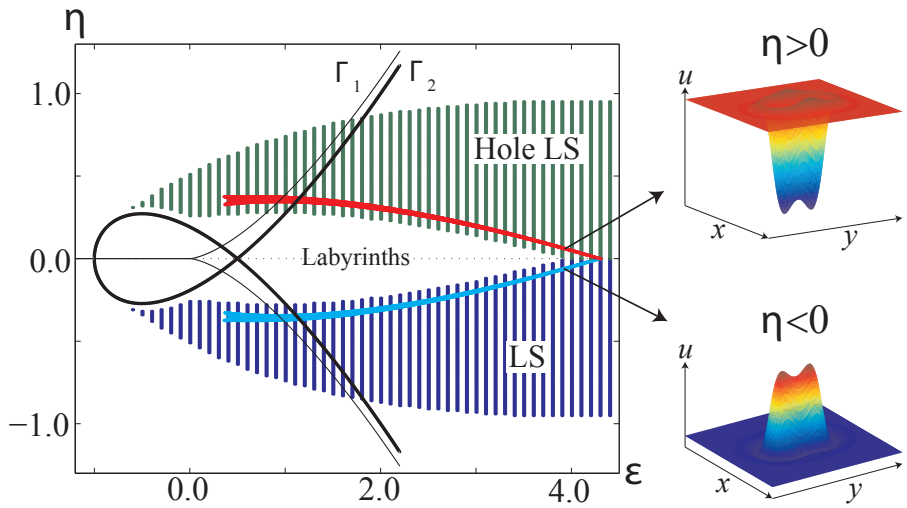

Figure 4.3: Bifurcation diagram of the 2D generalized Swift-Hohenberg Eq. (2.2) in (ϵ,η) space for $\nu = 2.0$. The light and solid curve Γ_1 and Γ_2 account for the imperfect pitchfork bifurcation and the spatial bifurcation of the uniform state, respectively. The shaded areas account for the zones where localized peaks (LS-zone) and localized holes (Hole LS-zone) are observed. The painted areas (light-blue and red) stand for the regions where rod structures have been observed. The insets correspond to the typical monitored rod structures.

curves Γ_1 and Γ_2 represent the saddle-node bifurcation and the threshold associated with a modulation or pattern forming or Turing instabilities of the homogeneous state, respectively [83, 84]. For negative ϵ, the system has only one homogeneous steady state, monostable region. For positive ϵ the system undergoes a bistable behavior between homogeneous steady states as result of the saddle-node bifurcation. Moreover, as a result of the spatial instability of the uniform state, the system also exhibits coexistence between patterns and uniform states (cf. Fig. 4.3). Near this type of bistability region one expects to observe localized structures [84]. The shaded zones in Fig. 4.3 account for the areas where circular localized peaks and holes are observed. When one decreases the value of the parameter $|\eta|$ (approaching zero) circular localized structures become unstable giving rise to labyrinthine pattern as described in Chapter 3. This transition occurs via fingering instability.

Unexpectedly, rod structures coexist with isotropic localized structures. Figure 4.3 depicts the region where the rod structures are observed.

Even though the Swift-Hohenberg model has been extensively studied since its deduction, no analytic expression is know for the localized solution. It is because these solutions are homoclinic solutions of the stationary dynamical system ($\partial_t u = 0$), which is chaotic when one replaces the time for the radial coordinate [96]. Under this consideration, the study of the rodlike structure will not lead to an analytic expression yet to the full characterization of its characteristic properties, bifurcations, and interaction. Numerical and geometrical methods are the most suitable tools for characterizing the localized structures. We have conducted various numerical simulations to validate our observations, in 2D we used both pseudo-spectral and finite differences methods, and in 3D we used an adaptive triangular finite element method. All the simulations exhibited stable rodlike structures.

4.3 One-dimensional interpretation

No definitive theory for two-dimensional localized structures has yet been formulated, therefore, the required physical and mathematical conditions for their existence and stability are not known. However, for one-dimensional systems, localized structures emerge as a family of stable fronts connecting an homogeneous with a pattern state in a bistable regime [97]. It is now known that coexistence (instead of bistability) is sufficient for the appearance of one-dimensional localized structures [98]. In this sense, the generation of two-dimensional localized structures can be regarded as an extension of one-dimensional localized structure, which is rotated over its axis thus generating an azimuthally symmetric localized structure. Nevertheless, the rodlike structure breaks the azimuthal symmetry.

Projecting over two orthogonal planes (γ_1 and γ_2). One can generate the equivalent to one-dimensional localized structures. The projection over the γ_1-plane (Fig 4.4.1) generates a one wavelength wide localized structure while the projection over the γ_1-plane (Fig 4.4.2) generates a two wavelength wide localized structure [85]. Hence, the two dimensional rod structure can be considered as the composition of two one-dimensional localized structures with different lengths.

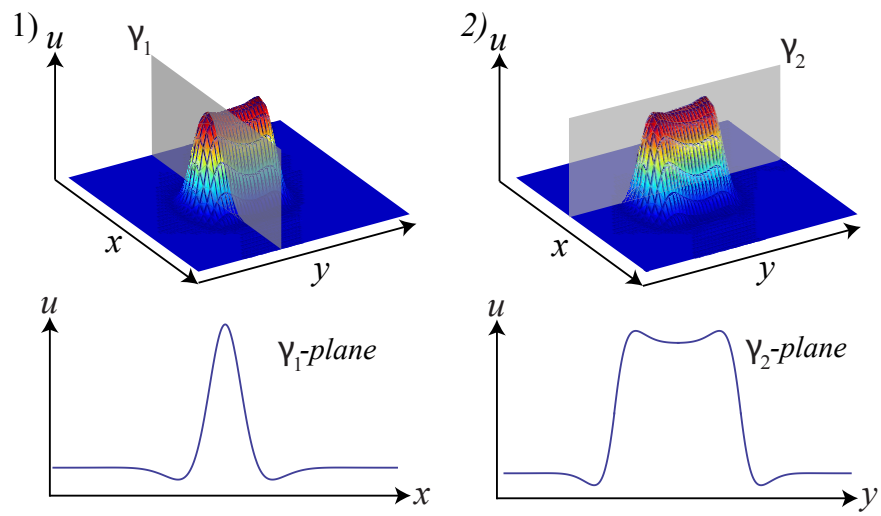

Figure 4.4: One-dimensional projections of the 2D rod structure and the respective projection over the: a) (x, u)-plane and b) (y, u)-plane. Numerical simulation of Eq. (2.2) with $\nu = 2.0$, $\eta = -0.355$, and $\epsilon = 1.2$.

As in one-dimensional localized structures of the generalized Swift-Hohenberg equation, the two dimensional structures possesses spatial oscillation tail of the field, which propagates radially from the bulk of the structure, these oscillations, that decay exponentially, stabilize the structure and allow the interaction between two or more structures by field interference [59].

4.4 Instabilities and bifurcation diagrams

The characterization of the phase space of the Swift-Hohenberg Eq. (2.2), Fig. 4.3, shows the existence of the rod structure for a narrow range of parameters η and ϵ. In all the range of stability, the rod structure coexists with stable circular localized spots. It was shown in the previous chapter that circular localized structures suffer from a curvature instability when leaving their stability zone thus generating an extended labyrinthine structure. In this section its shown how labyrinths can emerge—in zones where circular localized structures are stable—by the destabilization of the rod structure. It is also shown how the rod structure elongate into an infinite roll structure, decay into the simpler localized spot or even split into a bound state of two circular localized structures, depending on the parameters varied. Bifurcations suffered by the rod structure can be studied through monitoring the energy (Lyapunov functional) while modifying one parameter and fixing the others.

By variations of the parameters η or ϵ the rod structure is affected by saddle-node bifurcations characterized by a change of the energy which follows a square-root law near the threshold (see dotted lines in Fig. 4.5 and Fig. 4.8), and by a decay rate of the structure proportional to $(\alpha - \alpha_c)^{-1/2}$, where α is the parameter varied and α_c indicates the critical parameter value for which the bifurcation occurs [99], Figure 4.6 illustrates this type of dynamical behavior. Rod structures that exist at the right side of Γ_2-curve (cf. Fig. 4.3), exhibit only two bifurcations. The first occur when leaving the stability zone of the rod structure by decreasing ϵ (increasing η), causing an increment in the rod structures size and consequently an increment on its energy. Once the bifurcation takes place through the saddle-node mechanism, the system falls into the basin of attraction of the labyrinthine pattern.

The transitions from rod to labyrinthine pattern, changing the different control

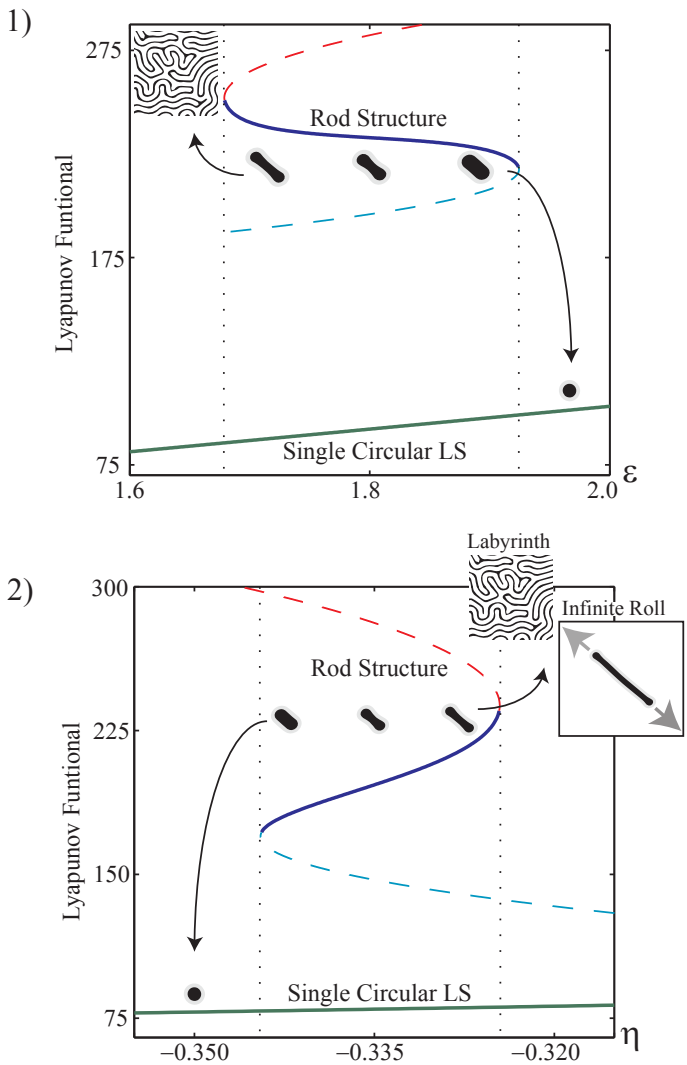

Figure 4.5: Bifurcation diagrams of rod structures as function of ϵ and η parameters. Saddle-node bifurcations, rod to circular localized structure, rod to labyrinth, and rod to infinite roll. For 1) $\eta = -0.320$ and 2) $\epsilon = 1.6$ and $\nu = 2.0$.

parameters are depicted in Figure 4.5. As labyrinths are extended patterns, their energy diverges. The second bifurcation suffered by the rod structure in this zone, takes place when increasing the value of ϵ (decreasing η), here, the rod structure shrinks subsequently reducing its energy, by saddle-node bifurcation rod structures decay into single localized spots, which are energetically more stable, in the Lyapunov sense. Figure 4.5 shows the transition from rod to localized spot. This rod to circular

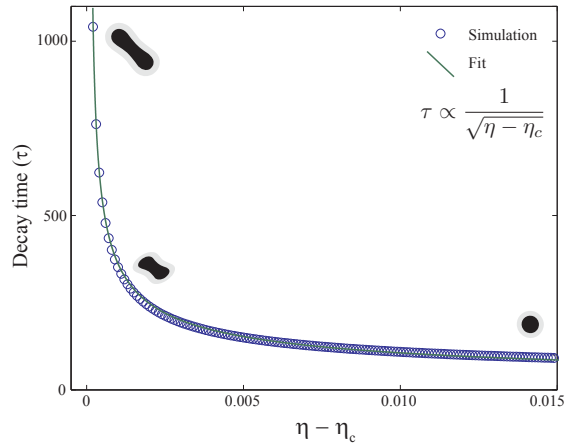

Figure 4.6: Decay rate as function η from a rod structure into a circular localized structure for the 2D generalized Swift-Hohenberg Eq. (2.2) with $\epsilon = 1.6$ and $\nu = 2.0$. The circles account for decay time obtained numerically. The solid curve is obtained using the expression $\tau = \tau_0/\sqrt{\eta - \eta_c}$ with fitting parameters $\eta_c = -0.3444$ and $\tau_0 = 11.61$ ($R^2 = 0.9647$).

structure bifurcation continues existing for values of η and ϵ to the left of Γ_2-curve. The decay rate from rod to localized spot is shown in Fig. 4.6, where, $\epsilon = 1.6$. The numeric decay rate law corresponds to the expected theoretical rate from a saddle-node bifurcation theory [99].

Another scenario emerges for values of η and ϵ to the left side of Γ_2-curve. Other two bifurcations are observed when overstepping the boundaries of the stability zone for the rod structure. For fixed values of ϵ and decreasing values of $|\eta|$ (see the transition ζ_4-curve in Fig. 4.7), the rod structure exhibits a continuous elongation similar to the case of the rod to labyrinth bifurcation, though in this case the elongation is permanent generating an infinitely long roll structure without transversal oscillations (see the inset in Fig. 4.5.2).

Different is the scenario when leaving the stability zone of the rod structure by the interior of the horseshoe-like arc, see Figure 4.7 for more detail, where a zoomed phase diagram of the rod structure is shown. By following the Γ_5-curve, a fourth bifurcation appears, where the rod structure becomes unstable, surface tension is

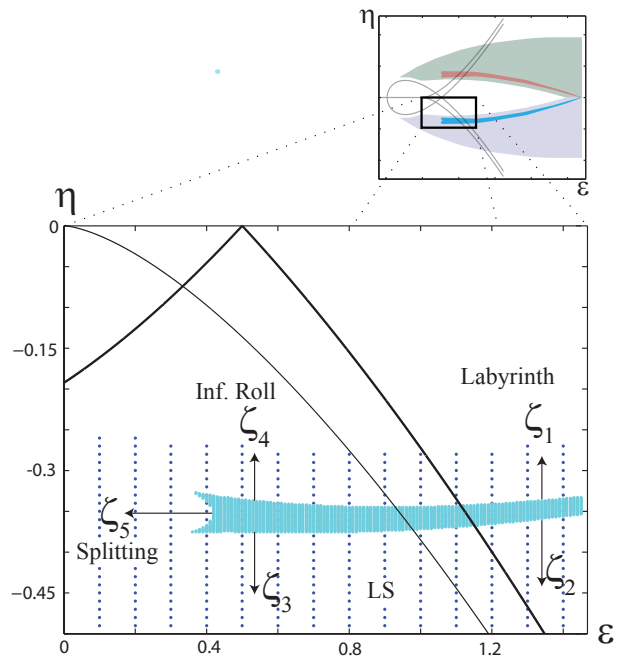

Figure 4.7: Zoomed phase diagram of rod structure. The different outcomes possible form the destabilization of a rod structure are shown. ζ_1-curve indicates the transition form rod to labyrinth bifurcation, ζ_2 and ζ_3-curves account for the transitions from rod to circular localized structure, ζ_4-curve stands for the transition from rod to infinite roll, and ζ_5-curve accounts for the transition between rod to binary state, for $\nu = 2.0$.

unable to keep the structure together leading to its splitting. Figure 4.8 depicts the bifurcation diagram observed in the horseshoe-like zone. Through this bifurcation two circular localized structures are generated by the collapse of the central part of the structure.

It is important to note that there is no transition from circular to rod structure, as the circular structure has always a lower energy. However, transitions from labyrinthine to rod structures are observed when entering with a labyrinth to the stability zone of the rod structure.

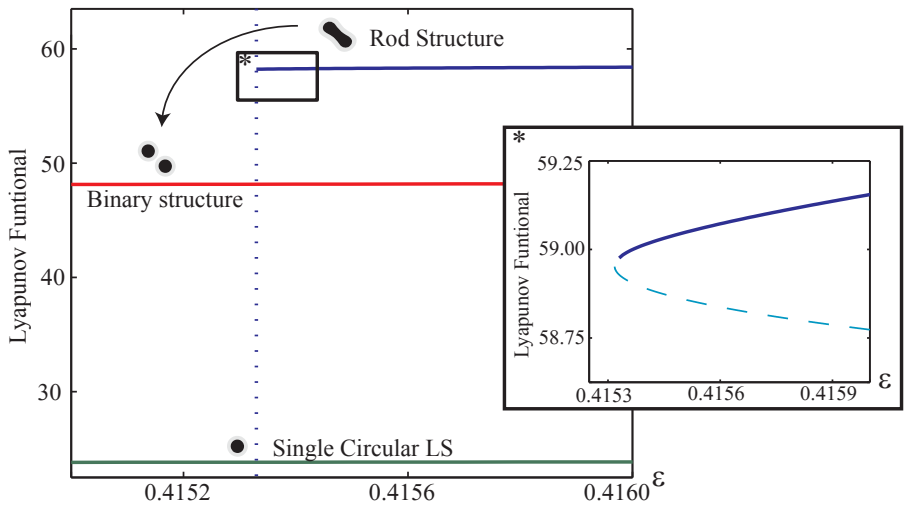

Figure 4.8: Saddle-node bifurcations for the splitting of a rod structure into a binary structure of the generalized Swift-Hohenberg Eq. (2.2) for $\nu = 2.0$ and $\eta = -0.350$. The inset corresponds to a zoom of the tip, where the dotted line depicts the square-root change in the energy proper of a saddle node bifurcation.

4.5 Interaction properties of the rod structure: dimer approach

It has been shown that the generalized Swift-Hohenberg model, allows the existence of multiple stable localized structures [58]. These (one or two dimensional) structures posses no compact support, thus, the frontier between the homogeneous state u_0 and the localized structure is not defined. Instead, the field oscillates decaying exponentially with the distance from the localized structure, these oscillations fluctuate around the homogeneous state with the characteristic wavelength of the system. The exponentially decaying tails will be addressed as the interaction field [31, 59, 100, 101].

4.5.1 Localized spots interaction

As mentioned before, no analytical expression is know for the localized structures in the generalized Swift-Hohenberg model, Eq. (2.2). Nevertheless, for long distance interaction only matters the asymptotic approximation of the decaying field is relevant. For circular localized structures, based on the linear perturbation theory, it is easy to show that the field $u(r)$ for distances from the localized structure much greater than the size of its core d, has the form

$$u(r \gg d) \approx u_0 + e^{-c_1 r} \cos(c_2 r) \tag{4.2}$$

where, $r = \sqrt{x^2 + y^2}$ is the radial coordinate, u_0 is the homogeneous state and

$$\begin{aligned} c_1 &= \mathrm{Re}\left[\sqrt{\frac{1}{2}(\sqrt{\nu^2 + 4\epsilon} \pm \nu)}\right], \\ c_2 &= \mathrm{Im}\left[\sqrt{\frac{1}{2}(\sqrt{\nu^2 + 4\epsilon} \pm \nu)}\right]. \end{aligned}$$

A system with two (or more) circular localized structures with initial given positions $\boldsymbol{r}_1$ and $\boldsymbol{r}_2$, respectively, evolves to a stationary equilibrium by the change of relative position between the structures $\boldsymbol{R} = \boldsymbol{r}_2 - \boldsymbol{r}_1$. The corresponding interaction fields from each particle interfere with each other generating interaction forces, which in turn, induce movement of the particle-like solutions. Aranson et al. in Ref. [59] showed that for two circular localized structures with interaction fields given by expression (4.2), the temporal evolution of $\boldsymbol{R}$ is

$$\frac{d\boldsymbol{R}}{dt} = \frac{\boldsymbol{R}}{R^2} \frac{d}{dR} \left[e^{-c_1 R} \cos(c_2 R)\right], \tag{4.3}$$

where $R = ||\boldsymbol{R}||$ is the magnitude of the vector of relative position.

4.5.2 Dimer approach

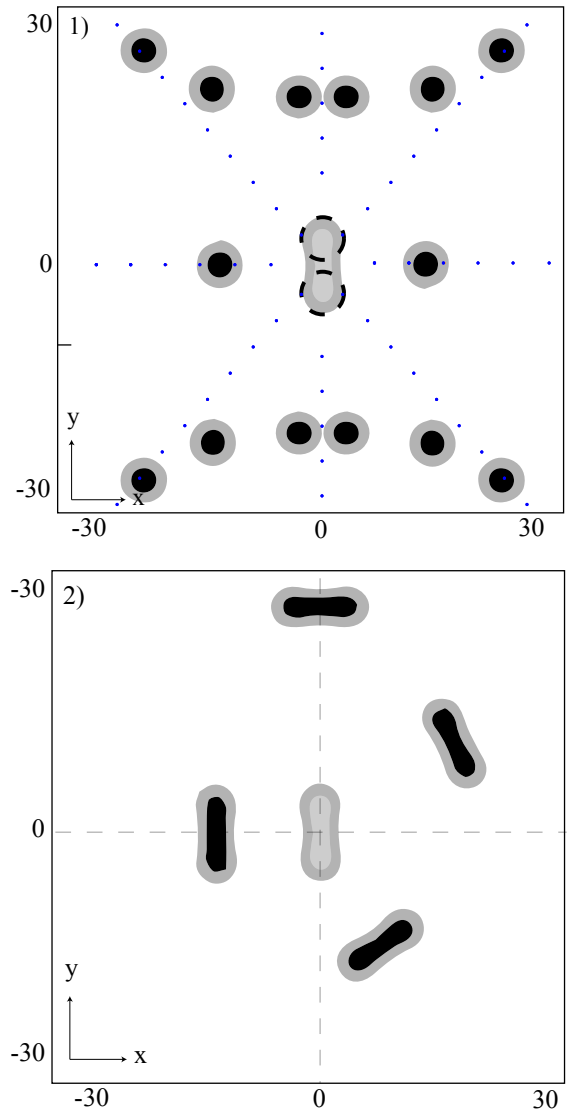

Figure 4.9: Dimer approach to rod structure. 1) Rod-LS numerical equilibrium points (black dots) and dimer-LS approximated analytical equilibriums (blue dots), the dimer is represented by black dashed lines. 2) Some characteristic points of equilibrium between rod structures. Simulations of the Swift-Hohenberg model, Eq. (2.2), with $\nu = 2.0$, $\eta = -0.355$, $\epsilon = 1.2$, and specular boundary condition, considering only two structures at a time, central rod structure is considered static.

The extension of the above calculation for rod structures requires the derivation of the asymptotic field for the rod structure, which must include an azimuthal de-

pendency given by the shape of the structure, not having this information makes the calculations non-viable. To avoid this impediment, the rod structure can be modeled as a dimer state, that is, the rod structure will be regarded as the composition of two circular localized spots separated by a distance d between the centers. Figure 4.9.1 shows a rodlike structure and the respective approximation of two localized spots, which are emphasized by dashed lines. Therefore, the interaction field of the rod structure is constructed by the composition of the corresponding interaction fields of the two localized spots. With the dimer approximation, considering a diluted regime, this is, evaluating the field at a distance r from the middle of the rod much larger than the size of the spots ($r \gg d$), the force field can be written as

$$\begin{aligned} \boldsymbol{F}_{dimer}(r,\theta) &= \frac{\boldsymbol{R}_-}{R_-^2}\frac{d}{dR_-}\left[e^{-c_1 R_-}\cos(c_2 R_-)\right] \\ &\quad + \frac{\boldsymbol{R}_+}{R_+^2}\frac{d}{dR_+}\left[e^{-c_1 R_+}\cos(c_2 R_+)\right], \end{aligned}$$

where $\boldsymbol{R}_\pm = \boldsymbol{r} \pm \boldsymbol{d}/2$, and $\boldsymbol{d}$ is a vector of size d, which points in the semi-major axis of the rodlike structure and $\boldsymbol{r}$ is the radial unit vector.

This field approximation yield the equilibrium points for a test structure shown as small blue spots in Fig. 4.9.1. Agreement with numerical observations for the interaction between a rod and a circular localized structure can only be seen for the structures further from the origin, as the validity of the force field approximation is valid only for $r \gg d$, however the approximation does not predict the existence of multiple diagonal equilibriums as observed in Fig. 4.9.1. More complex is the rod-rod interaction, for their azimuthal asymmetry reflected on its axial elongation. This adds and angular degree of freedom for the positioning of a rod structure at each equilibrium point (see Fig. 4.9.2). The variety of equilibriums exhibited by this new type of structure allow the existence of diverse complex arrangements when multiple

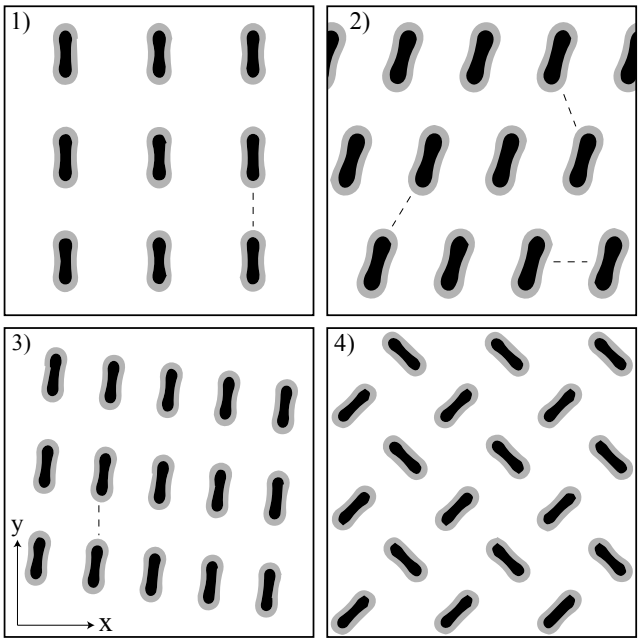

Figure 4.10: Tailored crystal-type configurations generated by the collocation of rod structures for the Swift-Hohenberg model, Eq. (2.2) with $\nu = 2.0$, $\eta = -0.355$, $\epsilon = 1.2$ and periodic boundary conditions.

rod structures are considered. Figure 4.10 shows some of the stable crystal-type structures, that we have constructed from rod-rod interaction.

The interaction of a larger number of rods (i.e. covering all the available space) increases the number of possible equilibrium configurations. The multiple interaction drives the system sometimes to equilibriums which were unstable in the rod-rod interaction scenario, in Figs. 4.10.1, 4.10.2, and 4.10.3, dashed lines indicate rod-rod equilibriums which are unstable in an isolated environment and stabilize under the presence of multiple structures. Crystal-type structure shows in Fig. 4.10.4 is constructed based on the T-like equilibrium position, orthogonal rod structures, exhibited by the rod-rod interaction.

4.6 Non-variational stabilization

The generalized Swift-Hohenberg model, Eq. (2.2), has a non-variational extension deduced in the context of liquid crystals for bouncing localized states [34] and deduced from chemical, biological and optical models [53] this equation reads (Lifshitz normal form)

$$\frac{\partial u}{\partial t} = \eta + \epsilon u - u^3 - \nu \nabla^2 u - \nabla^4 u + bu(\nabla^2 u) + c(\nabla u)^2, \tag{4.4}$$

which (excluding the case where $b = 2c$) is non-variational, this is, it is not derived from a Lyapunov functional. Thus, this model can exhibit complex and permanent behaviors, such as, the propagation of localized objects, oscillations, chaos and other spatiotemporal dynamics. The last two terms of Eq. (4.4) correspond, respectively, to nonlinear diffusion, being b the nonlinear diffusion coefficient, and nonlinear advection. Numerically, we have observed that for small range of parameters b and c,

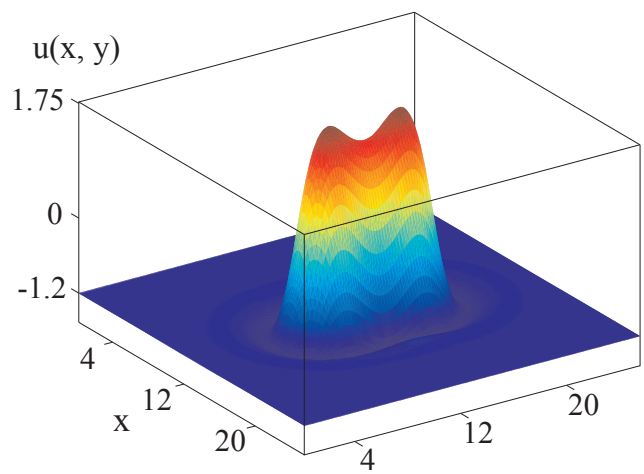

Figure 4.11: Stationary rod localized structure for the nonvariational Swift-Hohenberg model, Eq. (4.4), with $b = 0.01$, $c = -0.005$, $\nu = 2.0$, $\eta = -0.355$, and $\epsilon = 1.2$.

the rod structure remains stable by only changes on its dimensions (see Fig. 4.11).

For constant values of ϵ and η, increasing b or decreasing c affects the structure, by making it shorter. While decreasing b or increasing c enlarges the structure. For parameter b and c where the rod structures are larger, the evolution of the system is faster, for example, in the labyrinth formation or splitting process.

For fixed values of the parameters, $\epsilon = 1.2$, $\eta = -0.355$ and $\nu = 2.0$ the range of b and c for which the rod structure is stable are approximately $b = [-0.017, 0.015]$ and $c = [-0.007, 0.008]$. Despite the small range of b and c for which the rod is stable, the possibility of existence of rod structures in non variational systems opens the possibility for searching this structure in a wider variety of experiments.

4.7 Chapter summary

An asymmetric localized solution for the isotropic generalized Swift-Hohenberg model in two and three spacial dimensions has been revealed. This solution called rod structure breaks the azimuthal symmetry, remaining invariant only with respect to a rotation of π around any axis on the (x, y)-plane which contains the centre of the localized structure. The existence, bifurcation diagram, stability properties and interaction have been addressed. The question if this type of solution exist in other isotropic systems remains, so is the possibility of experimental observation.

The results presented in this chapter are under revision for publishing, a copy of the manuscript can be found in Appendix B.

Chapter 5

Universality of the curvature mechanism

The destabilisation of circular localized structures and the subsequent formation of labyrinthine structures has been deeply studied in the previous chapters in the context of the generalized Swift-Hohenberg equation (2.2). It has been shown that the localized structure to labyrinth transition occurs under the existence of bistability between homogeneous states and far from any pattern forming instability. In this chapter it will be shown that the curvature instability leading to labyrinths is universal and common to a wide variety of natural systems. First, the existence of the curvature mechanism will be presented in the context of vegetation dynamics though a generic interaction-redistribution model, then it will be shown that the mechanism is also present in chemical reactions through the Gray-Scott model.

5.1 Interaction-redistribution model

In this section a minimal but general model for vegetation pattern forming systems will be introduced. In this model the curvature instability mechanism also emerges in a regime of bistability of homogeneous steady states far from the pattern forming instability.

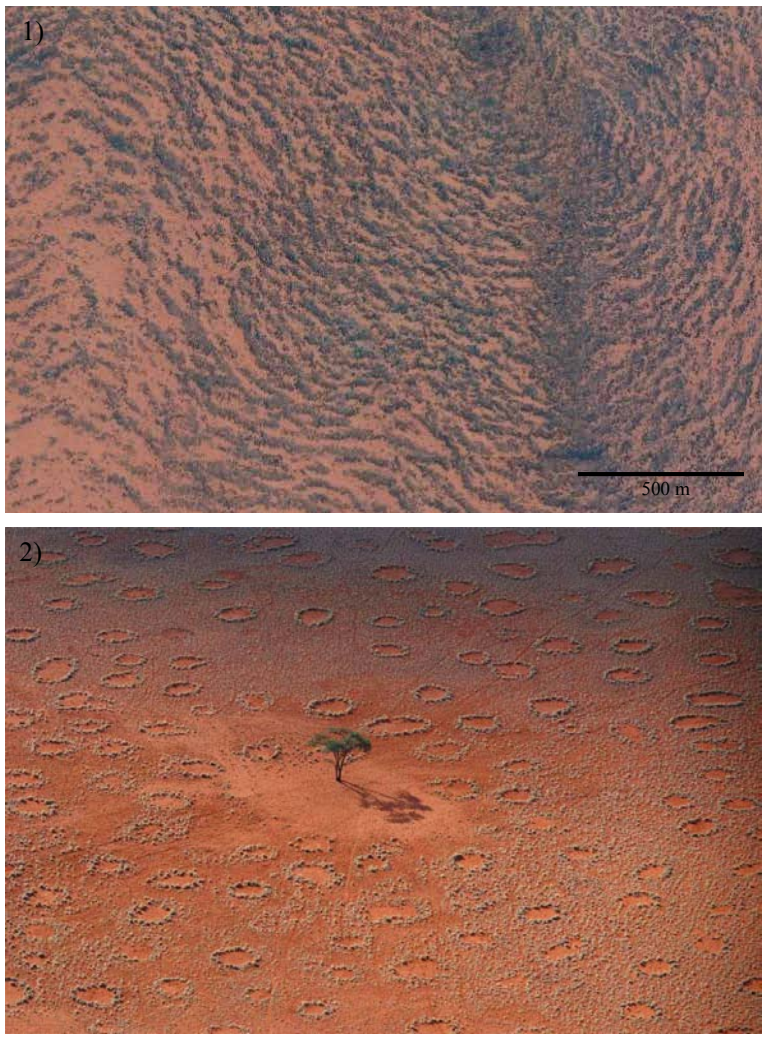

Figure 5.1: 1) Tiger bush patterns in central Australia [102], 2)Fairy circles in the desert of Namibia [103].

The emergence of spatial organization in extended landscapes has been an in-

triguing phenomena for both botanists and the non-linear science community for decades and is still a matter of great discussion [104, 105, 106]. One of the transversal agreements among scientists is that competition for soil resources such as water and nutrients leads to the self-organization of vegetation. Depending on the topography of the terrain, the climate conditions and the vegetation specie, the process of self-organization can lead to the formation of a wide variety of patterns, such as, tiger bush (see Fig. 5.1.1) [104], or fairy circles (see Fig. 5.1.2) [105, 106].

Taking into account the relation that exists between the structure of individual plants and the competition-facilitation interactions in a vegetation community is that generic interaction-redistribution models emerge [104, 107]. These models have been successful in the prediction of the existence of localized structures in arid and semi-arid environments where the resource scarcity induces high competition between plants through their root networks. In this context, a localized structure emerges as a patch of vegetation in an unpopulated homogeneous state. By considering a logistic equation with nonlocal coupling between plants, Tlidi et al. [45] where able via a weak gradient approximation, to deduce a mean-field nonlinear partial differential equation for the temporal evolution of the phytomass density $\rho(x, y, t)$:

$$\partial_t \rho = -\rho \left(\eta - \kappa\rho + \rho^2\right) + (\Delta - \Gamma\rho)\nabla^2\rho - \alpha\rho\nabla^4\rho, \tag{5.1}$$

where (x, y) and t are the spatial coordinates and time, respectively. This equation supposes an homogeneous and isotropic environment. The parameters: η accounts for the decrease-to-growth rate ratio; κ is the facilitation-to-competition susceptibility ratio; Δ is proportional to the square root of the facilitation-to-competition range ratio, this three parameters are positive-defined. The parameters Γ and α are the nonlinear diffusion coefficients. The existence of a nonlinear diffusion and

hyperdiffusion is fundamental for Eq. (5.1) to satisfy the physical constrain for the phytomass density $\rho(x, y, t) \geq 0$. However, presence of non-linear diffusion terms $u\nabla^2 u$ and $u\nabla^4 u$ render Eq. (5.1) nonvariational, thus, it cannot be written as the variation of a Lyapunov functional. Nonvariational systems can exhibit complex spatiotemporal dynamics, such as chaos, intermittency, among others. These nonvariational terms are imputable to the dispersion process. If the dispersion is negligible then equation (5.1) is similar to the variational Swift-Hohenberg, Eq. (2.1) where the coefficients of $\nabla^2 u$ and $\nabla^4 u$ are both independent of the field variable. The real order parameter equation (5.1) constitutes the simplest model of spatial dynamics in which competitive interactions between individuals occur locally.

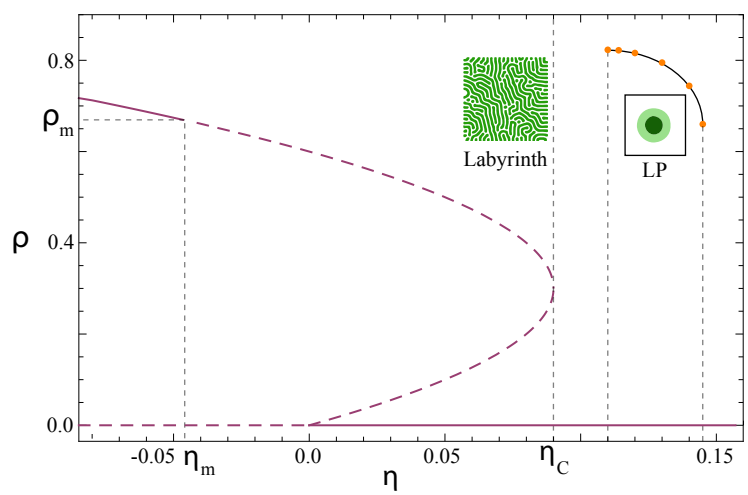

Figure 5.2: Bifurcation diagram of homogeneous plant population states (purple), dashed lines indicate unstable regime, and curve of stability of localized structures (dots). When the aridity η is decreased below η_c the curvature instability mechanism is observed.

The homogeneous solutions of Eq. (5.1) are (i) $\rho_s^0 = 0$, which correspond to a territory without vegetation, a bare state (ii) an two non-zero states given by $\rho_{s\pm} = (\kappa \pm \sqrt{\kappa^2 - 4\eta})/2$. For physical reasons phytomass density can only be positive or zero (see Fig. 5.2). When $\kappa \leq 0$, only the homogeneous steady state ρ_{s+}, defined is consistent, for $\eta < 0$. It decreases monotonously with μ and vanishes at $\eta = 0$.

When $\kappa > 0$, the viable homogeneous solution extends up to the limit point $\rho_L = \kappa/2$ and $\eta_L = \kappa^2/4$. In the range $0 < \eta < \eta_L$, the biomass density exhibits a bistable behavior: the stable homogeneous branches of solutions ρ_s^0 and ρ_{s+} coexist with the intermediate unstable branch ρ_{s-}. The upper homogeneous state ρ_{s+} undergoes a Turing instability characterized by the wavelength

$$\Lambda_m = 2\pi\sqrt{2\alpha}/\sqrt{\Gamma/\alpha - \Delta/\rho_m} \tag{5.2}$$

which measure the distance between two maxima or minima of the plant distribution. The threshold associated with this instability is solution of the following cubic equation:

$$(2\Gamma\rho_m - \Delta)^2 = 4\alpha\rho_m^2(2\rho_m - k). \tag{5.3}$$

There exist more than one threshold associated with the modulational instability. In the following, we focus on parameter regime where the uniform plant distribution exhibit bistability ($\kappa > 0$) and a portion of this state becomes unstable with respect to the Turing bifurcation ($\eta_m < \eta < \eta_L$). In this parameter range, any small fluctuation around the uniform plant distribution ρ_{s+} will trigger spontaneously the evolution of the system towards stationary, spatially periodic distributions of the biomass density which will invade the whole territory. However, when a stable localized vegetation patch is considered as an initial condition (high aridity), see Fig. 5.3.t_1, and the aridity is then varied in such quantity that the system reaches the coexistence of homogeneous states, then the localized structure suffers and elliptical deformation caused by the curvature instability and elongates into a rod structure (see Fig. 5.3.t_2) in a process identical as previously observed for the Swift-Hohenberg Eq. (2.1). Afterwards, the rod structure suffers from a transversal instability, here, the whole structure is compromised (see Fig. 5.3.t_3) and not only the central por-

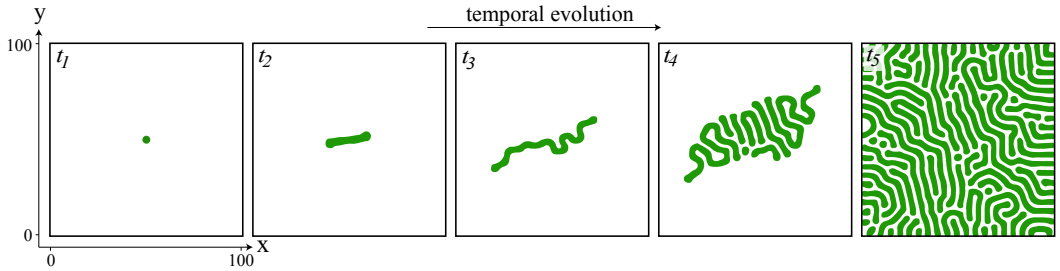

Figure 5.3: Curvature instability mechanism for the generation of a labyrinth from a localized patch as initial condition for the interaction-redistribution model Eq. (5.1). Simulation made for parameters $\eta = 0.085$, $\epsilon = 0.6$, $\Delta = 0.005$, $\Gamma = 0.5$ and $\alpha = 0.125$. Finite differences method was used with periodic boundary conditions, grid of 200×200 points and spacing $dx = 0.5$. Green indicates higher field values.

tion as in the Swift-Hohenberg case (Fig. 5.6.t_3). As time further increases, the labyrinthine structure invades all the system.

Here we have showed the appearance of the curvature instability mechanism over a localized vegetation patch which in turn generates the emergence of a labyrinthine structure in a generic interaction-redistribution model.

5.2 Gray-Scott model

Figure 5.4: Belousov-Zhabotinsky chemical reaction, concentrations of chemicals oscillate in time displaying astonishing spatial patterns [108].

Pushing further the idea of universality of the curvature instability mechanism for the formation of labyrinths we now enter the domain of chemical reactions. It is well known that the reaction and diffusion of the chemical components of a reaction can produce an immense variety of spatial structures, such as lamelar structures and self-replicating spots [109, 110], localized structures [111, 112] and Turing structure [113, 109, 114], and exhibit complex spatiotemporal dynamics, such as oscillatory dynamics (see Fig. 5.4), breathing localized structure and spatiotemporal chaos [115, 116, 117].

In a series of seminal works Peter Gray and Stephen K. Scott introduced a variant of the autocatalytic model of glycolisis first proposed by Evgeni Sel'kov [115]. This prototype autocatalytic reaction (i.e. the product of the reaction is also the catalyst) is described by two irreversible processes:

$$\begin{aligned} A + 2B &\rightarrow 3B \\ B &\rightarrow C \end{aligned} \tag{5.4}$$

where A, B and C are chemical species, C is a non-reactive product (inert) and the system is kept out-of-equilibrium by a constant injection of A (feeding) [118, 119, 116]. It has been shown that this simple model presents multistability, hysteresis cycles, patterns, oscillatory dynamics and other exotic patterns.

Through a rescaling and including the diffusion phenomena in the reactions, a non-linear partial differential equation can be deduced for the temporal evolution of the concentrations U and V of A and B, respectively [109]. This set of coupled equations are given by

$$\begin{aligned} \frac{\partial U}{\partial t} &= D_u \nabla^2 U - UV^2 + F(1-U), \\ \frac{\partial V}{\partial t} &= D_v \nabla^2 V + UV^2 - (F+k)V \end{aligned} \tag{5.5}$$

and are an example of reaction-diffusion equations, as they model the local evolution U and V, and the diffusion process of the chemical species. In Eq. (5.5) D_u and D_v correspond to the diffusion coefficients associated to U and V, respectively. F represents the feed rate of the reactive A and the dimensionless constant k (killing rate) accounts for the rate of the second reaction in Eq. (5.4). Alike the interaction-redistribution model presented for vegetation dynamics Eq. (5.1), the Gray-Scott model Eq. (5.5) does not have a known variational structure, which is the reason behind its rich phenomenology which includes, from oscillatory dynamics, self-replication [109] and chaos [117] and others mentioned before.

The existence and stability of patterns and localized spots (or single pulses) as homoclinic solutions of Eq. (5.5) has been well studied both in 1 and 2-dimensional cases [111, 120, 121, 122, 123]. This system supports a trivial homogeneous steady state $(U_0, V_0) = (1, 0)$ which is always stable. When the discriminator $d = 1 - 4(F + k)^2 > 0$ two additional homogeneous steady states $(U_\pm, V_\pm)$ appear, the first

$$(U_-, V_-) = \left(\frac{1}{2}(1+\sqrt{d}), \frac{F}{2(F+k)}(1-\sqrt{d}) \right) \tag{5.6}$$

is always unstable. The second state

$$(U_+, V_+) = \left(\frac{1}{2}(1-\sqrt{d}), \frac{F}{2(F+k)}(1+\sqrt{d}) \right) \tag{5.7}$$

is stable when $-V^2 + k < 0$ and $(F + k)(V^2 - F) > 0$. For $F > 1/4$ the system

only exhibits the trivial steady state. For $F < 1/4$ and $k < 1/16$ the system exhibits three homogeneous steady states (one unstable). The bifurcation diagram for the homogeneous states is shown in Fig. 5.5. For a detailed study on the bifurcations and instabilities of Eq. (5.5) see ref. [114].

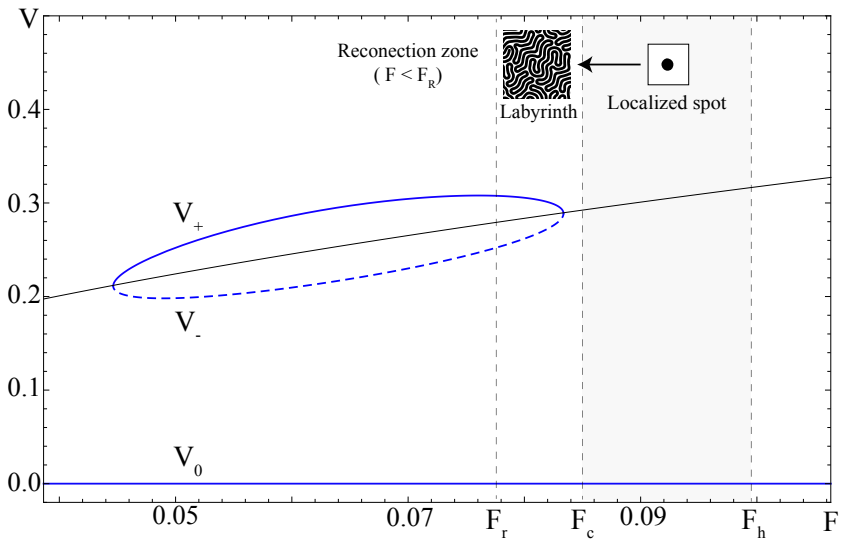

Figure 5.5: Bifurcation diagram for the concentration V for $k = 0.061$, homogeneous states (blue), dashed lines indicate unstable regime. The $\sqrt{F}$-curve shows the position of the saddle-node bifurcation. For $F_c < F < F_h$ stable localized structures are observed (numerically). When changing the feeding parameter for a localized structure to values $F_r < F < F_c$, the curvature instability mechanism is observed. Reconnection zone indicates the zone where a radial instability is observed and structures can reconnect (see. Fig. 5.7). Here $F_h = 0.097$, $F_c = 0.085$ and $F_r = 0.078$.

As indicated in Fig. 5.5, we have found that localized structures are stable when $F_c < F < F_h$. If F is increased further the system falls to the homogeneous state $V = 0$. When the parameter F is reduced below F_c, perturbations become unstable and the structure suffers a curvature instability characterized by the elongation of the structure (see Fig. 5.6). As observed for the modified Swift-Hohenberg equation (2.1) and for the interaction-redistribution model (5.1) the concentration field suffers then a transversal instability characterized by the wiggling of the central section of the structure. Non saturating evolution leads to the formation of a complex labyrinthine

structure as seen in Fig. 5.6.t_5.

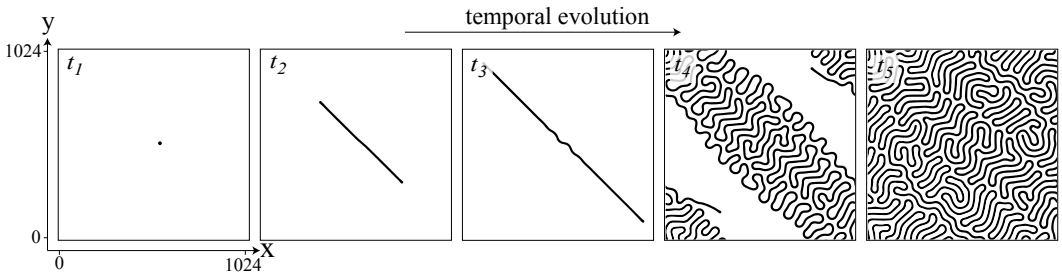

Figure 5.6: Curvature instability mechanism for the generation of a labyrinth from a localized concentration peak as initial condition for the Gray-Scott model (5.5). Simulation made for parameters $F = 0.080$, $k = 0.061$. Finite differences method was used with periodic boundary conditions, grid of 1024×1024 points and spacing $dx = 1$. Black indicates higher values of concentration V.

When the feeding parameter is decreased further ($F < F_r$), an initially circular localized structure suffers from a radial instability as seen in Fig. 5.7.t_2, there two spots where given as initial conditions. As the radius of the structures grow, they suffer from a curvature instability. Non saturation causes the structure to propagate. Differently from what is observed from every labyrinthine structure showed previously, here the tips merge, this causes reconnection of the structures. In the transition from t_4 to t_5 one can realize that the two initially distinct structures reconnect into one single labyrinth.

5.3 Labyrinth connectivities

The curvature instability of a localized structure was observed in the three systems presented previously which describe at least three different physical contexts. In the three cases (modified Swift-Hohenberg, interaction-redistribution and Gray-Scott models) an initially localized structure suffers from the curvature instability mechanism to finally fall into an extended labyrinthine structure. However each of these structures are different (see Figs. 3.3.6, 5.3.t_5, 5.6.t_5 and 5.7.t_6). Starting

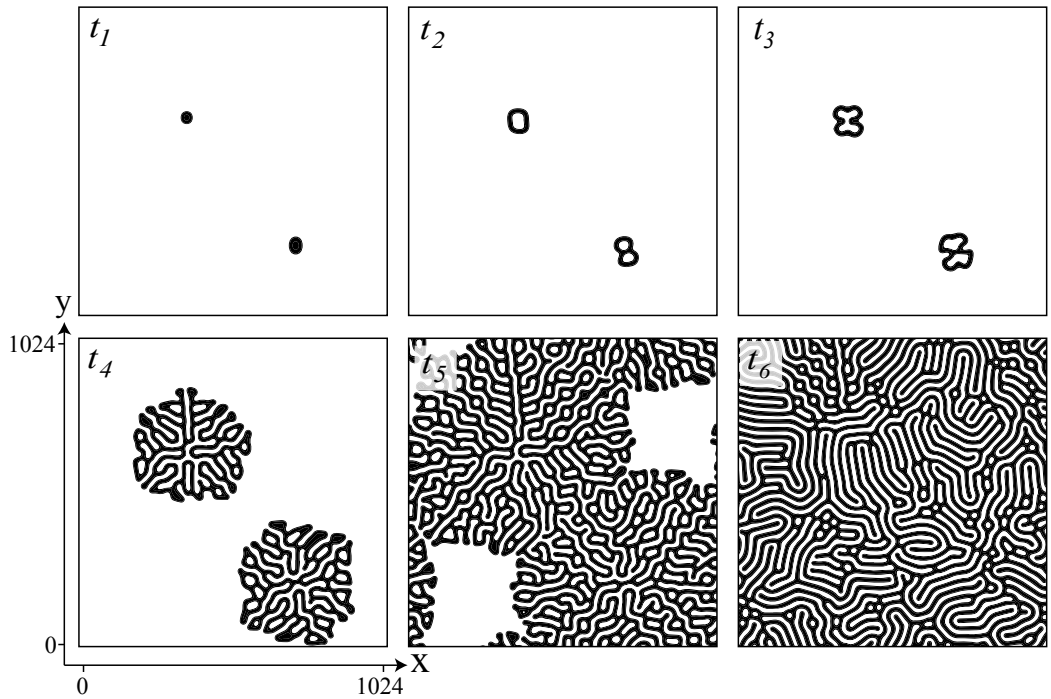

Figure 5.7: Alternative mechanism for the generation of a labyrinth from a localized concentration peak as initial condition for the Gray-Scott model (5.5). Simulation made for parameters $F = 0.070$, $k = 0.061$. In this parameter zone occurs reconnection between structures. Finite differences method was used with periodic boundary conditions, grid of 1024×1024 points and spacing $dx = 1$. Black indicates higher values of concentration V.

from a single localized structure the Swift-Hohenberg model Eq. (2.1), generates a single fully connected structure, this is, starting from any point of the labyrinth, one can go over the whole structure without leaving the higher value field. The same happens in the first labyrinth from the Gray-Scott model (c.f Fig. 5.6) only that in this case the structure shows no dislocations as the structure remains in a single line labyrinth. In the case of the interaction-redistribution model Eq. (5.3), starting from a single localized structure, the final labyrinthine state is disintegrated into a high number of small structures, thus, this labyrinth is highly disjoint. On contrary, when considering two initial structures in Fig. 5.7, the structures where able to reconnect increasing the connectivity from the initial state.

A classification of the labyrinth structures originated from localized initial states can be done based on the connectivity difference between the initial and the final states. Defining $\Delta = C_f - C_i$ as the difference between final C_f and initial C_i connectivities, where the connectivity is simply the number of disjoint structure in the system. Then, if $\Delta > 0$ we will say labyrinth is dissociative (the structure tends to divide), if $\Delta = 0$ it is neutral (each structure preserves its identity) and if $\Delta < 0$ the labyrinth is associative (structures tend to merge). We can conjecture after the previous observations that the type of labyrinth that a system exhibits will depend on the capacity of a structure of preserving its integrity, here, surface tension (or line tension) which keeps the structure together will play a fundamental role. In this sense, the type of labyrinths a system exhibits can give information of the line tension properties of the system.

5.4 Chapter summary

In this chapter the curvature instability mechanism for the destabilization of a localized structure leading to the formation of extended labyrinthine patterns has been shown to exist in a wide range of physical systems including in vegetation dynamics through a general interaction-redistribution model and in chemical reactions through the Gray-Scott reaction diffusion equations. It has been shown that depending not only in the context in which labyrinths emerge but also on the parameters considered for simulation/experimentation, different labyrinths emerge and even more, they can be classified as *associative*, *neutral* or *dissociative*, based on the difference between the initial and final connectivity of their structures.

The results presented in this chapter are under revision for publishing, a copy of the manuscript can be found in Appendix C.

Chapter 6

Self-replication in vegetation dynamics

In this chapter, we study a robust phenomenon observed in semi-arid ecosystems, by which localized vegetation patches split in a process called self-replication. By observation of real ecosystems and comparing with theoretical and numerical analysis we show an underlying process of self-organization leading to pattern formation mediated by the self-replication of patches.

6.1 Preliminary observations

In arid and semi-arid landscapes of the African, American, Asian and Australian continents, it is common to encounter a non-uniform vegetation cover which exhibits large spatial scale structures, generically called vegetation patterns [124, 125, 126]. These landscapes are characterized by either water limited resources and/or nutrient-poor territories. In the former case, the potential evapo-transpiration of the plants exceeds the water supply provided by rainfalls. At the level of individual plant,

the water scarcity provokes an hydric stress that affects both the plants survivability and the plant growth. At the community level, this hydric stress promotes clustering behaviour which induces the fragmentation landscapes. It is now generally admitted that this adaptation to hydric stress involves a symmetry-breaking modulational instability or Turing instability that leads to the establishment of a stable periodic pattern in an isotropic environmental conditions [104, 127, 126]. Vegetation patterns

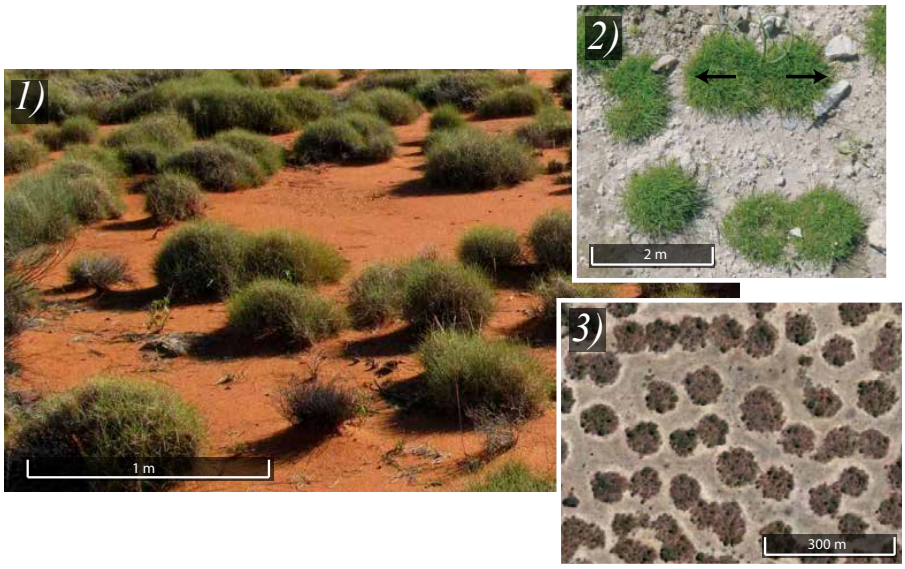

Figure 6.1: Localized patch instability. 1) Spinifex grassland, Yakabindi station, Western Australia (courtesy of Villis and Magi Nams). 2) Patterns of P. bulbosa observed in the Northern Negev [17]. 3) Satellite image showing localized vegetation patches, Zambia (Google Earth).

are not always periodic. The spatial distribution of vegetation cover, may consists of isolated or randomly distributed patches or gaps. Such patterns can form systems such as groves within grasslands [45, 128] or spots of bare soil within a grass matrix [129]. They consist of patches which are either isolated or part of large systems. In both cases, such patterns have been interpreted as localized structures. A well documented example are the so-called fairy circles, which consist of circular areas devoid of vegetation embedded in an herbaceous vegetation field. The aperiodic patterning

phenomenon is not specific to particular soils or plants. Localized vegetation patches or gaps may develop on soil ranging from sandy and silty to clayey and the nature of vegetation may consist of grasses, shrubs and trees. The surface of vegetation patch can vary from small clumps of grasses (0.5-2 m^2) to large groves of mulga (Acacia aneura) trees (100-1000 m^2), such as those observed in central Australia [130], see Fig. 6.1. On the other hand, the formation of localized pattern is an important issue not only in plant ecology context and environment science but also it is a multidisciplinary area of research involving physics, chemistry and mathematics [128].

However, localized vegetation patches may be unstable, and exhibit a curvature instability that leads to a splitting of the patch into two new patches. Examples of such behavior are shown in Fig. 6.1. This intriguing phenomenon often called spot-replication is well documented issue in the context of magnetic fluids [12], liquid crystals [66, 67], Chemical systems [68]-[76], in plant ecology [17], material science [77, 78], granular fluid systems [79, 80], and nonlinear optics [81].

In this chapter, we investigate the self-replication mechanism in natural ecosystems, and show that this phenomena is robust as it is observed in a wide range of species and size scales. We consider a general interaction-redistribution model, where simulations show that there exist a critical value of the level of the aridity under which a single circular patch grows up to a maximal diameter, the curvature instability leads to an elliptical deformation followed by patch multiplication. This process continue in time until the system reaches a self-organized vegetation pattern in an hexagonal structure. Afterwards, we address the spatial organization problem and show how self-replication mediates the spatial distribution and propagation of the vegetation.

6.2 Field observations

6.2.1 Location

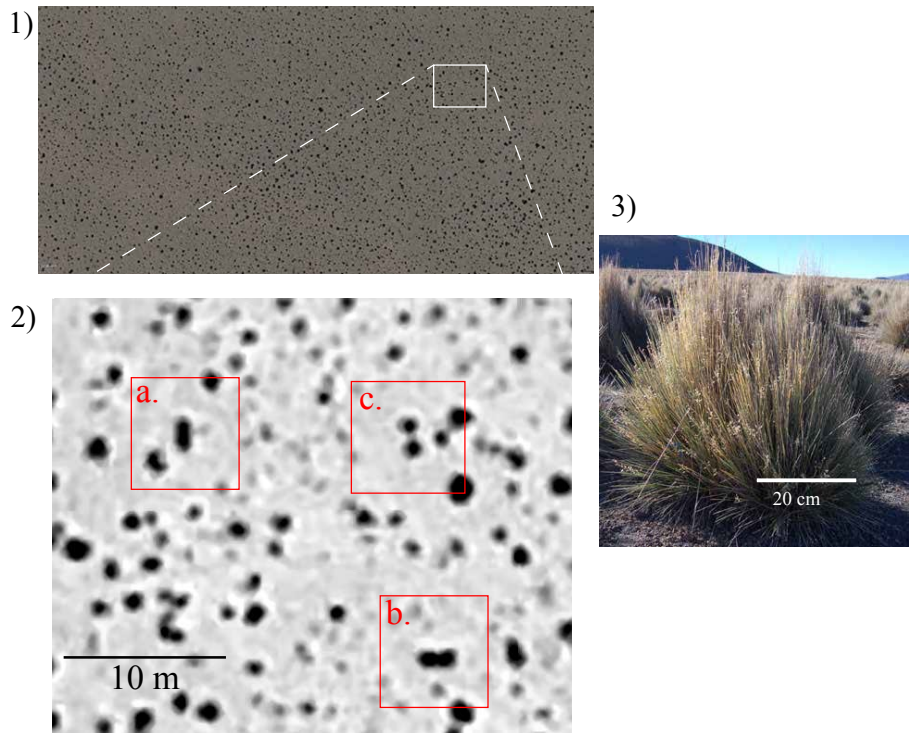

Figure 6.2: Study site, dark spots correspond to *Festuca orthophylla* tussocks. 1) Satellite image showing localized vegetation patches (Google Earth) in the Catamarca region, Argentina. b) Zoom of the region under study. c) Average size tussocks of *Festuca orthohylla* in the Sajama National Park in the Bolivian Altiplano [131].

The Andes highlands are semi-arid ecosystems with low amounts of available resources. In particular, the Catamarca region in NW-Argentina (-23.436253°, -65.976767° at 3424 m a.s.l.), the average annual rainfall reaches 369 mm (source CRU CL 2.0), with a maximum in January of 71 mm and a minimum in July of 6 mm, temperature varies from warm in the day to freezing temperatures in the night. Here, it is well known that *Festuca orthophylla* which produces tall, evergreen tussocks dominates the landscape over extended areas and periods of time

at elevations between 3225 and 4860 m a.s.l [132, 131]. This specie is present in a variety of cold climates, adapting to diverse rainfall and soil moisture conditions.

Festuca tussocks arrange in circular shape compact structures composed by thousands of tightly packed tillers. The size of the tussocks depends on the resources available and weather conditions of their location, for instance, in western Bolivia they can reach heights of 1.6 m [131]. An important characteristic of Festuca is their shallow rooting system, which has been reported to cover an area 6-fold the area of the above ground canopy [131]. This quality allows each plant to have access to the resources in a total area equivalent to 6-fold the area of the projected canopy, which is well known to be the most important mechanism to capture resources in highlands [131, 133]. This root distribution also allows tussock-tussock competition for resources, this will be important later on for understanding the spatial organization of the tussocks. The study site, was selected in order to have a minimal slope, and no topographic perturbations such as mountains, canyons, river or highways. The image obtained from Google Earth consists on a 4800x3562 pixels image (with a spatial resolution of 30cm), which corresponded to an area of 109.4 km^2 (384m x 285m), see Fig. 6.2.1.

Festuca structures are easily recognizable in the images for their high light absorption (they appear as black spots). As mentioned previously Festuca organizes in tightly packed structures of circular shape, however, there is an important number of structure that have lost their circular shape, this modulational instability is the mechanism by which a tussock deform into an elliptical shape and consequently splits into two independent tussocks, we term this process self-splitting (see Fig. 6.2.2). This process is common to a wide range of species and scales, as observed in Fig. 6.1, where self-replication can be observed for structures in the scale of meters to hundreds of meters.

6.2.2 Spatial distribution analysis

The field image (Fig. 6.2.1) was used to study the spatial distribution of the tussocks. Detection of patches was performed through filtering, noise reduction and contrast enhancement of the image. Objects touching the border of the image were removed as they may not be completely observed, thus, they could introduce erroneous measurements to the analysis. The size of the structures that can be detected is lower-bounded by the satellite spatial resolution, nevertheless, we can hypothesize that the spatial distribution will be dominated by the bigger tussocks as a consequence of their fully developed shallow root systems.

After the detection of the patches, the boundaries of each object and their properties (area, centroid position, perimeter and equivalent diameter) can be precisely computed. The relation of meters per pixel is extracted directly from the image (20 m/250 pixels). A total of 3204 structures where detected. The first analysis, corresponded to detailed characterization of individual plant properties such as nearest neighbor distance (NND), area covered and equivalent radius of each structure, this radius is calculated by comparing the area of the structure with that of a circle of that equivalent radius. The nearest neighbour distance is computed as the minimal boundary-to-boundary distance, this will allow us to extract some conclusions on the NND versus root sphere size. Canopy area and radius will be useful in understanding the underlying pattern emerging from redistribution and competition for resources. To expose the emergent spatial order in tussocks distribution, spatial Fourier analysis was performed in order to determine a characteristic wave number. For the effect of Fourier analysis, a square sub-figure was selected from the original one. Finally, we have computed the Voronoi tessellation for the centres of the structures. This analysis, suitable for studying the regularity of a pattern has been used previously

in aerial analysis to address pattern formation in vegetation structures [134]. For both NND and Voronoi cell computation, a subset of structures where selected such that they where far enough from the images border to avoid error induced from non visible structures.

6.2.3 Nearest neighbor distance and structure properties

From the remote sensing image analysis of the Catamarca region in NW-Argentina a total area of 109.4 km^2 (384m x 285m) was studied. Structures found in the analysis ranged from an area of 0.0128 m^2 to maximum area of 6.2528 m^2 with a mean of 0.95±0.79 m^2. By visual inspection, we have noticed that bigger structures are most probably evolving clusters of structures. The average equivalent radius was found to be 0.50±0.22 m. For calculating the minimal distance between the objects boundaries, only structures which are far enough from the image's border are considered, as the objects not captured in the image could be closer to these structures than the other observable ones. By this consideration, distances between 2837 objects are used. The distance between objects vary from 0.25 m to 4.63 m, and averaged a distance of 1.83±0.77 m (see. Fig. 6.3).

Considering the average size and NND, and assuming that the distance between tussock is set under the constrain that the root spheres do not overlap, we can estimate the projected root sphere size of an average tussock as the half of the NND, this results in a root sphere of 1.4 m radius and 6.3 m^2 area, which corresponds to an area of 6.7-fold the area of the average structure. This is in agreement with previous field observations [135].

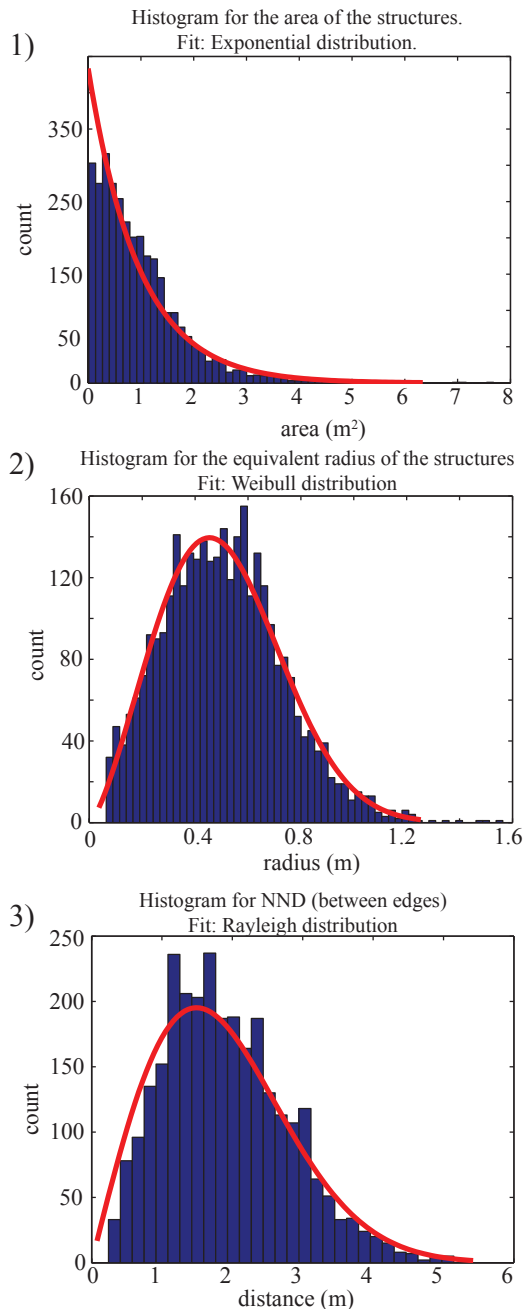

Figure 6.3: Histograms for 1) area, and 2) radius of the detected structures, and 3) nearest neighbour distance between them.

6.2.4 Fourier analysis

For the spatial Fourier analysis, we considered a square sub-figure of the original. This figure contained 1510 structures. The spatial Fourier transform is extensively

used by pattern formation community to evaluate the degree of order. Pronounced peaks in the 2D Fourier amplitude indicate not only the existence of a characteristic length in the system but also a preferred spatial direction for the formation of the pattern. From our spatial Fourier analysis we are unable to detect pronounced

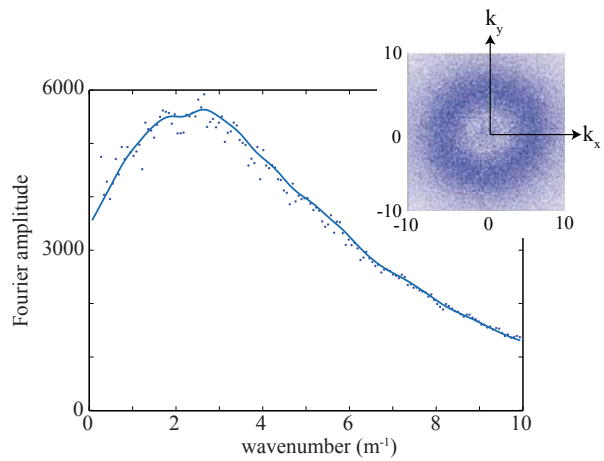

Figure 6.4: Circular integration for spatial Fourier transform. Inset shows the full spectrum of the detected structures.

peak in the spectrum, indicating that there in no preferred direction for a pattern to form, this is the same type of spectrum as the one observed for labyrinthine patterns [89]. However, in the circular integration of the spectrum, we observe a maximum wavenumber at k=2.4 m^{-1} (see Fig. 6.4), this is the first sign that the system is arranging in such a way that a characteristic length emerges ($L_c = 2\pi/k =$ 2.6 m). As one would expect this characteristic length is related to the interaction between tussocks, no-overlap (between tussock root spheres) is achieved in average if the distance between the centres of the structures is at least 2.4 m according to estimations made in the previous section from the histogram analysis. Root competition between plants generates a minimal distance between tussocks.

6.2.5 Voronoi cells characterization

One of the problems of detecting patterns in natural ecosystems is the existence of high scale perturbations such as terrain inhomogeneities, weather conditions, wind, animal presence, among others. All this external noise, alters the interaction between tussocks therefore, mangles their ability to form a regular pattern. With no regular pattern, the task of finding some type of unitary cell in the tussoks arrangement can be facilitated by the introduction of the Voronoi tessellation [136]. Considering the centre of a structures, the Voronoi cell associated with that structure will correspond to all the points that are closer to its centre than to the center of any other structure. In this sense, the Voronoi tessellation gives us information of the most probable cell

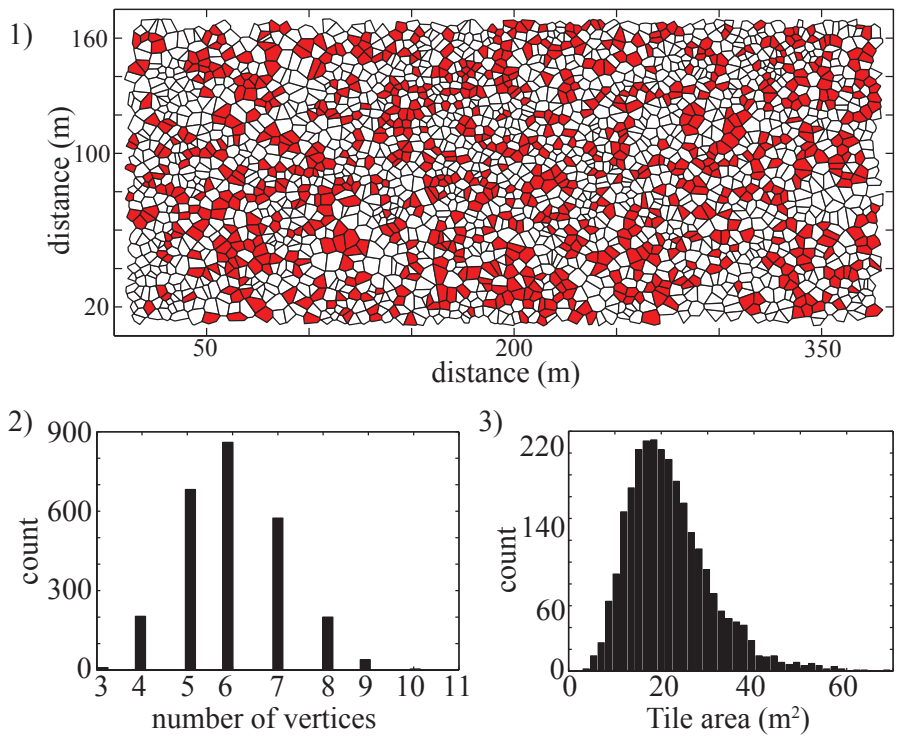

Figure 6.5: 1) Voronoi cell tessellation, 6-sided tiles are painted red. Histograms for 2) the number of vertices in each cell, and 3) the tile area.

arrangement. As it is observed in Fig. 6.5, the most probable vertex number is 6,

which strengthen the idea of the underlying tendency of Festuca tussocks to arrange in hexagons, this is reinforces by observing that 6-sided cells are clearly not randomly distributed but rather cluster in groups. Important data can also be extracted from the tile area, each tile represent the amount of land that is closer to a certain tussock than to any other, thus the nutrients present in that portion of soil will be more accessible for the center tussock. The average tile area is 21.8 m^2, which corresponds to equivalent radius of 2.63 m, almost twice the radius estimated for the root spheres. This means that even though when considering nearest neighbors, roots seem to determine the minimum distance, in a large scale, tussock disperse through the terrain. This can be understood as an exponential decay of the interaction between tussocks, where depending on the amount of space available, they will spread or tighten provided that the root spheres do not overlap.

6.3 Model equation for vegetation dynamics

In this section we will reintroduce the generic interaction-redistribution model (Eq. (5.1) presented in Chapter 5, here we will focus in the self-replication regime.

Pattern formation in vegetated environments has been extensively studied both experimentally and theoretically. It is well known that competition for resources such as water leads to self-organization phenomenon. This process leads to the formation of a wide range of patterns that depends on the characteristics of both the environment and the spatial distribution of underground root networks.

Several models describing vegetation patterns and self-organization in arid and semiarid landscapes have been proposed during last two decades. They can be classified into three types. The first approach often called generic interaction-redistribution models, are based on the relationship between the structure of individual plants and

the facilitation-competition interactions existing within plant communities [104, 137, 138, 107].The second approach is based on reaction-diffusion type of models, these take into account the influence of water transport by below ground diffusion and/or above ground run-off [139, 10]. The third approach focuses on the role of environmental randomness as a source of noise that induces symmetry breaking transitions [140, 141, 127].

In particular, the formation of localized structures in vegetation, also called localized vegetation patches has been studied in the case of poor resources, isotropic and homogeneous environment via a weak gradient approximation of the generalized logistic equation that described the non-local interaction between plants, a non-variational equation for the phytomass density $\rho(x, y, t)$ was derived in [45]

$$\partial_t \rho = -\rho \left(\eta - \kappa\rho + \rho^2\right) + (\Delta - \Gamma\rho)\nabla^2\rho - \alpha\rho\nabla^4\rho, \tag{6.1}$$

where (x, y) and t are the spatial coordinates and time, respectively. As stated in the previous chapter, this equation contains three positive defined control parameters: η that account for the decrease-to-growth rate ratio; κ is the facilitation-to-competition susceptibility ratio; Δ is proportional to the square root of the facilitation-to-competition range ratio. The parameters Γ and α are the nonlinear diffusion coefficients. The real order parameter equation (6.1) constitutes the simplest model of spatial dynamics in which competitive interactions between individuals occur locally.

The homogeneous steady states; ρ_s; solutions of Eq. (6.1) are (i) no plant state, $\rho_s^0 = 0$, which correspond to a territory devoid of vegetation and (ii) an homogeneous plant population $\rho_{s\pm} = (\kappa \pm \sqrt{\kappa^2 - 4\eta})/2$ where at each point of the territory, the vegetation production and death are exactly balanced. They should be real and

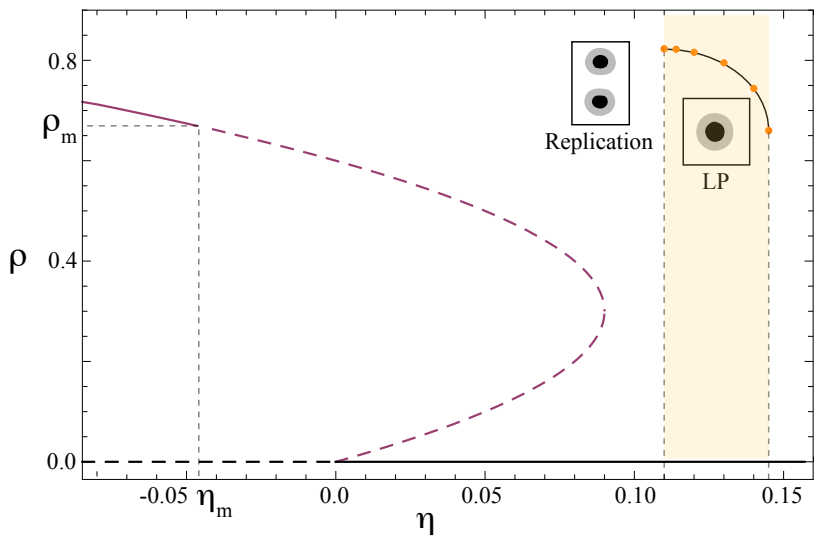

Figure 6.6: Bifurcation diagram of homogeneous plant population states (purple and black), dashed lines indicate unstable regime, and curve of stability of localized structures. The darkened area accounts for the region where localized patches (LP) are observed.

positive. Two situations must be distinguished according to the sign of κ. When $\kappa \leq 0$, only the homogeneous steady state ρ_{s+}, defines the biomass density, for $\eta < 0$. It decreases monotonously with μ and vanishes at $\eta = 0$. When $\kappa > 0$, the physical part of homogeneous branch of solution extends up to the limit point $\rho_L = \kappa/2$ and $\eta_L = \kappa^2/4$. In the range $0 < \eta < \eta_L$, the biomass density exhibits a bistable behavior: the stable homogeneous branches of solutions ρ_s^0 and ρ_{s+} coexist with the intermediate unstable branch ρ_{s-} as shown in Fig. 6.6. The former solution is always unstable even in the presence of homogeneous fluctuations.

The upper homogeneous state ρ_{s+} undergoes a modulational instability characterized by an intrinsic wavelength

$$\Lambda_m = 2\pi\sqrt{2\alpha}/\sqrt{\Gamma/\alpha - \Delta/\rho_m} \tag{6.2}$$

which measure the distance between two maxima or minima of the plant distribution.

The threshold associated with the modulational instability is solution of the following cubic equation:

$$(2\Gamma\rho_m - \Delta)^2 = 4\alpha\rho_m^2(2\rho_m - k) \tag{6.3}$$

There exist more than one threshold associated with the modulational instability. In the following, we focus on parameter regime where the uniform plant distribution exhibit bistability ($\kappa > 0$) and a portion of this state becomes unstable with respect to the Turing bifurcation ($\eta_m < \eta < \eta_L$) as shown in Fig. 6.6. In this parameter range, any small fluctuation around the uniform plant distribution ρ_{s+} will trigger spontaneously the evolution of the system towards stationary, spatially periodic distributions of the biomass density which will invade the whole territory. A detailed nonlinear analysis of two-dimensional periodic vegetation patterns such as stripes (often called Tiger bush, see Fig. 5.1.1), and hexagons consisting of either sparsely populated or bare areas alternate with dense vegetations patches have been reported in [137].

6.4 Field observations vs model

When increasing the aridity parameter η, the structures that appear first are gaps. They consist of spots of spare vegetation. The region where these localized patches are observed is depicted in Fig. 6.6. They are stable until they lose their stability towards the formation of localized patches. When decreasing the aridity, a single patch exhibits an elliptical deformation followed by splitting as shown in Fig. 6.7.t_3. This self-replicating process continues until the system is entirely occupied by spots. Only spots which have available space around them are able to replicate, because of this, only spots located in the edges can replicate. In the real ecosystem available space can be generated by the death of a plant by natural or external perturbations

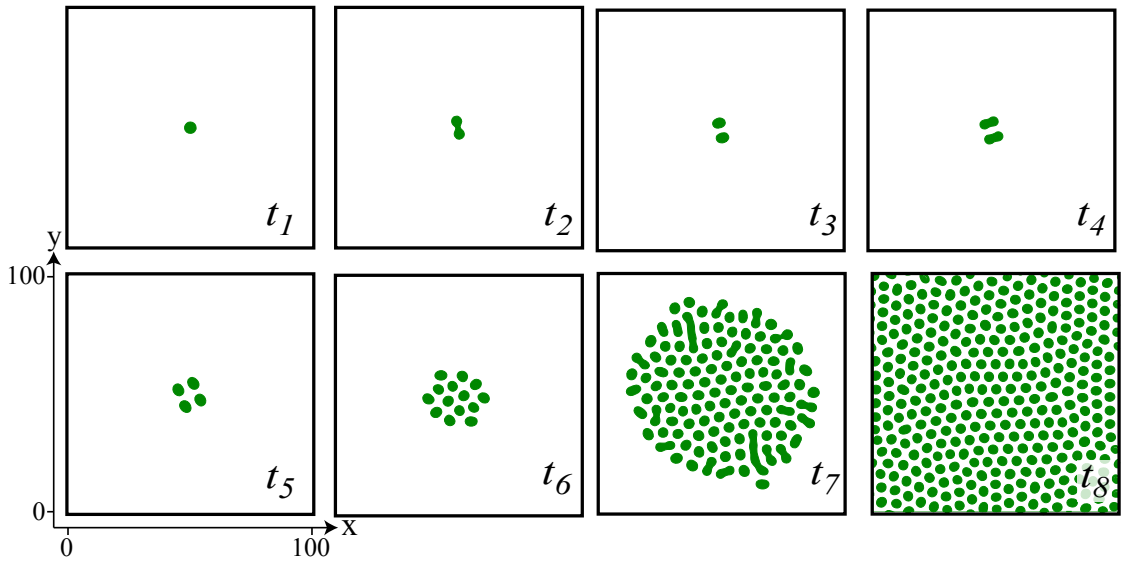

Figure 6.7: Temporal evolution of a single localized patch self-replication for the vegetation model Eq. (6.1). With $\eta = 0.1$, $\kappa = 0.6$, $\Delta = 0.02$ $\Gamma = 0.5$, and $\alpha = 0.125$, integration grid 200×200.

(animals, fires) this is the reason we can observe self-replication throughout all the territory analyzed previously.

The pattern obtained from the replication of a single spot is an hexagonal configuration, defects observed are induced by the boundary conditions, nevertheless, after a sufficiently long simulation time, the system arrives to a regular hexagonal pattern (Fig. 6.7.t_8). This regularity is not observed in the arrangement of Festuca tussocks observed in Fig. 6.2 as vegetation in a real ecosystem is not nucleated by a single spot but rather developed by the seed spreading by wind and animals thus generating multiple tussocks in different locations, each with the possibility of splitting to spread through the terrain.

To numerically test the effect of seed spreading, we have studied the evolution of the model with the initial condition of 155 randomly distributed spots (cf. Fig. 6.8.1), the aridity level allows each of the spots to self-replicate. With temporal evolution, communities of spots interact as the replicating process continues (see Fig.

6.8.2). By observing the evolution of these spots we can show that the self-replication process favors a spatial organization similar to the field observation. Initially, as seen

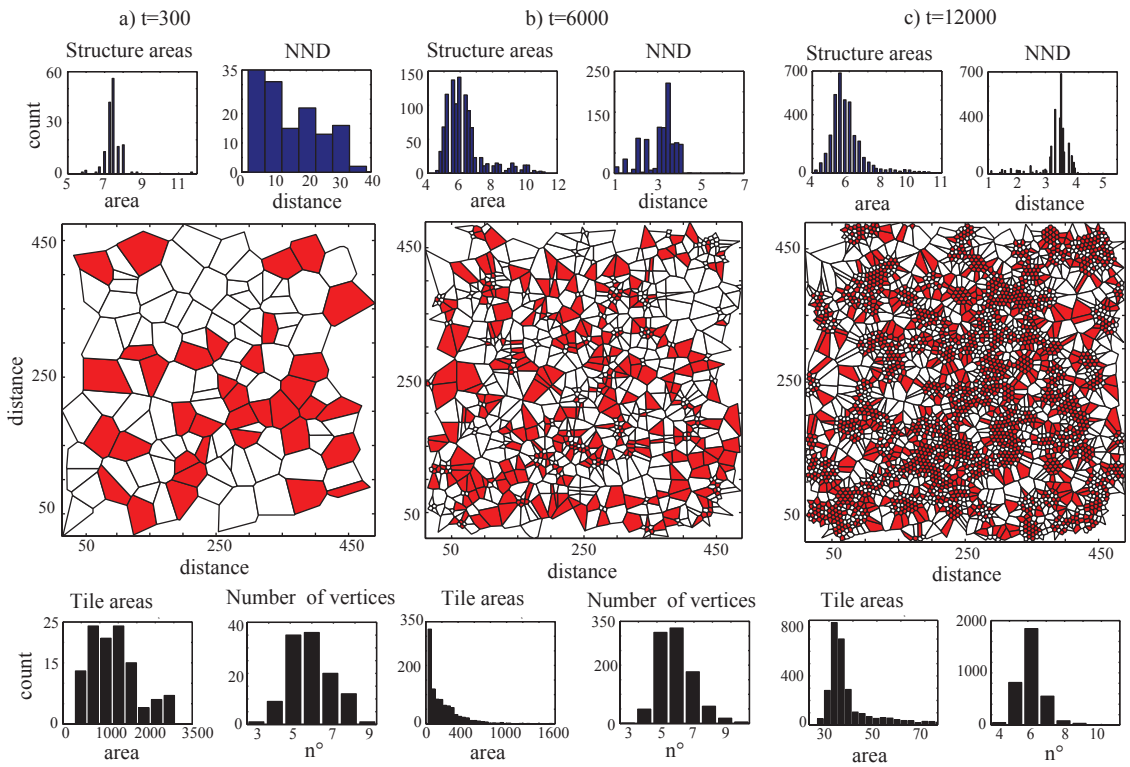

Figure 6.8: Numerical simulations of non-variational phytomass model (6.1) with 155 randomly distributed localized patches as initial conditions, with $\eta = 0.1$, $\kappa = 0.6$, $\Delta = 0.02$ $\Gamma = 0.5$, and $\alpha = 0.125$, integration grid of 1000×1000 points. At different evolution times, the Voronoi cell tessellation, histograms for number of vertices in each cell, tile area, nearest neighbor distance, and structure areas are analyzed for each time.

in Fig. 6.8, the system has no particular order, histograms do not show any clear trend, however, further evolving in time, (t=6000) self-replication has generated 1060 spots, for which characteristic values emerge for the areas of the structures and NND. The number of vertices histogram behave as observed for the Festuca tussocks. At time t=12000 the structure count is 3641, their areas and NND show a clear maximum value indicating an emergent ordering, the process of self-replication favors a dispersion of the structures and tile areas from the mean, as the observed

in the real ecosystem. In this line, the process of self-replication allows the system to spatially organize.

6.5 Chapter summary

In this chapter we have studied the self-replication phenomenon through a vegetation point of view. Observations made through remote sensing analysis of the Andes semi-arid ecosystem we have localized Festuca tussocks which by a modulational instability deform from circular to an elliptical shape, process after which the tussocks split into two new structures, we have observed this process in a variety of species and size scales. By statistical analysis we have encounter characteristic distributions which are signatures of an underlying self-organization process. Though a general interaction-redistribution model we have shown the existence of self-replication and the mechanism by which this phenomenon leads to the formation of an extended pattern. Comparison between numerical and field observations indicate intriguing similarities in the distribution of areas and distance between structures. Self-replication in vegetation give new lights on the way plants propagate and populate the semi-arid terrains. The results presented in this chapter are being prepared for publishing, a copy of the manuscript can be found in Appendix D.

Chapter 7

Conclusions and perspectives

The main objective of this thesis was to study the stability of two-dimensional localized structures, and to investigate how the destabilization due to the curvature could lead to the formation of extended patterns. To accomplish this objective, we first studied a prototype Swift-Hohenberg model, and then extended the result obtained to a wider variety of physical contexts. Later, through a generic interaction-redistribution model for vegetation dynamics we studied the curvature induced process of self-replication of localized spots.

In what follows we present the conclusions and perspectives of this thesis.

Curvature instability and labyrinthine patterns

- Using a canonical model, the process of destabilization by which a two-dimensional localized structure generates an extended labyrinthine pattern has been characterized. This process can be divided in different stages.

- The curvature of the localized spot induces the destabilization of an unstable mode of angular index $m = 2$. Such instability leads to an elliptical deforma-

tion of the localized spot leading to the generation of an elongated structure. Subsequently, it causes transversal oscillations. The local patterns formed are in turn unstable unchaining the formation of the labyrinth. This mechanism occurs far from any pattern forming instability and requires coexistence of homogeneous states.

- The phase space was characterized. Through numerical simulations we were able to construct the phase transition curve where an initially stable localized structure destabilized falling into the attraction basin of the labyrinthine extended pattern.

- The transition from localized structure to extended patterns can be observed in both variational and non-variational systems, thus it is not necessarily dominated by the minimization of a free energy.

Future research in this topic includes:

- ▷ Study through numerical linearization the stability of two dimensional localized structures and the unstable modes growth rates.

- ▷ Seek to describe the localized to extended pattern dynamics in cholesteric liquid-crystals from first principles.

- ▷ Define labyrinthine patterns. And explore the importance of pinning phenomena in the stabilization of labyrinthine structures.

- ▷ Study the instabilities of three-dimensional localized structures, preliminary work shows a rich variety of bifurcations.

Rodlike localized structure

- A non azimuthally symmetric localized solution for the prototype isotropic two and three dimensional Swift-Hohenberg equation has been found. This type of structures where reported for the first time in this work, they have been called rodlike or simply Rod localized structures.

- Numerically, the stability properties of two-dimensional rod localized structures was characterized. By the construction of the bifurcation diagram it was observed that he parameter region where 2D Rod localized structures exist is narrow, this can explain why they haven't been observed experimentally.

- The interaction properties of the structure were studied. The elongated shape of the structure allows for a wide variety of equilibriums. Complex lattices of equilibria can be constructed.

Future research in this topic includes:

- ▷ Search for experimental evidence of the Rod localized structure. We propose that the Liquid-Crystal Light Valve (LCLV) experiment is suitable for this task as it is a controlled and well known environment.

- ▷ Find Rod localized structures in other physical contexts.

- ▷ Study the three-dimensional case, this includes: stability, bifurcation diagram, interaction.

Universality of the curvature mechanism

- The curvature instability mechanism for the destabilization of a localized structure leading to the formation of extended labyrinthine patterns exist in a wide range of physical systems. In particular, in the context of vegetation dynamics, and autocatalytic chemical reactions.

- Depending on the model used different labyrinthine structures emerge from an initial localized structure. The parameters considered also affect the resulting patterns. These can be classified as *associative*, *neutral* or *dissociative*, based on the difference between the initial and final connectivity of their structures.

Future research in this topic includes:

- ▷ Find experimental evidence of the numerical observations made both in vegetation dynamics and chemical reactions.

- ▷ Study the importance of surface tension in the destabilization and labyrinth formation processes.

Self-replication in vegetation dynamics

- Self-replication of localized structures exists and was studied in the context of vegetation dynamics through a generic interaction-redistribution model.

- Field observations of semi-arid ecosystems show that a certain specie of plant exhibit self-replications process, plant tussocks suffer from a modulational instability which deforms their circular shape to an elliptical structure, process after which the tussocks split into two new structures, this process was observed in a variety of species and size scales.

- Comparison between theoretical, numerical analysis and field observations, show an underlying process by which self-replication mediates self-organization of structures leading to extended pattern formation. This is a mechanism by which vegetation extends to cover vast areas. It explains also the emergence of characteristic quantities observed in the statistical analysis of field observations.

Future research in this topic includes:

- ▷ Development of a complete theoretical analysis of the stability of localized structures. Preliminary work shows that localized structures can suffer from different modulational instabilities depending on the simulation parameters considered.

- ▷ Consider more realistic conditions, such as, spatial-dependence of resources and allometric factors in the theoretical description of the vegetation dynamics.

Bibliography

[1] R. Niebrugge. *Sand patterns pictures*. [Online; accessed December 1, 2014]. URL: http://www.wildnatureimages.com/sand_pattern_pictures.htm.

[2] Chiswick Chap. *Giant Puffer fish skin pattern*. [Online; accessed December 1, 2014]. 2012. URL: https://www.flickr.com/photos/tin-g/55563889/.

[3] tin.G. *viel gesundes grün*. [Online; accessed December 1, 2014]. 2005. URL: https://www.flickr.com/photos/tin-g/55563889/.

[4] _DJ_. *Human brain on white background*. [Online; accessed December 1, 2014]. 2005. URL: https://www.flickr.com/photos/flamephoenix1991/8376271918.

[5] P.B. Umbanhowar, F. Melo, and H.L. Swinney. "Localized excitations in a vertically vibrated granular layer". In: *Nature* 382.6594 (1996), pp. 793–796.

[6] P. Glansdorff and I. Prigogine. *Thermodynamic Theory of Structures, Stability and Fluctuations*. Wiley New York, 1971.

[7] M.C. Cross and P.C. Hohenberg. "Pattern formation outside of equilibrium". In: *Reviews of modern physics* 65.3 (1993), p. 851.

[8] Y. Pomeau and L.M. Pismen. *Patterns and interfaces in dissipative dynamics*. Springer, 2006.

[9] J. von Hardenberg. *The green grass grows*. [Online; accessed December 1, 2014]. 2001. URL: http://physics.aps.org/story/v8/st24.

[10] J. von Hardenberg et al. "Diversity of Vegetation Patterns and Desertification". In: *Phys. Rev. Lett.* 87 (19 2001), p. 198101. DOI: 10.1103/PhysRevLett.87.198101. URL: http://link.aps.org/doi/10.1103/PhysRevLett.87.198101.

[11] S.A. Langer, R.E. Goldstein, and D.P. Jackson. "Dynamics of labyrinthine pattern formation in magnetic fluids". In: *Physical Review A* 46.8 (1992), p. 4894.

[12] A.J. Dickstein et al. "Labyrinthine pattern formation in magnetic fluids". In: *Science-New York then Washington-* 261 (1993), pp. 1012–1012.

[13] Z. Khattari and Th.M. Fischer. "Shapes of Langmuir monolayer domains in confined geometries". In: *The Journal of Physical Chemistry B* 106.7 (2002), pp. 1677–1683.

[14] P. Heinig, L.E. Helseth, and Th.M. Fischer. "Relaxation of patterns in 2D modulated phases". In: *New Journal of Physics* 6.1 (2004), p. 189.

[15] R.A. Barrio et al. "A two-dimensional numerical study of spatial pattern formation in interacting Turing systems". In: *Bulletin of mathematical biology* 61.3 (1999), pp. 483–505.

[16] J.H.E. Cartwright. "Labyrinthine Turing pattern formation in the cerebral cortex". In: *Journal of theoretical biology* 217.1 (2002), pp. 97–103.

[17] E. Meron et al. "Vegetation patterns along a rainfall gradient". In: *Chaos, Solitons & Fractals* 19.2 (2004), pp. 367–376.

[18] V.B. Taranenko, K. Staliunas, and C.O. Weiss. "Pattern formation and localized structures in degenerate optical parametric mixing". In: *Physical review letters* 81.11 (1998), p. 2236.

[19] R. Gallego, M. San Miguel, and R. Toral. "Self-similar domain growth, localized structures, and labyrinthine patterns in vectorial Kerr resonators". In: *Physical Review E* 61.3 (2000), p. 2241.

[20] W. Lu and S.L. Lachinova. "Formation and transition of labyrinthine domain patterns in a nonlinear optical system". In: *Physical Review A* 63.1 (2000), p. 013807.

[21] C. Swann. *Bait ball of blue jack mackerel (Trachurus picturatus)*. [Online; accessed December 1, 2014]. URL: http://agentur-focus.de/Lightboxen/ANGEBOTE/FEATURES/2013/Tiere/SPLMakrelen/index.html.

[22] L.D. Landau and E.M. Lifshitz. "Statistical physics, part I". In: *Course of theoretical physics* 5, XIV (1980), p. 468.

[23] H-G Purwins, H.U. Bödeker, and Sh Amiranashvili. "Dissipative solitons". In: *Advances in Physics* 59.5 (2010), pp. 485–701.

[24] O. Descalzi et al. *Localized States in Physics: Solitons and Patterns: Solitons and Patterns*. Springer, 2011.

[25] W. van Saarloos and P.C. Hohenberg. "Fronts, pulses, sources and sinks in generalized complex Ginzburg-Landau equations". In: *Physica D: Nonlinear Phenomena* 56.4 (1992), pp. 303–367.

[26] Y. Pomeau. "Front motion, metastability and subcritical bifurcations in hydrodynamics". In: *Physica D: Nonlinear Phenomena* 23.1 (1986), pp. 3–11.

[27] P. Coullet, C. Riera, and Ch. Tresser. "Stable static localized structures in one dimension". In: *Physical review letters* 84.14 (2000), p. 3069.

[28] A.H. Eschenfelder. *Magnetic bubble technology*. Vol. 14. Springer-Verlag Berlin, 1980.

[29] K-J Lee et al. "Experimental observation of self-replicating spots in a reaction-diffusion system". In: *Nature* 369.6477 (1994), pp. 215–218.

[30] J. Wu, R. Keolian, and I. Rudnick. "Observation of a nonpropagating hydrodynamic soliton". In: *Physical review letters* 52.16 (1984), p. 1421.

[31] M.G. Clerc et al. "Soliton pair interaction law in parametrically driven Newtonian fluid". In: *Philosophical Transactions of the Royal Society A: Mathematical, Physical and Engineering Sciences* 367.1901 (2009), pp. 3213–3226.

[32] M.G. Clerc et al. "Liquid–solid-like transition in quasi-one-dimensional driven granular media". In: *Nature physics* 4.3 (2008), pp. 249–254.

[33] S. Pirkl, F. Ribiere, and P. Oswald. "Forming process and stability of bubble domains in dielectrically positive cholesteric liquid crystals". In: *Liquid Crystals* 13.3 (1993), pp. 413–425.

[34] M.G. Clerc, A. Petrossian, and S. Residori. "Bouncing localized structures in a liquid-crystal light-valve experiment". In: *Physical Review E* 71.1 (2005), p. 015205.

[35] U. Bortolozzo et al. "Bistability between different localized structures in nonlinear optics". In: *Physical review letters* 93.25 (2004), p. 253901.

[36] U. Bortolozzo et al. "Localized states in bistable pattern-forming systems". In: *Physical review letters* 96.21 (2006), p. 214501.

[37] O. Lioubashevski et al. "Oscillons and propagating solitary waves in a vertically vibrated colloidal suspension". In: *Physical review letters* 83.16 (1999), p. 3190.

[38] Y.A. Astrov and Y.A. Logvin. "Formation of clusters of localized states in a gas discharge system via a self-completion scenario". In: *Physical review letters* 79.16 (1997), p. 2983.

[39] R. Heinrichs, G. Ahlers, and D.S. Cannell. "Traveling waves and spatial variation in the convection of a binary mixture". In: *Physical Review A* 35.6 (1987), p. 2761.

[40] P. Kolodner, D. Bensimon, and C.M. Surko. "Traveling-wave convection in an annulus". In: *Physical review letters* 60.17 (1988), p. 1723.

[41] F.T. Arecchi, S. Boccaletti, and P.L. Ramazza. "Pattern formation and competition in nonlinear optics". In: *Physics Reports* 318.1 (1999), pp. 1–83.

[42] B. Schäpers et al. "Interaction of localized structures in an optical pattern-forming system". In: *Physical review letters* 85.4 (2000), p. 748.

[43] A. Kaminaga, V.K. Vanag, and I.R. Epstein. "A reaction–diffusion memory device". In: *Angewandte Chemie International Edition* 45.19 (2006), pp. 3087–3089.

[44] A. Kaminaga, V.K. Vanag, and I.R. Epstein. ""Black spots" in a surfactant-rich Belousov–Zhabotinsky reaction dispersed in a water-in-oil microemulsion system". In: *The Journal of chemical physics* 122.17 (2005), p. 174706.

[45] O. Lejeune, M. Tlidi, and P. Couteron. "Localized vegetation patches: a self-organized response to resource scarcity". In: *Physical Review E* 66.1 (2002), p. 010901.

[46] S. Barland et al. "Cavity solitons as pixels in semiconductor microcavities". In: *Nature* 419.6908 (2002), pp. 699–702.

[47] M'F. Hilali, G. Dewel, and P. Borckmans. "Subharmonic and strong resonances through coupling with a zero mode". In: *Physics Letters A* 217.4 (1996), pp. 263–268.

[48] R. Lefever et al. "Deeply gapped vegetation patterns: on crown/root allometry, criticality and desertification". In: *Journal of theoretical biology* 261.2 (2009), pp. 194–209.

[49] M. Tlidi, M. Georgiou, and P. Mandel. "Transverse patterns in nascent optical bistability". In: *Physical Review A* 48.6 (1993), p. 4605.

[50] J. Lega, J.V. Moloney, and A.C. Newell. "Swift-Hohenberg equation for lasers". In: *Physical review letters* 73.22 (1994), p. 2978.

[51] N. Stoop et al. "Curvature-induced symmetry breaking determines elastic surface patterns". In: *Nature materials* (2015).

[52] A.G. Vladimirov, R. Lefever, and M. Tlidi. "Relative stability of multipeak localized patterns of cavity solitons". In: *Physical Review A* 84.4 (2011), p. 043848.

[53] G. Kozyreff and M. Tlidi. "Nonvariational real Swift-Hohenberg equation for biological, chemical, and optical systems". In: *Chaos: An Interdisciplinary Journal of Nonlinear Science* 17.3 (2007), p. 037103.

[54] J. Swift and P.C. Hohenberg. "Hydrodynamic fluctuations at the convective instability". In: *Physical Review A* 15.1 (1977), p. 319.

[55] P. Mandel. "Theoretical problems in cavity nonlinear optics (hardback)". In: *Cambridge studies in modern optics* (1997).

[56] J. Lega, J.V. Moloney, and A.C. Newell. "Universal description of laser dynamics near threshold". In: *Physica D: Nonlinear Phenomena* 83.4 (1995), pp. 478–498.

[57] S. Longhi and A. Geraci. "Swift-Hohenberg equation for optical parametric oscillators". In: *Physical Review A* 54.5 (1996), p. 4581.

[58] M. Tlidi, P. Mandel, and R. Lefever. "Localized structures and localized patterns in optical bistability". In: *Physical review letters* 73.5 (1994), p. 640.

[59] I.S. Aranson et al. "Stable particle-like solutions of multidimensional nonlinear fields". In: *Physica D: Nonlinear Phenomena* 43.2 (1990), pp. 435–453.

[60] L.Y. Glebsky and L.M. Lerman. "On small stationary localized solutions for the generalized 1-D Swift–Hohenberg equation". In: *Chaos: An Interdisciplinary Journal of Nonlinear Science* 5.2 (1995), pp. 424–431.

[61] M'F Hilali et al. "Pattern selection in the generalized Swift-Hohenberg model". In: *Physical Review E* 51.3 (1995), p. 2046.

[62] M. Tlidi, P. Mandel, and R. Lefever. "Kinetics of localized pattern formation in optical systems". In: *Physical review letters* 81.5 (1998), p. 979.

[63] R. Richter and I.V. Barashenkov. "Two-dimensional solitons on the surface of magnetic fluids". In: *Physical review letters* 94.18 (2005), p. 184503.

[64] D.J.B. Lloyd et al. "Localized hexagon patterns of the planar Swift-Hohenberg equation". In: *SIAM Journal on Applied Dynamical Systems* 7.3 (2008), pp. 1049–1100.

[65] S. McCalla and B. Sandstede. "Snaking of radial solutions of the multidimensional Swift–Hohenberg equation: A numerical study". In: *Physica D: Nonlinear Phenomena* 239.16 (2010), pp. 1581–1592.

[66] P. Ribiere and P. Oswald. "Nucleation and growth of cholesteric fingers under electric field". In: *Journal de Physique* 51.16 (1990), pp. 1703–1720.

[67] P. Oswald, J. Baudry, and S. Pirkl. "Static and dynamic properties of cholesteric fingers in electric field". In: *Physics Reports* 337.1 (2000), pp. 67–96.

[68] J.E. Pearson. "Complex patterns in a simple system". In: *Science* 261.5118 (1993), pp. 189–192.

[69] M. Monine et al. "Modeling triangular titration fronts in the O2 + H2 reaction on a catalytic Rh (111) surface". In: *The Journal of chemical physics* 117.9 (2002), pp. 4473–4478.

[70] A.P. Muñuzuri, V. Pérez-Villar, and M. Markus. "Splitting of autowaves in an active medium". In: *Physical review letters* 79.10 (1997), p. 1941.

[71] T. Kolokolnikov and M. Tlidi. "Spot deformation and replication in the two-dimensional belousov-zhabotinski reaction in a water-in-oil microemulsion". In: *Physical review letters* 98.18 (2007), p. 188303.

[72] P.W. Davies et al. "Dividing blobs, chemical flowers, and patterned islands in a reaction-diffusion system". In: *The Journal of Physical Chemistry A* 102.43 (1998), pp. 8236–8244.

[73] C.B. Muratov and V.V. Osipov. "General theory of instabilities for patterns with sharp interfaces in reaction-diffusion systems". In: *Physical Review E* 53.4 (1996), p. 3101.

[74] A. Schaak and R. Imbihl. "Triangular-shaped reaction fronts in a catalytic surface reaction". In: *Chemical physics letters* 283.5 (1998), pp. 386–390.

[75] Y. Hayase and T. Ohta. "Sierpinski gasket in a reaction-diffusion system". In: *Physical review letters* 81.8 (1998), p. 1726.

[76] Y. Hayase and T. Ohta. "Self-replicating pulses and Sierpinski gaskets in excitable media". In: *Physical Review E* 62.5 (2000), p. 5998.

[77] X. Ren and J. Wei. "On the spectra of three-dimensional lamellar solutions of the diblock copolymer problem". In: *SIAM journal on mathematical analysis* 35.1 (2003), pp. 1–32.

[78] Y. Nishiura and H. Suzuki. "Higher dimensional SLEP equation and applications to morphological stability in polymer problems". In: *SIAM journal on mathematical analysis* 36.3 (2005), pp. 916–966.

[79] B. Sandnes et al. "Labyrinth patterns in confined granular-fluid systems". In: *Physical review letters* 99.3 (2007), p. 038001.

[80] B. Sandnes et al. "Patterns and flow in frictional fluid dynamics". In: *Nature communications* 2 (2011), p. 288.

[81] M. Tlidi, A.G. Vladimirov, and P. Mandel. "Curvature instability in passive diffractive resonators". In: *Physical review letters* 89.23 (2002), p. 233901.

[82] A. Hagberg et al. "Linear and nonlinear front instabilities in bistable systems". In: *Physica D: Nonlinear Phenomena* 217.2 (2006), pp. 186–192.

[83] P. Coullet, C. Riera, and Ch. Tresser. "Qualitative theory of stable stationary localized structures in one dimension". In: *Progress of Theoretical Physics Supplement* 139 (2000), pp. 46–58.

[84] F. Del Campo et al. "Effects of translational coupling on dissipative localized states". In: *Phys. Rev. E* 86 (2012), p. 036201.

[85] P. Coullet. "Localized patterns and fronts in nonequilibrium systems". In: *International Journal of Bifurcation and Chaos* 12.11 (2002), pp. 2445–2457.

[86] M. Tlidi et al. "Phase-separation dynamics of circular domain walls in the degenerate optical parametric oscillator". In: *Optics letters* 25.7 (2000), pp. 487–489.

[87] C. Chevallard et al. "Zig-zag instability of an Ising wall in liquid crystals". In: *EPL (Europhysics Letters)* 58.5 (2002), p. 686.

[88] H. Calisto et al. "Bubbles interactions in the Cahn-Hilliard equation". In: *Physical review letters* 85.18 (2000), p. 3805.

[89] M. Le Berre et al. "Example of a chaotic crystal: The labyrinth". In: *Physical Review E* 66.2 (2002), p. 026203.

[90] D. Walgraef. *Spatio-temporal pattern formation*. Springer, 1997.

[91] N. Verschueren et al. "Chaoticon: localized pattern with permanent dynamics". In: *Philosophical Transactions of the Royal Society A: Mathematical, Physical and Engineering Sciences* 372.2027 (2014), p. 20140011.

[92] E. Moses, J. Fineberg, and V. Steinberg. "Multistability and confined traveling-wave patterns in a convecting binary mixture". In: *Physical Review A* 35.6 (1987), p. 2757.

[93] M. Dennin et al. "Chaotic localized states near the onset of electroconvection". In: *Physical review letters* 77.12 (1996), p. 2475.

[94] S. Residori, U. Bortolozzo, and P.L. Ramazza. "Triangular optical localized structures and their transition to a turbulent-like extended state". In: *Journal of Low Temperature Physics* 145.1 (2006), pp. 277–285.

[95] R.M. Hornreich, M. Luban, and S. Shtrikman. "Critical Behavior at the Onset of k $\rightarrow$ -Space Instability on the λ Line". In: *Physical Review Letters* 35.25 (1975), p. 1678.

[96] P Coullet, C Elphick, and D Repaux. "Nature of spatial chaos". In: *Physical review letters* 58.5 (1987), p. 431.

[97] M.G. Clerc and C. Falcon. "Localized patterns and hole solutions in one-dimensional extended systems". In: *Physica A: Statistical Mechanics and its Applications* 356.1 (2005), pp. 48–53.

[98] U.Bortolozzo, M.G. Clerc, and S. Residori. "Solitary localized structures in a liquid crystal light-valve experiment". In: *New Journal of Physics* 11.9 (2009), p. 093037.

[99] S.H. Strogatz. *Nonlinear dynamics and chaos: with applications to physics, biology, chemistry, and engineering*. Westview press, 2014.

[100] K. Kawasaki and T. Ohta. "Kink dynamics in one-dimensional nonlinear systems". In: *Physica A: Statistical Mechanics and its Applications* 116.3 (1982), pp. 573–593.

[101] M.G. Clerc, S. Coulibaly, and D. Laroze. "Interaction law of 2D localized precession states". In: *EPL (Europhysics Letters)* 90.3 (2010), p. 38005.

[102] Google Earth (CNES/Astrium). *Tiger Bush*. (-23.503901°, 133.614643°). 2015.

[103] N. Juergensen. *Fairy Circles*. [Online; accessed May 25, 2015]. URL: http://www.livescience.com/39401-fairy-circles-get-new-explanation.html.

[104] R. Lefever and O. Lejeune. "On the origin of tiger bush". In: *Bulletin of Mathematical Biology* 59.2 (1997), pp. 263–294.

[105] N. Juergens. "The biological underpinnings of Namib Desert fairy circles". In: *Science* 339.6127 (2013), pp. 1618–1621.

[106] C. Fernandez-Oto et al. "Strong interaction between plants induces circular barren patches: fairy circles". In: *Philosophical Transactions of the Royal Society A: Mathematical, Physical and Engineering Sciences* 372.2027 (2014), p. 20140009.

[107] R. Martínez-García et al. "Vegetation pattern formation in semiarid systems without facilitative mechanisms". In: *Geophysical Research Letters* 40.23 (2013), pp. 6143–6147.

[108] Stephen W. Morris. *Belousov Zhabotinsky reaction*. [Online; accessed May 28, 2015]. 2004. URL: https://www.flickr.com/photos/nonlin/3572095252/.

[109] J.E. Pearson. "Complex patterns in a simple system". In: *Science* 261.5118 (1993), pp. 189–192.

[110] K.J. Lee and H.L. Swinney. "Lamellar structures and self-replicating spots in a reaction-diffusion system". In: *Physical Review E* 51.3 (1995), p. 1899.

[111] S. Koga and Y.Kuramoto. "Localized patterns in reaction-diffusion systems". In: *Progress of Theoretical Physics* 63.1 (1980), pp. 106–121.

[112] V.K. Vanag and I.R. Epstein. "Localized patterns in reaction-diffusion systems". In: *Chaos: An Interdisciplinary Journal of Nonlinear Science* 17.3 (2007), p. 037110.

[113] K.J. Lee et al. "Pattern formation by interacting chemical fronts". In: *Science* 261.5118 (1993), pp. 192–194.

[114] W. Mazin et al. "Pattern formation in the bistable Gray-Scott model". In: *Mathematics and Computers in Simulation* 40.3 (1996), pp. 371–396.

[115] E.E. Sel'Kov. "Self-Oscillations in Glycolysis". In: *European Journal of Biochemistry* 4.1 (1968), pp. 79–86.

[116] P. Gray and S.K. Scott. "Sustained oscillations and other exotic patterns of behavior in isothermal reactions". In: *The Journal of Physical Chemistry* 89.1 (1985), pp. 22–32.

[117] Y. Nishiura and D. Ueyama. "Spatio-temporal chaos for the Gray–Scott model". In: *Physica D: Nonlinear Phenomena* 150.3 (2001), pp. 137–162.

[118] P. Gray and S.K. Scott. "Autocatalytic reactions in the isothermal, continuous stirred tank reactor: isolas and other forms of multistability". In: *Chemical Engineering Science* 38.1 (1983), pp. 29–43.

[119] P. Gray and S.K. Scott. "Autocatalytic reactions in the isothermal, continuous stirred tank reactor: Oscillations and instabilities in the system A + 2B → 3B; B → C". In: *Chemical Engineering Science* 39.6 (1984), pp. 1087–1097.

[120] A. Doelman, R.A. Gardner, and T.J. Kaper. "Stability analysis of singular patterns in the 1D Gray-Scott model: a matched asymptotics approach". In: *Physica D: Nonlinear Phenomena* 122.1 (1998), pp. 1–36.

[121] J.K. Hale, L.A. Peletier, and W.C. Troy. "Exact Homoclinic and Heteroclinic Solutions of the Gray–Scott Model for Autocatalysis". In: *SIAM Journal on Applied Mathematics* 61.1 (2000), pp. 102–130.

[122] J. Wei. "Pattern formations in two-dimensional Gray–Scott model: existence of single-spot solutions and their stability". In: *Physica D: Nonlinear Phenomena* 148.1–2 (2001), pp. 20 –48.

[123] C.B. Muratov and V.V. Osipov. "Stability of the Static Spike Autosolitons in the Gray–Scott Model". In: *SIAM Journal on Applied Mathematics* 62.5 (2002), pp. 1463–1487.

[124] P. Greig-Smith. "Pattern in vegetation". In: *The Journal of Ecology* (1979), pp. 755–779.

[125] S.A. Levin. "The problem of pattern and scale in ecology: the Robert H. MacArthur award lecture". In: *Ecology* 73.6 (1992), pp. 1943–1967.

[126] E. Meron. *Nonlinear Physics of Ecosystems*. CRC Press, 2015.

[127] L. Ridolfi, P. D'Odorico, and F. Laio. *Noise-induced phenomena in the environmental sciences*. Cambridge University Press, 2011.

[128] D. D. Escaff et al. "Localized vegetation patterns, fairy circles, and localized patches in arid landscapes". In: *Phys. Rev. E* 91 (2 2015), p. 022924.

[129] M. Tlidi, R. Lefever, and A. Vladimirov. "On vegetation clustering, localized bare soil spots and fairy circles". In: *Dissipative Solitons: From Optics to Biology and Medicine*. Springer, 2008, pp. 1–22.

[130] D.L. Dunkerley. "Infiltration rates and soil moisture in a groved mulga community near Alice Springs, arid central Australia: evidence for complex internal rainwater redistribution in a runoff–runon landscape". In: *Journal of Arid Environments* 51.2 (2002), pp. 199–219.

[131] J.A.F. Monteiro. "Functional morphology and productivity of a Tussock grassland in the Bolivian Altiplano". PhD thesis. University of Basel, 2012.

[132] J.C. Ospina González, S.S. Aliscioni, and S.S. Denham. "Estudios taxonómicos en el género Festuca L.(Poaceae) de Argentina y Chile". In: *Gayana. Botánica* 70.1 (2013), pp. 01–15.

[133] E. Geyger. "Untersuchungen zum Wasserhaushalt der Vegetation im nordargentinischen Andenhochland". PhD thesis. PhD Thesis, Universität Göttingen, Göttingen, Germany, 1985.

[134] S. Getzin et al. "Adopting a spatially explicit perspective to study the mysterious fairy circles of Namibia". In: *Ecography* 38.1 (2015), pp. 1–11.

[135] J.A.F. Monteiro, E. Hiltbrunner, and C. Körner. "Functional morphology and microclimate of Festuca orthophylla, the dominant tall tussock grass in the Andean Altiplano". In: *Flora-Morphology, Distribution, Functional Ecology of Plants* 206.4 (2011), pp. 387–396.

[136] F. Aurenhammer. "Voronoi diagrams—a survey of a fundamental geometric data structure". In: *ACM Computing Surveys (CSUR)* 23.3 (1991), pp. 345–405.

[137] O. Lejeune and M. Tlidi. "A model for the explanation of vegetation stripes (tiger bush)". In: *Journal of Vegetation science* 10.2 (1999), pp. 201–208.

[138] E. Gilad et al. "Ecosystem engineers: from pattern formation to habitat creation". In: *Physical Review Letters* 93.9 (2004), p. 098105.

[139] C.A. Klausmeier. "Regular and irregular patterns in semiarid vegetation". In: *Science* 284.5421 (1999), pp. 1826–1828.

[140] P. D'Odorico, F. Laio, and L. Ridolfi. "Patterns as indicators of productivity enhancement by facilitation and competition in dryland vegetation". In: *Journal of Geophysical Research: Biogeosciences (2005–2012)* 111.G3 (2006).

[141] P. D'Odorico et al. "Noise-induced vegetation patterns in fire-prone savannas". In: *Journal of Geophysical Research: Biogeosciences (2005–2012)* 112.G2 (2007).

Appendices

Appendix A

This appendix is a copy of the paper entitled: **From localized spots to the formation of invaginated labyrinthine structures in a Swift-Hohenberg model.**

Paper published in the journal: *Communications in Nonlinear Science and Numerical Simulation.*

Corresponding author: Ignacio Bordeu Weldt.

DOI information: 10.1016/j.cnsns.2015.05.028

This work shows the results presented in Chapter 3.

A previous version of this manuscript was uploaded to *arXiv*, preprint arXiv:1505.05621.

Commun Nonlinear Sci Numer Simulat 29 (2015) 482–487

Contents lists available at ScienceDirect

Commun Nonlinear Sci Numer Simulat

journal homepage: www.elsevier.com/locate/cnsns

From localized spots to the formation of invaginated labyrinthine structures in a Swift–Hohenberg model

I. Bordeu [a,*], M.G. Clerc [b], R. Lefever [c], M. Tlidi [c]

[a] Departamento de Física, Facultad de Ciencias, Universidad de Chile, Santiago, Chile
[b] Departamento de Física, Facultad de Ciencias Físicas y Matemáticas, Universidad de Chile, Casilla 487-3, Santiago, Chile
[c] Département de Physique, Faculté des Sciences, Université Libre de Bruxelles (U.L.B.), CP 231, Campus Plaine, B-1050 Bruxelles, Belgium

ARTICLE INFO

Article history:
Received 6 April 2015
Revised 27 May 2015
Accepted 28 May 2015
Available online 5 June 2015

Keywords:
Nonlinear dynamics
Pattern formation in complex systems

ABSTRACT

The stability of a circular localized spot with respect to azimuthal perturbations is studied in a prototype variational model, namely, a Swift–Hohenberg type equation. The conditions under which the circular shape of the spot undergoes an elliptical deformation which transforms it into a rod-shaped structure are analyzed. As it elongates, the rod structure exhibits a transversal instability, generating an invaginated labyrinthine structure which invades all the space available.

© 2015 Elsevier B.V. All rights reserved.

1. Introduction

Several spatially extended systems that undergo a symmetry breaking instability close to a second-order critical point can be described by real order parameter equations in the form of Swift–Hohenberg type of models. These models, have been derived in various fields of nonlinear science such as hydrodynamics [1], chemistry [2], plant ecology [3], nonlinear optics [4–6], and elastic materials [7].

A complex Swift–Hohenberg equation was deduced in the context of lasers [8–10] and optical parametric oscillators [11]. Moreover, to describe the nascent optical bistability with transversal effect in nonlinear optical cavities a real approximation has been deduced [12] from laser equations. This approximation allowed the prediction of stable, single and clustered localized structures [12]. A detailed derivation of this equation from first principles can be found in Ref. [8]. In the present work, we show that this real modified Swift–Hohenberg equation (SHE) of the form

$$\partial_t u = \eta + \epsilon u - u^3 - \nu \nabla^2 u - \nabla^4 u \tag{1}$$

supports a curvature instability over localized structures that lead to an elliptical deformation, producing a rod-like structure. With the temporal evolution, the rod-like structure exhibits a transverse undulation, leading to the formation of invaginated structures. Such a structure is a labyrinthine pattern, characterized by its interconnected structure where the field value is high. The outer region or complement to the invaginated structure corresponds to low field value. This behavior occurs far from any pattern forming instability and requires a bistable behavior between homogeneous steady states. In Eq. (1), $u = u(x, y, t)$ is a real scalar field, x and y are spatial coordinates and t is time.

The parameter η represents the external forcing field which brakes the reflection symmetry $u \to -u$. The bifurcation parameter is ϵ. The coefficient ν may change the sign of the diffusive term ∇^2, and allows the pattern forming to take place [4,13–17].

* Corresponding author. Tel.: +56 978879738.
E-mail address: ibordeu@gmail.com (I. Bordeu).

http://dx.doi.org/10.1016/j.cnsns.2015.05.028
1007-5704/© 2015 Elsevier B.V. All rights reserved.

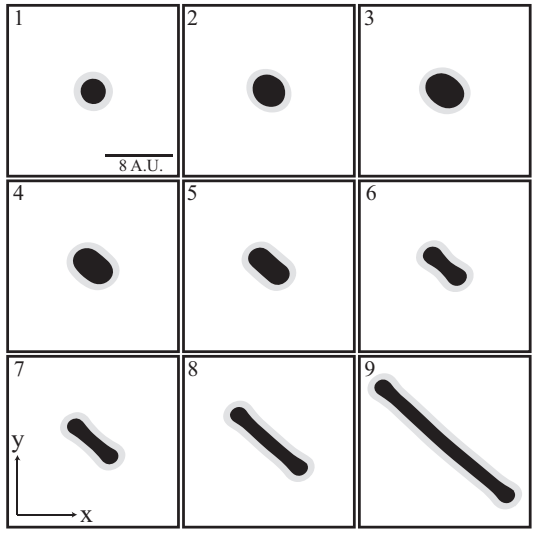

Fig. 1. Temporal evolution for; (1) $t = 0$; (2) $t = 125$; (3) $t = 175$; (4) $t = 225$; (5) $t = 275$; (6) $t = 340$; (7) $t = 350$; (8) $t = 360$; (9) $t = 400$, of a localized spot through an elliptical deformation into a rod-like structure for Eq. (1) with: $\eta = -0.065$; $\epsilon = 2.45$; $\nu = 2.0$. Minima are plain white. The image corresponds to a zoom of 16×16 points of a 512×512 points finite-difference simulation, with Neumann boundary conditions.

Depending on the context in which this equation is derived, the physical meaning of the field variable and parameters adopt particular meanings, for instance, in cavity nonlinear optics $u(x, y, t)$ corresponds to light field intensity, while parameters $\{\eta, \epsilon, \nu\}$ are associated with the injection field, the deviations of the cavity field, and cooperativity, respectively [12].

For certain ranges of parameter values, Eq. (1) exhibits stable circular localized structures. General properties such as existence, stability and dynamical evolution of these structures have been well studied (see Refs. [18–27]). Recent review on localized structures can be found in [28]. For $\eta < 0$ localized structures emerge as isolated peaks of the field $u(x, y, t)$, instead, for $\eta > 0$ localized structures appear as holes in the field. These localized structures have a fixed stable radius for each parameter value. Curvature instability of localized spot has been experimentally studied or theoretically predicted in magnetic fluids [29], liquid crystals [30,31], reaction–diffusion systems [32–40,40–43], plant ecology [44], material science [45,46], granular fluid systems and frictional fluids [47,48], and nonlinear optics [49]. The fingering instability of planar fronts leading to the formation of labyrinth structures has been reported by Hagberg et al. [50]. In this manuscript we shall focus on circular localized states.

2. Stability of localized spots

Considering fixed parameter values, starting with an azimuthally symmetric stationary localized structure. The structure is then perturbed, this perturbation grows radially as shown in Fig. 2(1). The circular shape becomes unstable at some critical radius. The elliptical shape elongate into a rod-like structures as shown in Fig. 1. This elongation proceeds until a critical size is reached beyond which a transversal instability onset the appearance of fingers near the midsection of the structure (see Fig. 2(3)). The finger continues their elongation, and the amplitude of oscillation increases (Fig. 2(4) and (5)). The dynamic of the system does not saturate and for a long time evolution, the rod-like structure invades the whole space available in (x, y)-plane as shown in Fig. 2(6). This invaginated structure is stationary solutions of the SHE. The dynamic described previously has been observed in cholesteric liquid crystals under the presence of an external electric field [30,31], where an initially circular structure of cholesteric phase suffers from a curvature instability, transversal oscillations and develops into an extended labyrinthine structure. The characterization of this dynamic is an open problem.

For $\nu = 2$, the bifurcation diagram of the model Eq. (1) in the parameter space (ϵ, η) is shown in Fig. 3. For $\epsilon > 0$ the system undergoes a bistable regime between homogeneous steady states. For $\epsilon < 0$, the system possesses only one homogeneous steady state. The curve Γ_1 represents the pitchfork bifurcation, where the coordinates of the limit points of the bistable curve are given by $\eta_\pm = \pm 2(\epsilon/3)^{3/2}$. The threshold associated with a symmetry breaking or Turing instability is provided by the curve Γ_2. The coordinates of the symmetry breaking instabilities thresholds are $\eta_\pm = \pm\sqrt{(\nu^2 + 4\epsilon)/3}(\nu^2 - 8\epsilon)/24$. The Γ_1 and Γ_2 curves are well known in the literature [51,52]. We have built numerically the curve Γ_3, which separates the zone of bistability where localized structures are stable, zone II, from the zone where they are unstable, zone I. The transition from localized structures to labyrinthine patterns take place when crossing from the I-zone to the II-zone, through the Γ_3-curves indicated in Fig. 3. This transition occurs via fingering instability at the Γ_3-curves delimiting the parameter domain I and II. In the limit of the classical Swift–Hohenberg equation, $\eta = 0$, there is no observation of fingering instability, instead, at the transition from II-zone to I-zone, localized structures only grow radially. The destabilization of these structures into labyrinthine structures may be observed, as a result of size effect phenomenon due to boundary conditions. In contrast, for $\eta \neq 0$ the transition from the II-zone to the I-zone

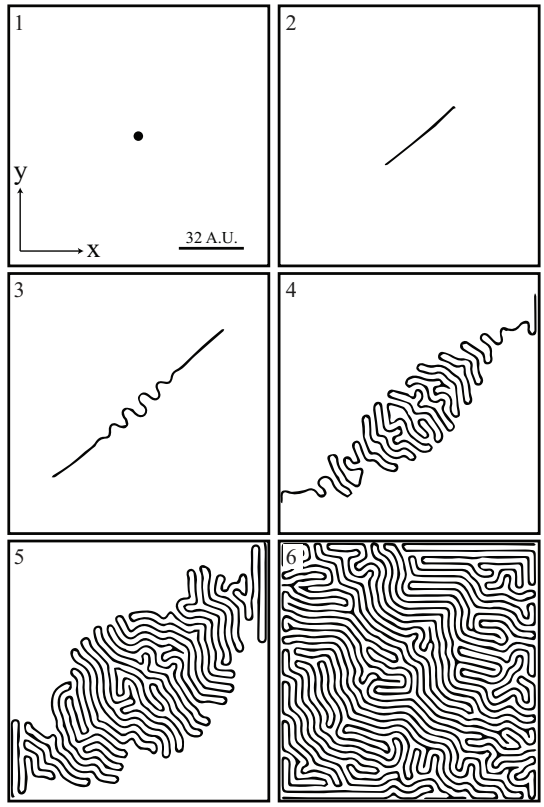

Fig. 2. Transition from a single localized spot to invaginated pattern. Temporal evolution with Neumann boundary conditions and with the same parameters as in Fig. 1. (1) $t = 0$, localized spot, (2) $t = 600$, rod-like structure, (3) $t = 1900$, transverse undulation of the rod-like structure, (4) $t = 2800$, (5) $t = 3700$, localized transient patterns, and (6) $t > 15{,}000$, stationary invaginated labyrinth pattern. Minima are plain white and the mesh integration is 512×512 points. Simulation done with finite-difference method.

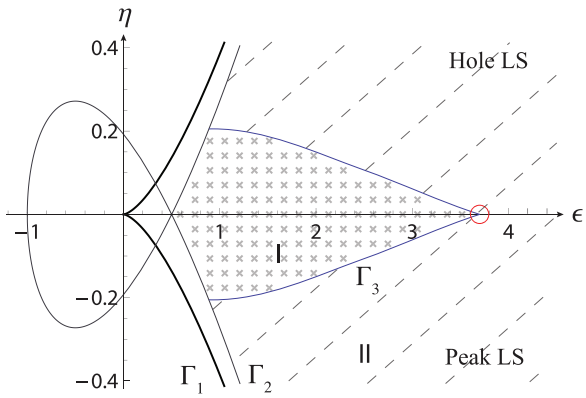

Fig. 3. Bifurcation diagram of Eq. (1) in (ϵ, η) space for $\nu = 2.0$. In II-zone (dashed black), stable circular localized structures are observed. In I-zone (gray crosses) generation of labyrinthine structures are observed from localized structures. The transition curve Γ_3 was constructed numerically.

of a localized spot induces a curvature instability, giving rise to an unstable rod structure which exhibits transversal oscillations and develops into an extended labyrinthine structure.

In what follows, we first study the stability of a circular localized spot with respect to azimuthal perturbations. This linear analysis allows us to evaluate the threshold above which the transition from localized spot to a rod-like structure takes place. Then, a linear stability analysis of the rod-like structure is performed, to determine the conditions under which the transversal oscillations occur for the SH equation.

Starting from a stationary solution with rotational symmetry (i.e. circular localized structure) $u = u_s(r)$ where r is the radial coordinate. Then, the solution is perturbed $u(r, \theta, t) = u_s(r) + \delta u(r) e^{\lambda_m t} \cos(m\theta)$, where θ is the angular coordinate, and $\delta u(r) \ll 1$. It should be noted that the perturbation mode $m = 2$ represents an elongation of the circular structure into an elliptical shape. Using polar representation of Eq. (1), considering the above perturbation and parameters in Eq. (1) at linear order in W

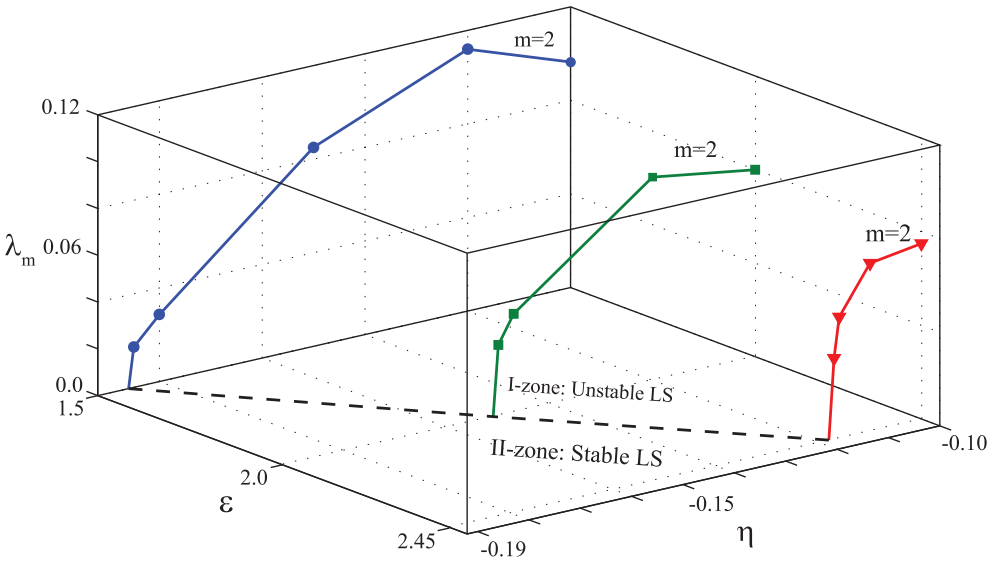

Fig. 4. Dots show the growth rate λ_m of the most unstable perturbation mode obtained numerically for different values of ϵ. Dashed line separates zones of stable and unstable localized structures (see Fig. 3). Parameters: $\nu = 2$; $dx = 0.5$; $dt = 0.03$. Periodic boundary conditions were used.

one obtains

$$\frac{\partial W}{\partial t} = \mathcal{L}W \tag{2}$$

where the linear operator $\mathcal{L} \equiv \epsilon + 3u_s^2(r) - \nu\nabla^2 - \nabla^4$ is explicitly dependent on the radial coordinate. Analytical calculations are not accessible when the operator is inhomogeneous.

However, by direct simulation of Eq. (1) with an initially stationary localized structure one can find the growth rate of the most unstable mode. First for fixed values of the parameters $\{\eta, \epsilon, \nu\}$ a stationary localized spot is considered as initial condition. Note that the radius of localized spot is determined by a balance between the interface energy and the energy difference between the homogeneous states which are proportional to ν and η, respectively. The radius of the localized structures r_s is proportional to ν/η [53]. Afterwards, the system is perturbed by homogeneous noise, this type of perturbation can be regarded as a linear combination of all the angular modes m. However, the most unstable mode (the one with largest eigenvalue λ_m) dominates the temporal dynamics and is the only one observable. By considering the stability of the localized spot for different values of the parameter η under homogeneous noise perturbations we can determine that the most unstable mode ($\lambda_2 > 0$) is $m = 2$ as observed in Fig. 4. This mode deforms the circular localized spot into an elliptically shaped structure as shown in Fig 2(2).

3. Transversal instability of rod structures and emergence of labyrinthine patterns

The SHE Eq. (1) admits a single stripe-like solution [21,54]. In order to evaluate the threshold over which transversal oscillations appear, we perform the stability analysis of a rod-like structure, by a method similar to the one performed in Ref. [50]. For this purpose we perturb the single stripe solution as $u = u_f(\boldsymbol{\xi}) + W(\boldsymbol{x}, \boldsymbol{X_0})$ where u_f is the single stripe solution and $\boldsymbol{\xi} = \boldsymbol{x} - \boldsymbol{X_0}(y, t)$ the relative position, $\boldsymbol{X_0}$ is the field that accounts for the shape and evolution of the rod, and $W(\boldsymbol{x}, \boldsymbol{X_0}) \ll 1$ is a non-linear correction of a single stripe. Applying this ansatz in Eq. (1) at first order in W and applying the solvability condition [16], the following equation is obtained for the dynamic of $\boldsymbol{X_0}$

$$\partial_t X_0 = -\Delta'\partial_{yy}X_0 + 6\beta'\partial_y^2 X_0(\partial_y X_0)^2 - \partial_y^4 X_0, \tag{3}$$

where

$$\beta' = \frac{\langle \partial_{\xi\xi} u_f | \partial_{\xi\xi} u_f \rangle}{\langle \partial_\xi u_f | \partial_\xi u_f \rangle}, \text{ and } \Delta' = (\nu - 2\beta'). \tag{4}$$

Thus $\boldsymbol{X_0}$ satisfies a nonlinear diffusion equation. This equation describes the dynamics of an interface between two symmetric states [55,56]. This model is well known for exhibiting a zigzag instability. Analogously, to the previous section, when $\Delta < 0$ the single stripe solution is stable, and for $\Delta > 0$, the solution is unstable as result of the curvature instability. From Eq. (3) one expects to observe the single stripe becomes unstable by the emergence of undulations. Fig. 5 illustrates the manifestation of this undulations under the consideration of an infinitely long rod-like structure, to avoid border effects. Note that similar dynamical behavior is observed in the propagation of cholesteric finger in liquid crystals [30,31]. Later, this undulated stripe is replaced by the emergence of facets that form a zigzag structure. However the higher nonlinear terms control the evolution of the single stripe, then the dynamics of initial zigzag is replaced by the growth of undulations without saturation as it is depicted in Fig. 2(4).

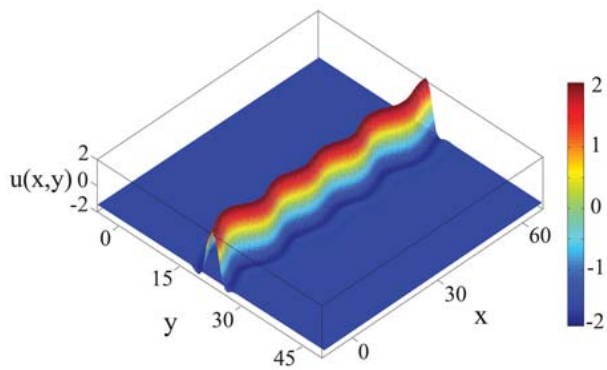

Fig. 5. Transversal instability of a single infinite stripe of Eq. (1). Image shows a section of a 256 × 256 points simulation with boundary conditions using a pseudo-spectral code. Parameters: $\eta = -0.065$, $\epsilon = 2.45$, $\nu = 2$, $dx = 0.5$, and $dt = 0.03$.

Therefore, the system displays the emergence of a roll-like transverse pattern which is formed in the midsection of the structure and invades the system generating invaginated structure (see Fig. 2(5)).

4. Conclusions

In this paper we have described the stability of localized spot in a modified Swift–Hohenberg equation. First, the bifurcation diagram was constructed, showing the possible solutions that appear in different parameter regimes. Afterwards, it was shown that the angular index $m = 2$ becomes unstable as consequence of curvature instability. Such instability leads to an elliptical deformation of the localized spot.

When angular index $m = 2$ becomes unstable, the curvature instability of localized spot produces an elliptical deformation leading to the generation of a rod-like structure. Subsequently, it causes undulations in the rod-like structure. The spatiotemporal evolution leads to the formation of invaginated labyrinthine structures. To understand this dynamics, we have performed the analytical stability analysis of a single stripe localized structure.

It should be noted that by an offset transformation, $u \to u + u_0$, where u_0 is a constant, Eq. (1) can be rewritten in such a way that the constant parameter η is removed and a quadratic nonlinearity appears. This quadratic model is equivalent to Eq. (1). The model with a quadratic nonlinearity has been well studied (see the textbook [16] and the references therein). This equivalence implies that the results of the present work are also valid for physical systems described by the quadratic model.

Acknowledgments

M.G.C. thanks the financial support of FONDECYT project 1150507. I.B. thanks the support from CONICYT, Beca de Magister Nacional and the Departamento de Postgrado y Postítulo of the Vicerrectoria de Asuntos Académicos, Universidad de Chile. M.T. received support from the Fonds National de la Recherche Scientifique (Belgium). M.T acknowledges the financial support of the Interuniversity Attraction Poles program of the Belgian Science Policy Office, under grant IAP 7–35 photonics@be.

References

[1] Swift J, Hohenberg PC. Phys Rev A 1977;15:319.
[2] Hilali M'F, Dewel G, Borckmans P. Phys Lett A 1996;217:263.
[3] Lefever R, Barbier N, Couteron P, Lejeune O. J Theor Biol 2009;261:194.
[4] Tlidi M, Georgiou M, Mandel P. Phys Rev A 1993;48:4605.
[5] Kozyreff G, Chapman SJ, Tlidi M. Phys Rev E 2003;68:015201.
[6] Clerc MG, Petrossian A, Residori S. Phys Rev E 2005;71:015205(R).
[7] Stoop N, Lagrange R, Terwagne D, Reis PM, Dunkel J. Nat Mater 2015;14:337.
[8] Mandel P. Theoretical problems in cavity nonlinear optics. New York: Cambridge University Press; 1997.
[9] Lega J, Moloney JV, Newell AC. Phys Rev Lett 1994;73:2978.
[10] Lega J, Moloney JV, Newell AC. Physica D 1995;83:478.
[11] Longhi S, Geraci A. Phys Rev A 1996;54:4581.
[12] Tlidi M, Mandel P, Lefever R. Phys Rev Lett 1994;73:640.
[13] Cross MC, Hohenberg PC. Rev Mod Phys 1993;65:851.
[14] Hohenberg PC, Halperin BI. Rev Mod Phys 1977;49:435.
[15] Aranson IS, Malomed BA, Pismen LM, Tsimring LS. Phys Rev E 2000;62:R5.
[16] Pismen LM. Patterns and interfaces in dissipative dynamics. Berlin, Heidelberg: Springer Series in Synergetics; 2006.
[17] Vladimirov AG, Lefever R, Tlidi M. Phys Rev A 2011;84:043848.
[18] Aranson IS, Gorshkov KA, Lomov AS, Rabinovich MI. Physica D 1990;43:435.
[19] Glebsky LYu, Lerman LM. Chaos 1995;5:424.
[20] Hilali MF, Métens S, Borckmans P, Dewel G. Phys Rev E 1995;51:2046.
[21] Tlidi M, Mandel P, Lefever R. Phys Rev Lett 1998;81:979.
[22] Coullet P, Riera C, Tresser C. Phys Rev Lett 2000;84:3069.
[23] Richter R, Barashenkov IV. Phys Rev Lett 2005;94:184503.

[24] Burke J, Knobloch E. Phys Rev E 2006;73:056211.
[25] Lloyd DJB, Sandstede B, Avitabile D, Champneys AR. J Appl Dyn Syst 2008;7:1049.
[26] McCalla S, Sandstede B. Physica D 2010;239:1581.
[27] Knobloch E. Annu Rev Condens Matter Phys 2015;6:325.
[28] Tlidi M, Staliunas K, Panajotov K, Vladimiorv AG, Clerc M. Phil Trans R Soc A 2014;372:20140101.
[29] Dickstein AJ, Erramilli S, Goldstein RE, Jackson DP, Langer SA. Science 1993;261:1012.
[30] Ribiere P, Oswald P. J Phys 1990;51:1703.
[31] Oswald P, Baudry J, Pirkl S. Phys Rep 2000;337:67.
[32] Pearson JE. Science 1993;261:189.
[33] Lee K, McCormick WD, Pearson JE, Swinney HL. Nature (London) 1994;369:215.
[34] Munuzuri AP, Perez-Villar V, Markus M. Phys Rev Lett 1997;79:1941.
[35] Kaminaga A, Vanag VK, Epstein IR. Angew Chem 2006;45:3087.
[36] Kaminaga A, Vanag VK, Epstein IR. J Chem Phys 2005;122:174706.
[37] Kolokolnikov T, Tlidi M. Phys Rev Lett 2007;98:188303.
[38] Davis PW, Blanchedeau P, Dulos E, De Kepper P. J Phys Chem A 1998;102:8236.
[39] Muratov CB, Osipov VV. Phys Rev E 1996;53:3101; Muratov CB. Phys Rev E 2002;66:066108.
[40] Monine M, Pismen L, Bar M, Or-Guil M. J Chem Phys 2002;117:4473.
[41] Schaak A, Imbihl R. Chem Phys Lett 1998;283:368.
[42] Hayase Y, Ohta T. Phys Rev Lett 1998;81:1726.
[43] Hayase Y, Ohta T. Phys Rev E 2000;62:5998.
[44] Meron E, Gilad E, von Hardenberg J, Shachak M. Chaos Solitons Fractals 2004;19:367.
[45] Ren X, Wei J. SIAM J Math Anal 2003;35:1.
[46] Nishiura Y, Suzuki H. SIAM J Math Anal 2004;36:916.
[47] Sandnes B, Knudsen HA, Maloy KJ, Flekkoy EG. Phys Rev Lett 2007;99:038001.
[48] Sandnes B, Flekkoy EG, Knudsen HA, Maloy KJ, See H. Nat Commun 2011;2:288.
[49] Tlidi M, Vladimirov AG, Mandel P. Phys Rev Lett 2002;89:233901.
[50] Hagberg A, Yochelis A, Yizhaq H, Elphick C, Pismen L, Meron E. Physica D 2006;217:186.
[51] Coullet P, Riera C, Tresser C. Prog Theor Phys Suppl 2000;139:46.
[52] del Campo F, Haudin F, Rojas RG, Bortolozzo U, Clerc MG, Residori S. Phys Rev E 2012;86:036201.
[53] Coullet P. Int J Bifur Chaos 2002;12:2445.
[54] Tlidi M, Mandel P, Le Berre M, Ressayre E, Tallet A, Di Menza L. Opt Lett 2000;25:487.
[55] Chevallard C, Clerc M, Coullet P, Gilli J-M. Europhys Lett 2002;58:686.
[56] Calisto H, Clerc M, Rojas R, Tirapegui E. Phys Rev Lett 2000;85:3805.

Appendix B

This appendix is a copy of the manuscript entitled: **Rod-like localized structure in isotropic pattern forming systems.**

Preprint submitted to the journal *Physical Review E.*

Corresponding author: Ignacio Bordeu Weldt.

This work shows the results presented in Chapter 4.

Rod-like localized structure in isotropic pattern forming systems

Ignacio Bordeu
Departamento de Física, Facultad de Ciencias, Universidad de Chile, Santiago, Chile.

Marcel G. Clerc*
Departamento de Física, Facultad de Ciencias Físicas y Matemáticas, Universidad de Chile, Casilla 487-3, Santiago, Chile.

Stationary two dimensional localized structures have been observed in a wide range of dissipative systems. The existence, stability properties, dynamical evolution and bifurcation diagram of an azimuthal symmetry breaking, rod-like, localized structure in the isotropic prototype model of pattern formation, the Swift-Hohenberg model, is studied. These rod-like structures persist under the presence of non gradients perturbations. Based on a dimer approximation, the interaction of rod-like structures is studied. This allows us to envisage the possibility of different crystal-like configurations. Numerical simulations show a fair agreement with the theoretical predictions.

PACS numbers: 05.45.Yv, 05.45.-a, 89.75.Kd

I. INTRODUCTION

Macroscopic systems under the influence of injection and dissipation of energy, momenta, and matter often lead to the formation of spatial structures [1–3]. These patterns can be extended, this is, they involve the whole spatial physical system, or localized, which are patterns that exists only on a portion of the spatial system [4–6]. From the dynamical system point of view, one dimensional localized structures are homoclinic connections of the stationary dynamical system involving a stable and an unstable manifold of a given equilibrium [7, 8]. The possibility of coexistence with different equilibria enriches the variety of possible homoclinic structures. For example, in the case of coexistence between a uniform and a pattern state, the heteroclinic entanglement generates the nucleation of a family of localized structures [8, 9], which are organized by a snaking bifurcation diagram [10, 11]. In recent decades, localized structures have been observed in different fields such as in magnetic materials [12], chemical reactions [15], vertically driven Newtonian fluid [13, 14], granular media [16, 17], liquid crystals [18], liquid crystal light valve [19–21], colloidal fluids [22], electrical discharges [23], thermal convection [24, 25], and non-linear optics [26, 27], to mention a few. In most of these observations the localized states are two-dimensional objects with circular symmetry.

Localized structures are particle-type solutions for nonlinear equations, as they exhibit a series of characteristics often attributed to particles such as a size, a position, and a velocity defined by the parameters of the system, and an interaction law between them. Localized structures have attracted the interest of the scientific community because of their potential applications in optical information storage and processing [28]. Isotropic systems, systems with translational and rotational invariance, usually exhibit localized patterns which are az-

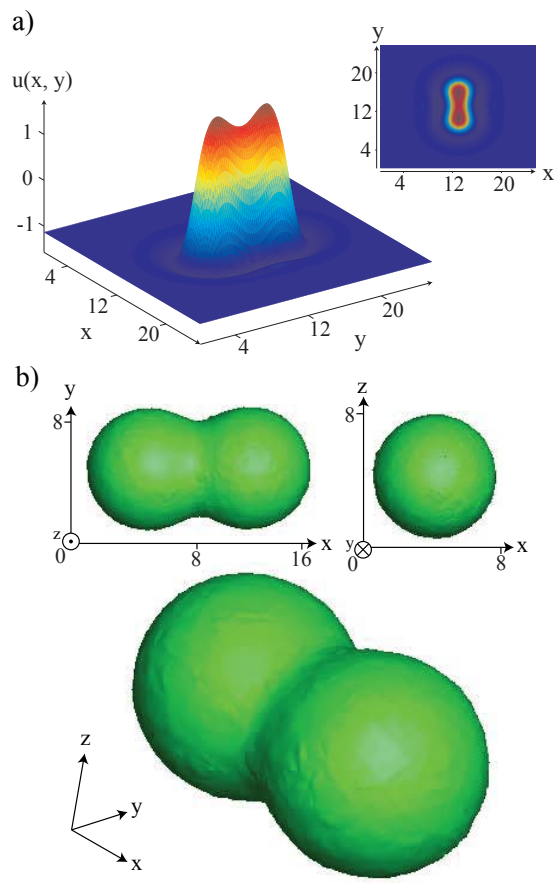

FIG. 1. (Color online) Stationary rod localized structure of, a) 2D Swift-Hohenberg model, Eq. (1), with $\nu = 2.0$, $\eta = -0.355$, and $\epsilon = 1.2$. Inset is a colormap of the rod localized structure, and b) 3D Swift-Hohenberg model, image shows the iso-surface for $u = 0.2$ with $\nu = 2.0$, $\eta = -0.37$, and $\epsilon = 1.5$. Simulations in 2D and 3D where made using pseudo-spectral and adaptive finite elements methods, respectively. Both with Neumann boundary conditions.

* marcel@dfi.uchile.cl

imuthally symmetric, that is, the localized states have a circular symmetry. Spatial breaking of symmetry tends to deform the localized structures and even can generate propagation of them, this is the case of the worm structures observed in binary liquids [24, 29] and electroconvection cells [30]. In the liquid crystal light valve experiment triangular localized structures have been observed by controlling the optical feedback [20]. Numerical simulations of the model describing this system also exhibits this type of intriguing localized state. Indeed, triangular structures are inherently two-dimensional due to the rotational symmetry breaking. There is not a global geometric theory to explain the origin of these structures and a characterization of the different possible localized structures without rotational symmetry.

In this paper, we show the existence, stability properties, dynamical evolution and bifurcation diagram of an elongated structure, non azimuthally symmetric, in a prototype isotropic two-dimensional model, The Swift-Hohenberg equation. We call this structure a *rod structure*. Figure 1 illustrates the typical observed rod structure in 2D and 3D systems. For 2D structures, based on the dimer approximation, we study the complex interaction scenario of rod structures. Which have a complex network of equilibria. This allows us to imagine the possibility of different crystal-like configurations. Numerical simulations show a fair agreement with these predictions.

The manuscript is organized as follows: In Sec. II, the generalized Swift-Hohenberg model and its dynamical evolution features are introduced. In particular, the phase space for the rod localized structures is presented. In Sec. III, the composition of the rod-like structure is analyzed as composition of one-dimensional structures. The different instabilities and bifurcation diagrams of rod structures are analyzed in Sec. IV. Interaction properties of rod structures using dimer approach is studied in Sec. V. Our conclusions and remarks are left to the final section.

II. GENERALIZED SWIFT-HOHENBERG EQUATION

Let us consider a prototype model which exhibits both localized and extended patterns. This is a natural variant of the Swift-Hohenberg equation [31], which is an isotropic, reflection symmetry, and real order parameter nonlinear equation deduced originally to describe the pattern formation of Benard convection [31]. This generalization includes an extra term which breaks the field reflection symmetry. It has been deduced in various field on nonlinear science such as chemistry [32], plant ecology [33], and nonlinear optics [34, 35]. This equation applies to a wide range of systems that undergo a symmetry breaking instability—often called Turing instability[2, 4]—close to a second-order critical point marking the onset of a hysteresis loop, which corresponds to a Lifshitz point [4, 36, 37]. The generalized Swift-Hohenberg equation reads

$$\frac{\partial u}{\partial t} = \eta + \epsilon u - u^3 - \nu \nabla^2 u - \nabla^4 u, \tag{1}$$

where $u = u(x, y, t)$ is a real scalar field, x and y are spatial coordinates and t is time. Depending on the context in which this equation has been derived, the physical meaning of the field variable $u(x, y, t)$ could be the electric field, deviation of molecular orientations, phytomass density, or chemical concentration. The control or the bifurcation parameter ϵ measures the input field amplitude, the aridity parameter, or chemical concentration. The η parameter breaks the reflection symmetry $u \to -u$, thus it accounts for the asymmetry between homogeneous states. When this parameter is ignored, $\eta = 0$, one gets the Swift-Hohenberg equation [31]. The parameter ν stands for the diffusion coefficient, when this parameter is negative, it realizes anti diffusion process ($\nu > 0$). The 2D Laplacian operator $\nabla^2 = \partial^2_{xx} + \partial^2_{yy}$ and the 2D bilaplacian operator ∇^4 act on the plane (x, y). Thus the first three terms on the right hand side of Eq. (1) account for homogeneous or local nonlinear dynamics, the fourth and the fifth term stand for the transport mechanisms or spatial coupling via diffusion and hyperdiffusion, respectively. It should be noted that by a displacement of the field $u \to u + u_0$, where u_0 is a constant, Eq. (1) can be rewritten by removing the parameter η but including an extra term quadratic in u, the equation including the quadratic term has been widely studied in various contexts (see the textbook [3] and references therein). An important property of Eq. (1) is that it possess a gradient form, i.e.

$$\frac{\partial u}{\partial t} = -\frac{\delta F[u, \nabla u, \nabla^2 u]}{\delta u}, \tag{2}$$

with the functional

$$F \equiv \iint_{\mathbb{R}^2} \left(-\eta u - \epsilon \frac{u^2}{2} + \frac{u^4}{4} - \nu \frac{(\nabla u)^2}{2} + \frac{(\nabla^2 u)^2}{2} \right) dxdy. \tag{3}$$

Note that using the solutions of Eq. (1), this functional satisfies

$$\frac{dF}{dt} = -\iint_{\mathbb{R}^2} dxdy \, (\partial_t u)^2 \leq 0. \tag{4}$$

Hence, F is a Lyapunov functional that can only decrease in the course of time. This functional guarantees that time evolution proceeds toward the state for which the functional has the smallest possible value which is compatible with the system boundary conditions. Any initial distribution $u(x, y, t)$ (or $u(x, y, z, t)$ in the 3D case) evolves towards a homogeneous or inhomogeneous (periodic or localized) stationary state corresponding to a local or global minimum of F. The analysis of the functional F is provided in Ref. [38].

The generalized Swift-Hohenberg equation exhibits coexistence between homogeneous and pattern states

[39, 40], thus allowing the stability of localized structures. These are localized structures in the sense of integral boundedness

$$\iint_{\mathbb{R}^2} |u_{ls}(x,y)|^2 dxdy < +\infty, \tag{5}$$

where, $u_{ls} \equiv u(x,y) - u_0$ is the relative field of the localized structure with respect to the homogeneous state wherein sustained the localized structure u_0. This homogeneous state is a stable solution to the cubic equation $\eta + \epsilon u - u^3 = 0$. For a certain range of parameters $\{\eta, \epsilon\}$ two different localized structures are stable, the first, is the well known circular (azimuthally symmetric) localized structure [47]. Notwithstanding, we have found a second type of localized structure corresponds to a novel class of localized structures at least in two and three-dimensional isotropic systems. This structure is a rod-like stable localized structure, it break the azimuthal symmetry, remaining invariant only with respect to a rotation of π around any axis on the (x,y)-plane which contains the center of the localized structure. Figure 1 shows the typical rod-like stable localized structures exhibited by both the 2D and 3D Swift-Hohenberg Eq. (1). In order to figure out the conditions under which the rod structure emerges, the analysis of the bifurcation diagram must be done for the model under study.

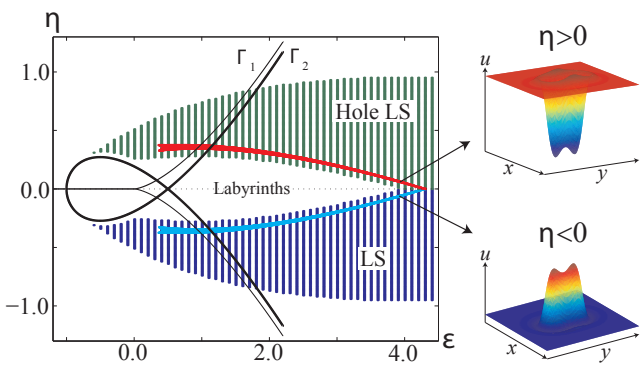

FIG. 2. (Color online) Bifurcation diagram of the 2D generalized Swift-Hohenberg Eq. (1) in (ϵ,η) space for $\nu = 2.0$. The light and solid curve Γ_1 and Γ_2 account for the saddle-node bifurcation and the spatial bifurcation of the uniform state, respectively. The shaded areas account for the zones where localized peaks (LS-zone) and localized holes (Hole LS-zone) are observed. The painted areas stand for the region where rod structures have been observed. The insets correspond to the typical monitored rod structures.

For a fixed value of the diffusion coefficient $\nu = 2.0$, typical bifurcation diagram of the model Eq. (1) in the parameter space (ϵ, η) is shown in Fig. 2. The curves Γ_1 and Γ_2 represent the saddle-node bifurcation and the threshold associated with a modulation or pattern forming or Turing instabilities of the homogeneous state observed for large negative ϵ, respectively [39, 40]. For negative ϵ, the system has only one homogeneous steady state, monostable region. For positive ϵ the system undergoes a bistable behavior between homogeneous steady states as result of the saddle-node bifurcation (cf. Fig. 2). Moreover as a result of the spatial instability of the uniform state (cf. Fig. 2), the system also exhibits coexistence between patterns and uniform states. Near this type of bistability region one expects to observe localized structures. The shaded zones in Fig. 2 account for the areas where localized peaks and localized holes are observed. When one decreases the parameter η localized structures become unstable giving rise to labyrinthine pattern [41]. This transition occurs via fingering instability. Unexpectedly, rod structures coexist with isotropic localized structures. Figure 2 depicts the region where the rod structures are observed.

Even though the Swift-Hohenberg model has been extensively studied since its deduction, no analytic expression is know for the localized solution. It is because these solutions are homoclinic solutions of the stationary dynamical system ($\partial_t u = 0$), which is chaotic when one replaces the time for the radial coordinate [42]. Under this consideration, the study of the rod-like structure will not lead to an analytic expression yet to the full characterization of its characteristic properties, bifurcations, and interaction. Thus the numerical and geometrical methods are the most suitable tools for characterizing the localized structures. We have conducted numerical simulations using a pseudo-spectral method, and verified with a finite-difference method.

III. COMPOSITION OF THE ROD STRUCTURE: ONE-DIMENSIONAL CORRESPONDENCE

No definitive theory for two-dimensional localized structures has yet been formulated, therefore, the required physical, hence, mathematical conditions for their existence and stability are not known. However, for one-dimensional systems, localized structures emerge as a

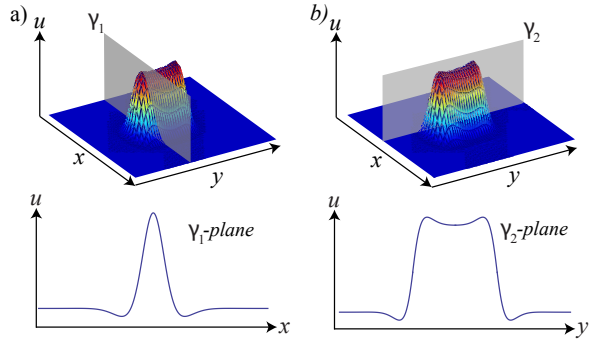

FIG. 3. (Color online) One-dimensional projections of the 2D rod structure and the respective projection over the: a) (x,u)-plane and b) (y,u)-plane. Numerical simulation of Eq. (1) with $\nu = 2.0$, $\eta = -0.355$, and $\epsilon = 1.2$.

family of stable fronts connecting an homogeneous with a pattern state in a bistable regime [43]. It is now known that coexistence (instead of bistability) is sufficient for the appearance of one-dimensional localized structures [44]. In this sense, the generation of two-dimensional localized structures can be regarded as an extension of one-dimensional localized structure, which is rotated over its axis thus generating an azimuthally symmetric localized structure. Nevertheless, the rod-like structure has no azimuthal symmetry. We can projected over two orthogonal planes (γ_1 and γ_2). These projections generate the equivalent to one-dimensional localized structures. The projection over the γ_1-plane (Fig 3a) generates a one wavelength wide localized structure while the projection over the γ_1-plane (Fig 3b) generates a two wavelength wide localized structure [8]. Hence, the two dimensional rod structure can be considered as the composition of two one-dimensional localized structures with different lengths.

As in one-dimensional localized structures of the generalized Swift-Hohenberg equation, the two dimensional structures possesses spatial oscillation tail of the field, which propagates radially from the bulk of the structure, these oscillations, that decay exponentially, stabilize the structure and allow the interaction between two or more structures by field interference [45].

IV. INSTABILITIES AND BIFURCATION DIAGRAMS

The characterization of the phase space of the Swift-Hohenberg Eq. (1), see Fig. 2, shows the existence of the rod structure for a wide range of parameters η and ϵ. In all these zones of stability the rod structure coexists with stable localized spots. It has been shown that circular localized structures suffer from a curvature instability when leaving their stability zone thus generating an extended labyrinthine structure [41]. In this section its shown how labyrinths can emerge—in zones where circular localized structures are stable—by the destabilization of the rod structure. Its also shown how the rod structure elongate into an infinite roll structure, decay into the simpler localized spot or even split into a bound state of two circular localized structures, depending on the parameters varied. Bifurcations suffered by the rod structure can be studied through monitoring the energy (Lyapunov functional) while modifying one parameter and fixing the others.

By variations of the parameters η or ϵ the rod structure is affected by saddle-node bifurcations characterized by the square-root law of the energy near the threshold and by a decay rate of the structure proportional to $(\alpha - \alpha_c)^{-1/2}$, where α is the parameter varied and α_c indicates the critical parameter value for which the bifurcation occurs [46]. Figure 4 illustrates this type of

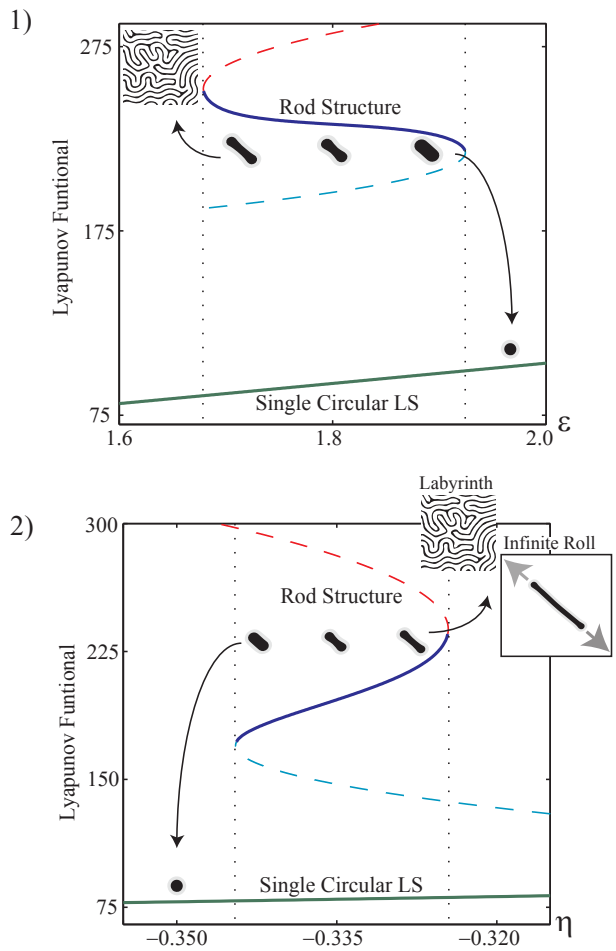

FIG. 5. (Color online) Bifurcation diagrams of rod structures as function of ϵ and η parameters. Saddle-node bifurcations, rod to circular localized structure, rod to labyrinth, and rod to infinite roll. For 1) $\eta = -0.320$ and 2) $\epsilon = 1.6$ and $\nu = 2.0$.

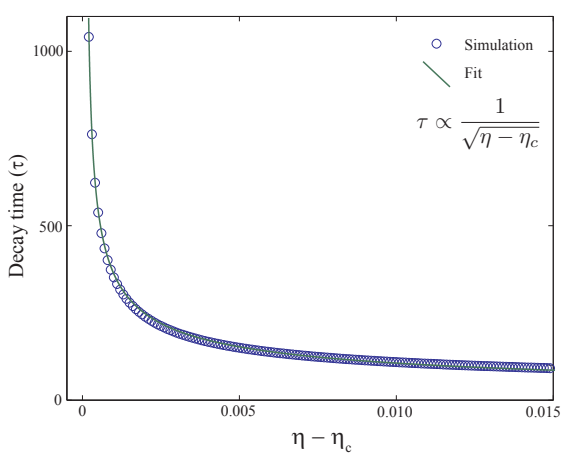

FIG. 4. Decay rate as function η from a rod structure into a circular localized structure for the 2D generalized Swift-Hohenberg Eq. (1) with $\epsilon = 1.6$ and $\nu = 2.0$. The circles account for decay time obtained numerically. The solid curve is obtained using the expression $\tau = \tau_0/\sqrt{\eta - \eta_c}$ with fitting parameters $\eta_c = -0.3444$ and $\tau_0 = 11.61$ ($R^2 = 0.9647$).

dynamical behavior. Rod structures that exist at the right side of Γ_2-curve (cf. Fig. 2), exhibit only two bifurcations. The first occur when leaving the stability zone of the rod structure by decreasing ϵ (increasing $|\eta|$), causing an increment in the rod structure size and consequently an increment on its energy. Once the bifurcation takes place through the saddle-node mechanism, the system falls into the basin of attraction of labyrinthine pattern. Figure 5 depicts the transition from rod to labyrinthine pattern, changing the different control parameters. As labyrinths are extended patterns, their energy diverges. The second bifurcation suffered by the rod structure in this zone, takes place when increasing the value of ϵ (decreasing $|\eta|$), here, the rod structure shrinks subsequently reducing its energy, by saddle-node bifurcation rod structures decay into single localized spots, which are energetically more stable in the Lyapunov sense. Figure 5 shows the transition from rod to localized spot. This rod to circular structure bifurcation continues existing for values of η and ϵ to the left of Γ_2-curve. The decay rate from rod to localized spot is shown in Fig. 4, where, $\epsilon = 1.6$. The numeric decay rate law corresponds to the expected theoretical rate from a saddle-node bifurcation theory [46].

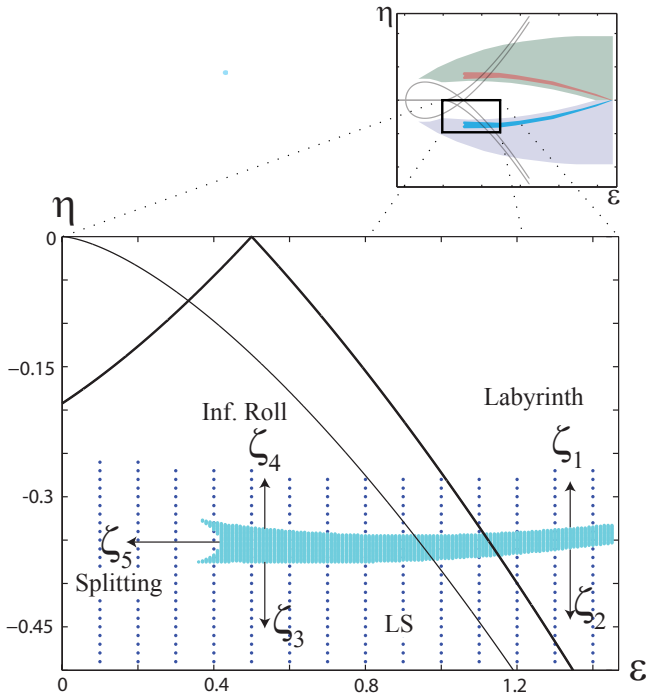

FIG. 6. (Color online) Zoomed phase diagram of rod structure, which shows the different outcomes possible form the destabilization of a rod structure. ζ_1-curve indicates the transition form rod to labyrinth bifurcation, ζ_2 and ζ_3-curve account for the transition between rod to circular localized structure, ζ_4-curve stands for the transition from rod to infinite roll, and ζ_5-curve accounts for the transition between rod to binary state, for $\nu = 2.0$.

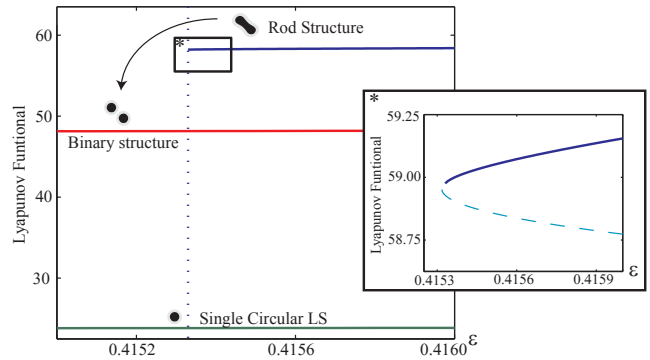

FIG. 7. (Color online) Saddle-node bifurcations for the splitting of a rod structure into a binary structure of the generalized Swift-Hohenberg Eq. (1) for $\nu = 2.0$, $\eta = -0.350$For 1) $\eta = -0.320$ and 2) $\epsilon = 1.6$. The inset corresponds to a zoom of the tip of the saddle-node bifurcation.

Another scenario emerges for values of η and ϵ to the left side of Γ_2-curve. Other two bifurcations are observed when overstepping the boundaries of the stability zone for the rod structure. For fixed values of ϵ and decreasing values of $|\eta|$ (see the transition ζ_4-curve in Fig. 6), the rod structure exhibits a continuous elongation similar to the case of the rod to labyrinth bifurcation, though in this case the elongation is permanent generating an infinitely long roll structure without transversal oscillations (see the inset in Fig. 5.2). Different is the scenario when leaving the stability zone of the rod structure by the interior of the horseshoe-like arc. Figure 6 shows a zoomed phase diagram of rod structure, the horseshoe-like arc is represented by ζ_5-curve. Following this route, a fourth bifurcation appears, where the rod structure becomes unstable, surface tension is unable to keep the structure together leading to its splitting. Figure 7 depicts the bifurcation diagram observed in the horseshoe-like zone. Through this bifurcation two circular localized structures are generated by the collapse of the central part of the structure.

V. INTERACTION PROPERTIES OF ROD STRUCTURE: DIMER APPROACH

It has been shown that the generalized Swift-Hohenberg model, allows the existence of multiple stable localized structures [47]. These (one or two dimensional) structures posses no compact support, thus, the frontier between the homogeneous state u_0 and the localized structure is not defined. Instead, the field oscillates decaying exponentially with the distance from the localized structure, these oscillations fluctuate around the homogeneous state with the characteristic wavelength of the system. The exponential tail will be addressed as the interaction field [14, 45, 48, 49].

A. Localized spots interaction

As mentioned before, no analytical expression is know for the localized structures in the generalized Swift-Hohenberg model, Eq. (1). Nevertheless, for interaction matter only the asymptotic approximation of the decaying field is relevant. Based on the linear perturbation theory, it is easy to show that the field $u(r)$ (with $r = \sqrt{x^2 + y^2}$ is the radial coordinate) has the form

$$u(r) \approx u_0 + e^{-c_1 r} \cos(c_2 r) \tag{6}$$

where, u_0 is the homogeneous state, and

$$c_1 = \mathrm{Re}\left[\sqrt{\frac{1}{2}(\sqrt{\nu^2 + 4\epsilon} \pm \nu)}\right],$$
$$c_2 = \mathrm{Im}\left[\sqrt{\frac{1}{2}(\sqrt{\nu^2 + 4\epsilon} \pm \nu)}\right].$$

A system with two (or more) localized structures with initial given positions $\boldsymbol{r}_1$ and $\boldsymbol{r}_2$, respectively, evolves to a stationary equilibrium by the change of relative position between the structures $\boldsymbol{R} = \boldsymbol{r}_2 - \boldsymbol{r}_1$. The corresponding interaction fields from each particle interfere with each other generating interaction forces, which in turn, induce movement of the particle-like solutions. Aranson et al. in Ref. [51] showed that for two circular localized structures with interaction fields given by expression (6), the temporal evolution of $\boldsymbol{R}$ is

$$\frac{d\boldsymbol{R}}{dt} = \frac{\boldsymbol{R}}{R^2}\frac{d}{dR}\left[e^{-c_1 R}\cos(c_2 R)\right], \tag{7}$$

where $R = ||\boldsymbol{R}||$ is the magnitude of the vector of relative position.

B. Dimer approach

The extension of the above calculation for rod structures requires the derivation of the asymptotic field for the rod structure, which must include an azimuthal dependency given by the shape of the structure, not having this information makes the calculations non-viable. To avoid this impediment, the rod structure can be modeled as a dimer, that is, the rod structure is composed by two localized spots separated by a distance d between the centers. Figure 8.1 shows a rod-like structure and the respective approximation of two localized spots, which are emphasized by dashed lines. Therefore, the interaction field of the rod structure is constructed by the composition of the corresponding interaction fields of the two localized spots. With the dimer approximation, considering a diluted regime, this is, evaluating the field at a distance r from the middle of the rod much larger than the size of the spots ($r \gg d$), the force field can be written

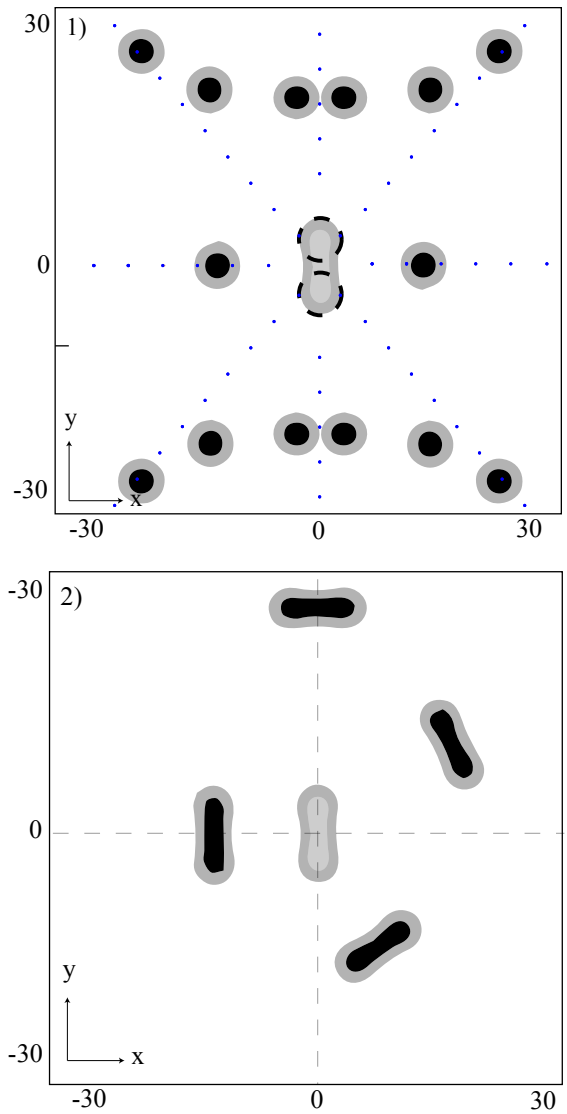

FIG. 8. (Color online) Dimer approach to rod structure. 1) Rod-LS numerical equilibrium points (black dots) and dimer-LS approximated analytical equilibriums (blue dots), the dimer is represented by black dashed lines. 2) Some characteristic points of equilibrium between rod structures. Simulations of the Swift-Hohenberg model, Eq. (1), with $\nu = 2.0$, $\eta = -0.355$, $\epsilon = 1.2$, and specular boundary condition, considering only two structures at a time, central rod structure is considered static.

as

$$\boldsymbol{F}_{dimer}(r,\theta) = \frac{\boldsymbol{R}_-}{R_-^2}\frac{d}{dR_-}\left[e^{-c_1 R_-}\cos(c_2 R_-)\right] \frac{\boldsymbol{R}_+}{R_+^2}\frac{d}{dR_+}\left[e^{-c_1 R_+}\cos(c_2 R_+)\right],$$

where $\boldsymbol{R}_\pm = \boldsymbol{r} \pm \boldsymbol{d}/2$, and $\boldsymbol{d}$ is a vector of size d, which points in the semi-major axis of the rod-like structure and $\boldsymbol{r}$ is the radial unit vector.

This field approximation yield the equilibrium points

for a test structure shown as small blue spots in Fig. 8.1. Agreement with numerical observations for the interaction between a rod and a circular localized structure can only be seen for the structures further from the origin, as the validity of the force field approximation is valid only for $r \gg d$, however the approximation does not predict the existence of multiple diagonal equilibriums as observed in Fig. 8.1. More complex is the rod-rod interaction, for their azimuthal asymmetry reflected on its axial elongation. This adds and angular degree of freedom for the positioning of a rod structure at each equilibrium point (see Fig. 8.2). The variety of equilibriums exhibited by these new type of structure allow the existence of diverse complex arrangements when multiple rod structures are considered. Figure 9 shows some of the stable crystal-type structures, that we have constructed from rod-rod interaction.

The interaction of a larger number of rods (i.e. covering all the available space) increases the number of possible equilibrium configurations. The multiple interaction drives the system sometimes to equilibriums which were unstable in the rod-rod interaction scenario, in Figs. 9.1, 9.2, and 9.3, dashed lines indicate rod-rod equilibriums which are unstable in an isolated environment and stabilize under the presence of multiple structures. Crystal-type structure shows in Fig. 9.4 is constructed based on the T-like equilibrium position, orthogonal rod structures, exhibited by the rod-rod interaction.

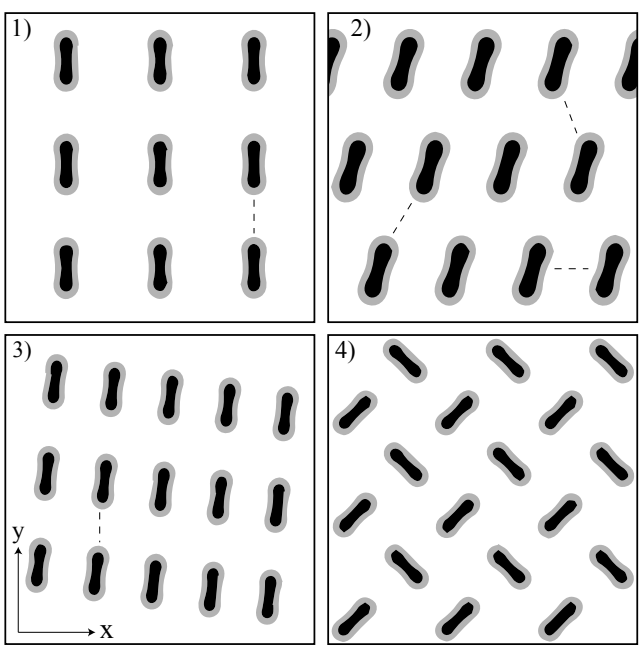

FIG. 9. (Color online) Tailored crystal-type configurations generated by the collocation of rod structures for the Swift-Hohenberg model, Eq. (1) with $\nu = 2.0$, $\eta = -0.355$, $\epsilon = 1.2$ and periodic boundary conditions.

VI. NON-VARIATIONAL STABILIZATION

The generalized Swift-Hohenberg model, Eq. (1), has a non-variational extension deduced in the context of liquid crystals for bouncing localized states [52] and deduced from chemical, biological and optical models [53] this equation reads (Lifshitz normal form)

$$\frac{\partial u}{\partial t} = \eta + \epsilon u - u^3 - \nu \nabla^2 u - \nabla^4 u + b u (\nabla^2 u) + c (\nabla u)^2, \quad (8)$$

which (excluding the case where $b = 2c$) is non-variational, this is, it is not derived from a Lyapunov functional. Thus, this model can exhibit complex and permanent behaviors such as oscillations, chaos and other spatiotemporal dynamics. The last two terms of Eq. (8) correspond, respectively, to nonlinear diffusion, being b the nonlinear diffusion coefficient, and nonlinear advection.

Numerically, we have observed that for small range of parameters b and c, the rod structure persists by only changes on its spatial size. For constant values of ϵ and η, increasing b or decreasing c, affects the structure, by making it shorter. While decreasing b or increasing c enlarges the structure, making it longer. For a larger stable rod structure, the bifurcation characteristic times τ are smaller, thus, decreasing b (or increasing c) triggers a faster dynamic of the system, for example, in the labyrinth formation process or splitting. For fixed values of the parameters, $\epsilon = 1.2$, $\eta = -0.355$ and $\nu = 2.0$ the range of b and c for which the rod structure is stable are approximately $b = [-0.017, 0.015]$ and $c = [-0.007, 0.008]$. Despite the small range of b and c for which the rod is stable, the possibility of existence of rod structures in non variational systems opens the possibility for searching this structure in a wider range of experimental set-ups.

VII. CONCLUSIONS

An asymmetric localized solution for the isotropic generalized Swift-Hohenberg model in two and three space dimensions has been found. This solution called rod structure breaks the azimuthal symmetry, remaining invariant only with respect to a rotation of π around any axis on the (x, y)-plane which contains the centre of the localized structure. The existence, bifurcation diagram, stability properties and interaction have been addressed. The question if this type of solution exist in other isotropic systems remain, so is the possibility of experimental observation.

ACKNOWLEDGMENTS

M.G.C. thanks the financial support of FONDECYT project 1150507. I.B. is supported by CONICYT, Beca de Magister Nacional numero XXXXXX.

[1] P. Glansdorff and I. Prigogine, *Thermodynamic Theory of Structures, Stability and Fluctuations* (Wiley, New York, 1971).

[2] G. Nicolis and I. Prigogine, *Self-Organization in Non Equilibrium Systems* (J. Wiley & Sons, New York, 1977).

[3] L. M. Pismen, *Patterns and Interfaces in Dissipative Dynamics* (Springer, Berlin, 2006).

[4] M. C. Cross, P. C. Hohenberg, Rev. Mod. Phys. **65**, 851 (1993).

[5] H.G. Purwins, H.U. Bodeker and S. Amiranashvili, Adv. Phys. **59**, 485 (2010);

[6] O. Descalzi, M. Clerc, S. Residori, and G. Assanto, Localized States in Physics: Solitons and Patterns (Springer, New York, 2011);

[7] W. van Saarloos, and P.C. Hohenberg, Phys. Rev. Lett. **67**, 749 (1990).

[8] P. Coullet. Int. J. Bifurcation and Chaos, **12**, 2445 (2002).

[9] P. Coullet, C. Riera, C. Tresser, Phys Rev. Lett. **84**, 3069 (2000).

[10] P. D. Woods and A. R. Champneys, Physica D **129**, 147 (1999); P. Coullet, C. Riera, and C. Tresser, Phys. Rev. Lett. **84**, 3069 (2000).

[11] F. Haudin, R. G. Rojas, U. Bortolozzo, S. Residori, and M.G. Clerc, Phys. Rev. Lett. **107**, 264101 (2011).

[12] H. A. Eschenfelder, *Magnetic Bubble Technology* (Springer Verlag, Berlin, 1981).

[13] J. Wu, R. Keolian and I. Rudnick, Phys. Rev. Lett. **52**, 1421 (1984).

[14] M.G. Clerc, S. Coulibaly, N. Mujica, R. Navarro, and T. Sauma, Phil. Trans. R. Soc. A **367**, 3213 (2009).

[15] K-Jin Lee, W. D. McCormick, J. E. Pearson, and H. L. Swinney, Nature (London) **369**, 215 (1994).

[16] P. Umbanhowar, F. Melo, H, Sweeney, Nature **382**, 793 (1996).

[17] M.G. Clerc, P. Cordero, J. Dunstan, K. Huff, N. Mujica, D. Risso, and G. Varas, Nature Physics, **4**, 249 (2008).

[18] S. Pirkl, P. Ribiere, and P. Oswald, Liq. Cryst. **13**, 413 (1993),

[19] M.G. Clerc, A. Petrossian and S.Residori, Phys. Rev. E **71**, 015205 (2005).

[20] U. Bortolozzo, L. Pastur, P.L. Ramazza, M.tlidi, and G. Kozyreff, Phys. Rev. Lett. **93**, 253901 (2004).

[21] U. Bortolozzo, M.C. Clerc, C. Falcon, S. Residori, and R. Rojas, Phys. Rev. Letts. **96**, 214501 (2006).

[22] O. Lioubashevski, Y. Hamiel, A. Agnon, Z. Reches, and J. Fineberg, Phys Rev. Lett. **83**, 3190 (1999).

[23] Y. Astrov, Y. Logvin, Phys. Rev. Lett. **79**, 2983 (1997).

[24] R. Heinrichs, G. Ahlers, and D. S. Cannell, Phys. Rev. A **35**, R2761 (1987).

[25] P. Kolodner, D. Bensimon, and C. M. Surko, Phys. Rev. Lett. **60**, 1723 (1988).

[26] F.T Arecchi, S. Boccaletti, P.L. Ramazza, Phys. Rep. **318**, 1 (1999).

[27] B. Schapers, M. Feldmann, T. Ackemann, W. Lange, Phys. Rev. Lett. **85**, 748 (2000).

[28] S. Barland et al., Nature (London) **419**, 699 (2002).

[29] E. Moses, F. Fineberg, and V. Steinberg, Phys. Rev. A **35**, 2757 (1987).

[30] M. Dennin, G. Ahlers, and D.S. Cannell, Phys. Rev. Lett. **77**, 2475 (1996).

[31] J. Swift and P. C. Hohenberg, Phys. Rev. A **15**, 319 (1977).

[32] MF. Hilali, G. Dewel, and P. Borckmans, Phys. Lett. A **217**, 263 (1996).

[33] R. Lefever, N. Barbier, P. Couteron, and O. Lejeune, J. Theor. Biol. **261**, 194 (2009).

[34] M. Tlidi, M. Georgiou, and P. Mandel, Phys. Rev. A **48**, 4605 (1993).

[35] J. Lega, J. V. Moloney, and A. C. Newell, Phys. Rev. Lett. **73**, 2978 (1994).

[36] L. D. Landau and E. M. Lifshitz, *Statistical Physics*, (Pergamon Press, New York, 1968) 2nd ed., Chap. XIV.

[37] R. M. Hornreich and M. Luban, Phys. Rev. Lett. **35**, 1678 (1975); R. M. Hornreich, J. Magn. Magn. Mater., 15, 387 (1980).

[38] A.G. Vladimirov, R. Lefever, and M. Tlidi, Phys. Rev. A **84**, 043848 (2011).

[39] P. Coullet, C. Riera, and C. Tresser, Prog. Theor. Phys. Supp. **139**, (2000).

[40] F. del Campo, F. Haudin, R. G. Rojas, U. Bortolozzo, M.G. Clerc and S. Residori Phys. Rev. E **86**, 036201 (2012).

[41] I. Bordeu, M.G. Clerc, R. Lefever, and M. Tlidi, submitted to Communications in Nonlinear Science and Numerical Simulation.

[42] P. Coullet, C. Elphick, and D. Repaux, Phys. Rev. **58**, 431 (1987).

[43] M.G. Clerc and C. Falcon, Physica A **356**, 48 (2005).

[44] U. Bortolozzo, M.G. Clerc, and S Residori, New J. Phys. **11**, 093037 (2009).

[45] I. Aranson, K. Gorshkov, A. Lomov, and M. Rabinovich, Physica D **43**, 435 (1990).q

[46] S. H. Strogatz, *Nonlinear Dynamics and Chaos: With Applications to Physics, Biology, Chemistry and Engineering*, (Addison-Wesley, Reading, MA, 1994).

[47] M. Tlidi, P. Mandel, And R. Lefever, Phys. Rev. Lett. **73**, 640. (1994)

[48] K. Kawasaki and T. Otha, Physica (Amsterdam) A **116**, 573 (1982).

[49] M.G. Clerc, S. Coulibaly and D. Laroze, EPL, **90**, 38005 (2010).

[50] Y. Pomeau, Physica D **23**, 3 (1986).

[51] I.S. Aranson, K.A. Rorshkov, A.S. Lomov, and M.I. Rabinovich, Physica D **43**, 435 (1990).

[52] M. G. Clerc, A. Petrossian, and S. Residori, Phys.Rev.E **71**, 015205(R) (2005).

[53] G. Koryreff and M. Tlidi, Chaos: An Interdisciplinary Journal of Nonlinear Science **17**, 037103 (2207).

Appendix C

This appendix is a copy of the manuscript entitled: **Labyrinthine dissipative patterns.**

Preprint submitted to the *Journal of Physics: Conference Series.*

Corresponding author: Ignacio Bordeu Weldt.

This work shows the results presented in Chapter 5.

Labyrinthine dissipative patterns

I Bordeu

Departamento de Fsica, Facultad de Ciencias, Universidad de Chile, Santiago, Chile.

E-mail: ibordeu@gmail.com

Abstract. A wide range of physical systems exhibit labyrinthine patterns as transient or steady states. One of the routes by which labyrinths emerge is through the destabilization of a localized structure through a curvature instability. In this work we will study the emergence of labyrinths through this mechanism in different physical contexts, ranging from non-linear cavity optics, vegetation dynamics and chemical reactions. Furthermore it will be shown that the resulting labyrinths can be classified depending on their connectivity properties.

1. Introduction

Systems which are kept out of thermodynamic equilibrium can exhibit multistability of states. These states can be homogeneous or inhomogeneous. The latter are sustained by the injection and dissipation of energy and/or momentum, and correspond to a mechanism by which systems self-organize [1, 2], minimizing–at least locally–some physical quantity. In variational systems this quantity is their energy, sometimes called nonequilibrium or Lyapunov potential [3]. Is in this context that spatial structures emerge. These structures can be localized, this is, they are finite domains that occupy only a portion of the available space, or extended, corresponding to periodic spatial structures which possess a characteristic wavelength that define them [4, 5, 6].

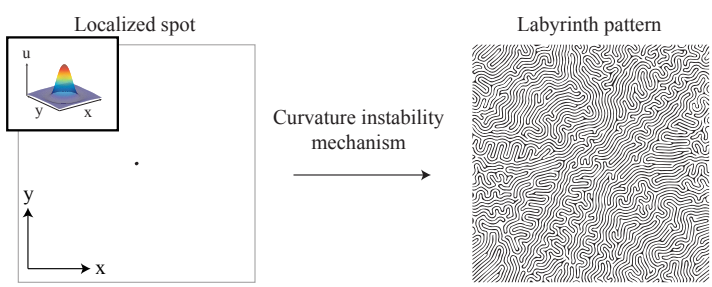

Figure 1. Curvature instability mechanism: Initially circular localized structure (left) and time evolved extended labyrinthine pattern final state (right) for Eq. (1). Parameters $\eta = -0.065$, $\epsilon = 2.45$, $\nu = 2.0$. Pseudo-spectral simulation (periodic boundary conditions), grid of 1024×1024 points and spacing $dx = 0.5$. Black indicates higher field values.

It has been observed that a wide range of dissipative systems exhibit a state (or multiple states) of equilibrium in which labyrinth structures are formed, such as, experimental observations in magnetic fluids [7], cholesteric liquid crystals [8, 9], Langmuir monolayers

[10], vegetation patterns [11], nonlinear cavity optics [12], among others. Such structures are characterized by having a well defined wavelength but a small correlation length, this is, the pattern has no privileged direction, generating in this way a sophisticated spatial structure [13]. This definition is purely statistical, thus, based on the average spatial distribution of the structure. In this work it will be shown that the route by which a localized structure evolves into a labyrinth reported in ref. [14] is universal, thus, observed in a wide range of physical systems. First, through a paradigmatic nonlinear equation, a modified Swift-Hohenberg equation [15], the route by which a localized spot loses stability to form a labyrinth pattern will be introduced. Here, an initially localized structure suffers an elliptical deformation and elongates, this elongation generates a rod-like structure, which in turn, suffers from a transversal instability propagating to all available space in the form of a labyrinth structure [14]. Based on this result, I will test the universality of the mechanism presented by showing its existence in other physical contexts. Namely, through a general competition-redistribution type of model and through the Gray-Scott reaction-diffusion model it will be shown that the transition from localized to extended structure is also observed in the context of dynamic vegetation and chemical reactions, respectively. The different types of labyrinths observed will lead us to define a simple classification of the labyrinth structures based on their connectivity properties.

2. From a localized spot to a extended labyrinth

2.1. Modified Swift-Hohenberg equation

It has been recently described how a localized structure loses stability, elongating and suffering a transversal instability to then generate an extended labyrinthine pattern [14]. Here, a generalization of the Swift-Hohenberg equation is presented. This is a real isotropic, symmetric under reflection, nonlinear partial differential equation. It was deduced originally to describe the amplitude of the pattern formed by Benard convection cells [15]. The modified Swift-Hohenberg equation includes an extra term which breaks the field reflection symmetry. It was deduced as an approximation to the Maxwell-Bloch equations, in the context of non-linear cavity optics to describe the nascent optical bistability with transversal effect [16, 17]. The modified Swift-Hohenberg equation reads

$$\frac{\partial u(x,y,t)}{\partial t} = \eta + \epsilon u(x,y,t) - u(x,y,t)^3 - \nu\nabla^2 u(x,y,t) - \nabla^4 u(x,y,t), \tag{1}$$

where $u = u(x,y,t)$ is a real scalar field, x and y are spatial coordinates and t is time. The field $u(x,y,t)$ accounts for the amplitude of the electric field and the bifurcation parameter ϵ measures the input field amplitude. The η parameter breaks the field reflection symmetry $u \to -u$. The parameter ν stands for the diffusion coefficient, positive values of ν lead to a pattern forming instability. The 2D Laplacian operator $\nabla^2 = \partial^2_{xx} + \partial^2_{yy}$ and the 2D bilaplacian operator ∇^4 act on the transverse plane (x,y), and they stand for the transport mechanisms or spatial coupling. It should be noted that by a displacement of the field $u \to u + u_0$, where u_0 is a constant term, Eq. (1) can be rewritten by removing the parameter η but including a term proportional to u^2, the equation including the quadratic term has been widely studied in various contexts (see the textbook [4] and the references therein).

The modified Swift-Hohenberg equation (1) possess a gradient form, i.e.

$$\frac{\partial u}{\partial t} = -\frac{\delta F[u, \nabla u, \nabla^2 u]}{\delta u}, \tag{2}$$

where F is the Lyapunov functional or energy [18] and reads

$$F \equiv \iint_{\mathbb{R}^2} dxdy \left[-\eta u - \epsilon\frac{u^2}{2} + \frac{u^4}{4} - \nu\frac{(\nabla u)^2}{2} + \frac{(\nabla^2 u)^2}{2} \right] \tag{3}$$

here its clear that the η term accounts for the asymmetry between the homogeneous states. By using the solutions of Eq. (1), this functional satisfies

$$\frac{dF}{dt} = -\iint_{\mathbb{R}^2} dxdy\,(\partial_t u)^2 \leq 0. \tag{4}$$

This property guarantees that a system described by Eq. (1) evolves towards a state of minimal energy. The modified Swift-Hohenberg equation exhibits for $\epsilon > 0$ coexistence between homogeneous and pattern states [19, 20], this allows the existence of stable localized structures.

This localized structures are azimuthally symmetric and occupy only a portion of the available space (see Fig. 1 left image).

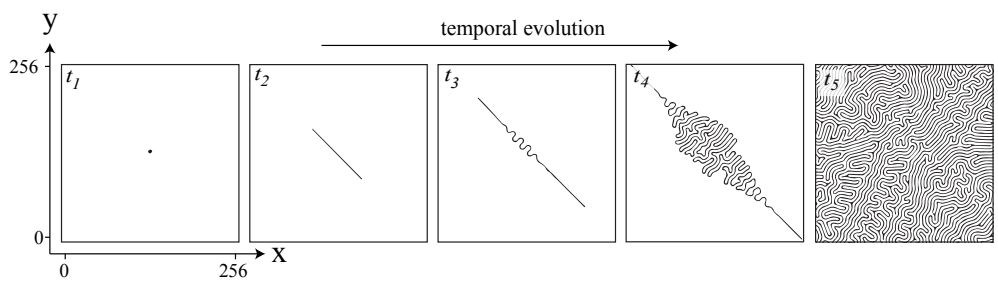

Figure 2. Curvature instability mechanism for the generation of a labyrinth from a localized structure as initial condition for the modified Swift-Hohenberg equation (1). Simulation made for parameters $\eta = -0.065$, $\epsilon = 2.45$, $\nu = 2.0$. Pseudo-spectral method was used by periodic boundary conditions, grid of 1024×1024 points and spacing $dx = 0.5$. Black indicates higher field values.

As described in reference [14] Eq. (1) supports a curvature instability over localized spots. This instability deforms the spot into an elongated elliptical shape, producing a rod-like structure. This rod structure suffers from a transversal instability, undulations appear in its core. The non-saturating dynamics that follow take the system into an extended seemingly disordered structure that covers all the available space. Such structure shall be called a labyrinthine pattern or simply labyrinth, which is characterized for not having a global order. Due to the variational origin of Eq. (1) and given that the temporal dynamic moves towards a minimum of the Lyapunov functional Eq. (4), we know that the labyrinthine structure will reach a stationary state asymptomatically. In this case, the labyrinth is composed by a single interconnected structure or invaginated structure [14] (which protrudes from the more stable homogeneous state). Defects such as, dislocations, disinclination, and phase fronts contribute to the spatial disorder of the labyrinth. This behaviour occurs far from any pattern forming instability and exists in a regime of bistability between homogeneous steady states.

3. Vegetation and chemical reaction models

The curvature instability mechanism for the formation of labyrinthine patterns from initially localized structures requires of few ingredients as the phenomena is observed even in the simplest of the pattern forming equations as is Eq. (1).

3.1. Competition-redistribution model

In this section, a minimal but general model for vegetation pattern forming systems will be introduced. In this model the curvature instability mechanism also emerges in a regime of bistability of homogeneous steady states far from the pattern forming instability.

The emergence of spatial organization in extended landscapes has been an intriguing phenomena for both botanists and non-linear science community for decades and are still a matter of great discussion [21, 22, 23]. One of the transversal agreements among scientists is that competition for soil resources such as water and nutrients leads to self-organization of vegetation. Depending on the topography of the terrain, the climate conditions and the vegetation specie, the process of self-organization leads to the formation of a wide variety of patterns, such as, tiger bush [21], or fairy circles [22, 23].

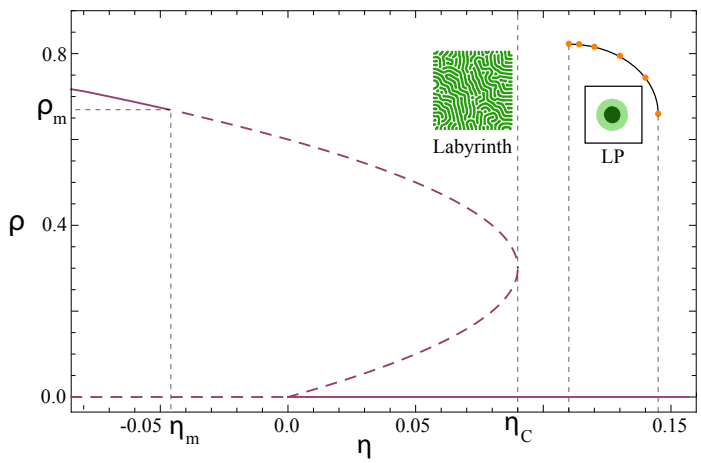

Figure 3. Bifurcation diagram of homogeneous plant population states (purple), dashed lines indicate unstable regime, and curve of stability of localized structures (dots). When the aridity η is decreased below η_c the curvature instability mechanism is observed.

Taking into account relation that exists between the structure of individual plants and the competition-facilitation interactions in a vegetation community is that the generic interaction-redistribution models emerge [24, 26]. These models have been successful in the prediction of formation of localized structures in arid and semi-arid environments where the resource scarcity induces high competition between plants through their root networks. In this context, a localized structure emerges as a patch of vegetation in an unpopulated homogeneous state. By considering a logistic equation with nonlocal coupling between plants, Tlidi et al. [27] where able via a weak gradient approximation, to deduce a mean-field nonlinear partial differential equation for the temporal evolution of the phytomass density $\rho(x, y, t)$:

$$\partial_t \rho = -\rho\left(\eta - \kappa\rho + \rho^2\right) + (\Delta - \Gamma\rho)\nabla^2\rho - \alpha\rho\nabla^4\rho, \tag{5}$$

where (x, y) and t are the spatial coordinates and time, respectively. This equation supposes an homogeneous and isotropic environment. The parameters: η accounts for the decrease-to-growth rate ratio; κ is the facilitation-to-competition susceptibility ratio; Δ is proportional to the square root of the facilitation-to-competition range ratio, this three parameters are positive-defined. The parameters Γ and α are the nonlinear diffusion coefficients. The existence of a nonlinear diffusion and hyperdiffusion is fundamental for Eq. (5) to satisfy the physical constrain for the phytomass density $\rho(\boldsymbol{r}, t) \geq 0$. However presence of non-linear diffusion terms $u\nabla^2 u$ and $u\nabla^4 u$ render Eq. (5) nonvariational, thus, it cannot be written ar the variation of a Lyapunov functional. Nonvariational systems can exhibit complex spatiotemporal dynamics, such as chaos, intermittency, among others. These nonvariational terms are imputable to the dispersion process. If the dispersion is negligible then equation (5) is similar to the variational

Swift-Hohenberg, Eq. (1) where the coefficients of $\nabla^2 u$ and $\nabla^4 u$ are both independent of the field variable.

The real order parameter equation (5) constitutes the simplest model of spatial dynamics in which competitive interactions between individuals occur locally.

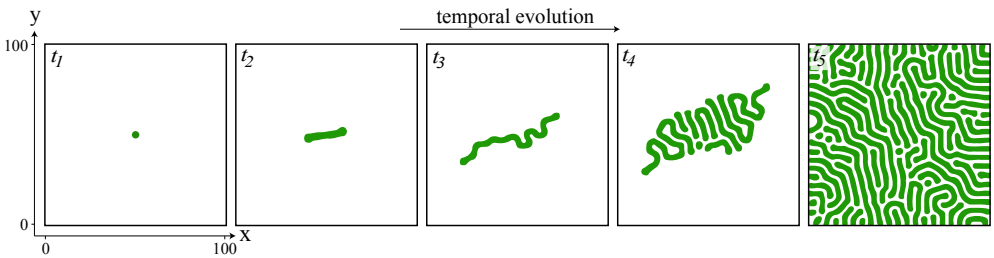

Figure 4. Curvature instability mechanism for the generation of a labyrinth from a localized patch as initial condition for the interaction-redistribution model Eq. (5). Simulation made for parameters $\eta = 0.085$, $\epsilon = 0.6$, $\Delta = 0.005$, $\Gamma = 0.5$ and $\alpha = 0.125$. Finite differences method was used by periodic boundary conditions, grid of 200×200 points and spacing $dx = 0.5$. Green indicates higher field values.

The homogeneous solutions of Eq. (5) are (i) $\rho_s^0 = 0$, which correspond to a territory without vegetation (ii) an two non-zero states given by $\rho_{s\pm} = (\kappa \pm \sqrt{\kappa^2 - 4\eta})/2$. For physical reasons phytomass density can only be positive or zero (see Fig. 3). When $\kappa \leq 0$, only the homogeneous steady state ρ_{s+}, defined is consistent, for $\eta < 0$. It decreases monotonously with μ and vanishes at $\eta = 0$. When $\kappa > 0$, the viable homogeneous solution extends up to the limit point $\rho_L = \kappa/2$ and $\eta_L = \kappa^2/4$. In the range $0 < \eta < \eta_L$, the biomass density exhibits a bistable behaviour: the stable homogeneous branches of solutions ρ_s^0 and ρ_{s+} coexist with the intermediate unstable branch ρ_{s-}.

The upper homogeneous state ρ_{s+} undergoes a Turing instability characterized by the wavelength

$$\Lambda_m = 2\pi\sqrt{2\alpha}/\sqrt{\Gamma/\alpha - \Delta/\rho_m} \tag{6}$$

which measure the distance between two maxima or minima of the plant distribution. The threshold associated with the this instability is solution of the following cubic equation:

$$(2\Gamma\rho_m - \Delta)^2 = 4\alpha\rho_m^2(2\rho_m - k). \tag{7}$$

There exist more than one threshold associated with the modulational instability. In the following, we focus on parameter regime where the uniform plant distribution exhibit bistability ($\kappa > 0$) and a portion of this state becomes unstable with respect to the Turing bifurcation ($\eta_m < \eta < \eta_L$). In this parameter range, any small fluctuation around the uniform plant distribution ρ_{s+} will trigger spontaneously the evolution of the system towards stationary, spatially periodic distributions of the biomass density which will invade the whole territory.

However, when a stable localized vegetation patch is considered as an initial condition (high aridity), see Fig. 3, and the aridity is then varied in such quantity that the system reaches the coexistence of homogeneous states, then the localized structure suffers and elliptical deformation caused by the curvature instability and elongates into a rod structure (see Fig. 4.t$_2$) in a process identical as previously observed for Eq. (1). Afterwards, the rod structure suffers from a transversal instability, only that in this case, the whole structure is compromised (see Fig. 4.t$_3$) and not only the central portion as in the Swift-Hohenberg case (Fig. 6.t$_3$). As time further increases, the labyrinthine structure invades all the system.

Here we have showed the appearance of the curvature instability mechanism over a localized structure which by turn generates the emergence of a labyrinthine structure.

3.2. Gray-Scott model

Pushing further the idea of universality of the curvature instability mechanism for the formation of labyrinths we now enter the domain of chemical reactions. It is well known that the reaction and diffusion of the components of a chemical reaction can produce an immense variety of spatial structures, such as lamelar structures and self-replicating spots [31, 28], localized structures [29, 30] and Turing structure [32, 31, 33], and exhibit complex spatiotemporal dynamics, such as oscillatory dynamics, breathing localized structure and spatiotemporal chaos [34, 35, 36].

In a series of seminal works P. Gray and S.K. Scott introduced a variant of the autocatalytic model of glycolisis first proposed by E.E. Sel'kov [34]. This prototype autocatalytic reaction (i.e. the product of the reaction is also the catalyst) is described by two irreversible processes:

$$\begin{aligned} A + 2B &\rightarrow 3B \\ B &\rightarrow C \end{aligned} \tag{8}$$

where A, B and C are chemical species, C is a non-reactive product (inert) and the system is kept out-of-equilibrium by a constant injection of A, called feeding [37, 38, 35]. Here, they show that this simple model presents multistability, hysteresis cycles, patterns, oscillatory dynamics and other exotic patterns.

Through a rescaling and including the diffusion phenomena in the reactions, a non-linear partial differential equation can be deduced for the temporal evolution of the concentrations U and V of A and B, respectively [31], this set of equations

$$\begin{aligned} \frac{\partial U}{\partial t} &= D_u \nabla^2 U - UV^2 + F(1-U), \\ \frac{\partial V}{\partial t} &= D_v \nabla^2 V + UV^2 - (F+k)V \end{aligned} \tag{9}$$

are an example of reaction-diffusion equations, as they model the local evolution U and V, and the diffusion process of the chemical species. In Eq. (9) D_u and D_v correspond to the diffusion coefficients associated to U and V, respectively. F represents the feed rate of the reactive A and dimensionless constant k (killing rate) accounts for the rate of the second reaction in Eq. (8). Alike the interaction-redistribution model presented for vegetation dynamics Eq. (5), the Gray-Scott model Eq. (9) does not have a known variational structure, which is the reason behind its rich phenomenology which includes, from oscillatory dynamics, self-replication [31] and chaos [36] and others mentioned before.

The existence and stability of patterns and localized spots (or single pulses) as homoclinic solutions of Eq. (9) has been well studied both in 1 and 2-dimensional cases [29, 39, 40, 41, 42]. This system supports a trivial homogeneous steady state $(U_0, V_0) = (1, 0)$ which is always stable. When the discriminator $d = 1-4(F+k)^2 > 0$ two additional homogeneous steady states $(U_\pm, V_\pm)$ appear, the first

$$(U_-, V_-) = \left(\frac{1}{2}(1+\sqrt{d}), \frac{F}{2(F+k)}(1-\sqrt{d}) \right) \tag{10}$$

is always unstable. The second state

$$(U_+, V_+) = \left(\frac{1}{2}(1-\sqrt{d}), \frac{F}{2(F+k)}(1+\sqrt{d})\right) \tag{11}$$

$$\tag{12}$$

is stable when $-V^2 + k < 0$ and $(F+k)(V^2 - F) > 0$. For $F > 1/4$ the system only exhibits the trivial steady state. For $F < 1/4$ and $k < 1/16$ the system exhibits three homogeneous steady states (one unstable). The bifurcation diagram for the homogeneous states is shown in Fig. 5. For a detailed study on the bifurcations and instabilities of Eq. (9) see ref. [33].

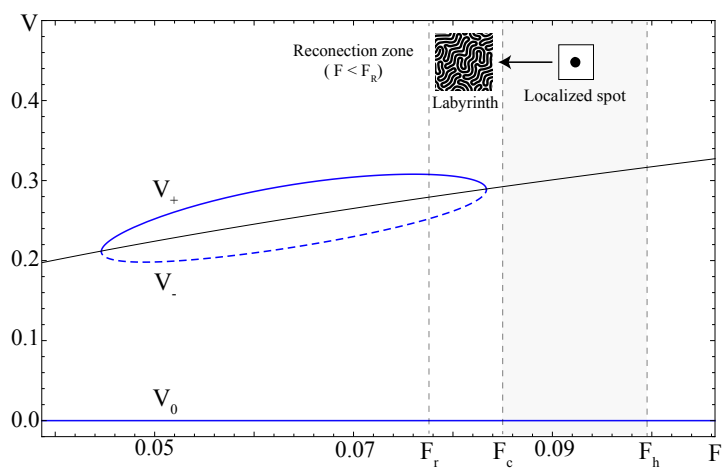

Figure 5. Bifurcation diagram the concentration V for $k = 0.061$, homogeneous states (blue), dashed lines indicate unstable regime. The $\sqrt{F}$-curve shows the position of the saddle-node bifurcation. For $F_c < F < F_h$ stable localized structures are observed (numerically). When changing the feeding parameter for a localized structure to values $F_r < F < F_c$, the curvature instability mechanism is observed. Reconnection zone indicates the zone where a radial instability is observed and structures can reconnect (see. Fig. 7). Here $F_h = 0.097$, $F_c = 0.085$ and $F_r = 0.078$.

As indicated in Fig. 5, localized structures live in $F_c < F < F_h$, is F is increased further the system falls to the homogeneous state $V = 0$. When the parameter F is reduced below F_c, perturbations become unstable and the structure suffers a curvature instability characterized by the elongation of the structure (see Fig. 6). As observed for the modified Swift-Hohenberg equation (1) and for the interaction-redistribution models (5) the concentration field suffers then a transversal instability characterized by the wiggling of the central section of the structure. Non saturating evolution leads to the formation of a complex labyrinthine structure as seen in Fig. 6.t_5.

When the feeding parameter is decreased further ($F < F_r$), an initially circular localized structure suffers from a radial instability as seen in Fig. 7.t_2, there two spots where given as initial conditions. As the radius of the structures grow, they suffer from a curvature instability. Non saturation causes the structure to propagate. Differently from what is observed from every labyrinthine structure showed previously, here the tips merge, this causes reconnection of the structures. In the transition from t_4 to t_5 one can realize that the two initially distinct structures reconnect into one single labyrinth.

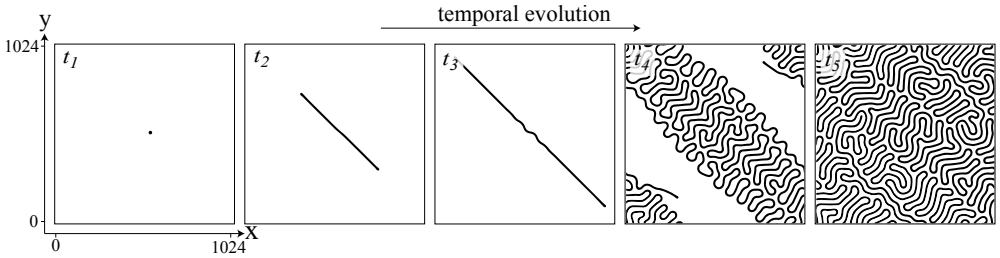

Figure 6. Curvature instability mechanism for the generation of a labyrinth from a localized concentration peak as initial condition for the Gray-Scott model (9). Simulation made for parameters $F = 0.080$, $k = 0.061$. Finite differences method was used with periodic boundary conditions, grid of 1024×1024 points and spacing $dx = 1$. Black indicates higher values of concentration V.

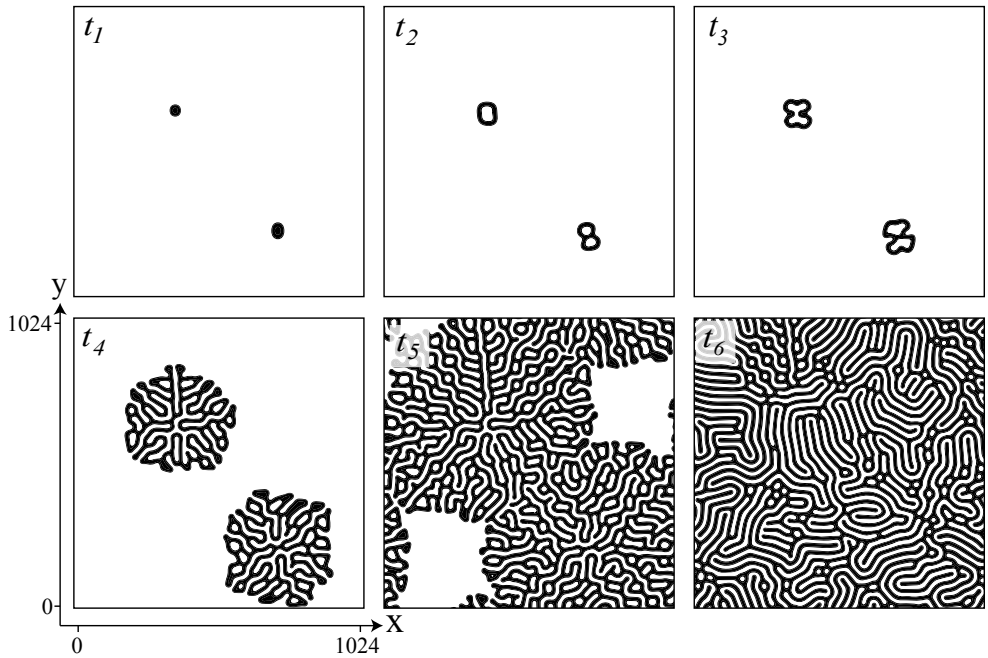

Figure 7. Alternative mechanism for the generation of a labyrinth from a localized concentration peak as initial condition for the Gray-Scott model (9). Simulation made for parameters $F = 0.070$, $k = 0.061$. In this parameter zone occurs reconnection between structures. Finite differences method was used with periodic boundary conditions, grid of 1024×1024 points and spacing $dx = 1$. Black indicates higher values of concentration V.

4. Labyrinth connectivities

The curvature instability of a localized structure was observed in the three systems presented previously. In the three cases (modified Swift-Hohenberg, interaction-redistribution and Gray-Scott models) an initially localized structure suffers from the curvature instability mechanism to finally fall into an extended labyrinthine structure. However each of these structures are different (see Figs. 2.t_5, 4.t_5, 6.t_5 and 7.t_6). Starting from a single localized structure the Swift-Hohenberg model Eq. (1), generates a single fully connected structure, this is, starting from any

point of the labyrinth, one can go over the whole structure without leaving the higher value field. The same happens in the fist labyrinth from the Gray-Scott model (c.f Fig. 6) only that in this case the structure shows no dislocations as the structure remains in a single line labyrinth. In the case of the interaction-redistribution model Eq. (4), starting from a single localized structure, the final labyrinthine state is disintegrated into a high number of small structures, thus, this labyrinth is highly disjoint. On contrary, when considering two initial structures in Fig. 7, the structures where able to reconnect increasing the connectivity from the initial state.

A classification of the labyrinth structures originated from localized initial states can be done based on the connectivity difference between the initial and the final states. If $\Delta = C_i - C_f$, where C_i and C_f are the initial and final number of disjoint structure, then, if $\Delta < 0$ we will say labyrinth is dissociative (the structure tends to divide), if $\Delta = 0$ it is neutral (structures preserve their identity) and if $\Delta > 0$ the labyrinth is associative (structures tend to merge). We can conjecture after the previous observations that the type of labyrinth that a system exhibits will depend on the capacity of a structure of preserving its integrity, here, surface tension (or line tension) which keeps the structure together will play a fundamental role. In this sense, the type of labyrinths a system exhibits can give information of the line tension properties of the system.

5. Conclusions

In this work the curvature destabilization of a localized structure had been show as a mechanism for the generation of extended labyrinthine patterns. Furthermore, the mechanism has been showed to exist in a wide range of physical systems including in vegetation dynamics through a general interaction-redistribution model and in chemical reactions through the Gray-Scott reaction diffusion equations. It has been shown that depending not only in the context in which labyrinths emerge but also on the parameters considered for simulation/experimentation different labyrinths emerge and even more, they can be classified as *associative*, *neutral* or *dissociative*, based on the difference between the initial and final connectivity of their structures. Future work will address quantitatively the effect of surface tension in the type of labyrinth formed.

Acknowledgements

I want to thank Professor Marcel G. Clerc for his constant support and valuable commentaries in the development of this work. I also wish to thank Professor Mustapha Tlidi for sharing with me his knowledge on vegetation dynamics. I also wish to thank the financial support from CONICYT, Beca de Magíster Nacional and the Departamento de Postgrado y Postítulo of the Vicerrectoría de Asuntos Académicos, Universidad de Chile.

References

[1] Glansdorff P and Prigogine I 1971 *Thermodynamic Theory of Structures, Stability and Fluctuations* (Wiley, New York).
[2] Nicolis G and Prigogine I 1977 *Self-Organization in Non Equilibrium Systems* (J. Wiley & Sons, New York).
[3] Graham R and Tel T 1984 *Phys. Rev. Lett.* **52** 1.
[4] Pismen L M 2006 *Patterns and Interfaces in Dissipative Dynamics* (Springer, Berlin).
[5] Cross M C and Hohenberg P C 1993 *Rev. Mod. Phys.* **65** 851.
[6] Descalzi O, Clerc M G, Residori S, and Assanto G 2011 *Localized States in Physics: Solitons and Patterns* (Springer, New York).
[7] Dickstein A J, Erramilli S, Goldstein R E, Jackson D P, and Langer S A 1993 *Science* **261**.
[8] Ribiere P and Oswald P 1990 *Journal de Physique* **51** 16.
[9] Oswald P, Baudry J, and Pirkl S 2000 *Physics Reports* **337** 1.
[10] Heinig P, Helseth L E, and Fischer Th M 2004 *New. J. Phys.* **6** 189.
[11] von Hardenberg J, Meron E, Shachak M, and Zarmi Y 2001 *Phys. Rev. Lett.* **87** 19.
[12] Taranenko V B, Staliunas K, and Weiss C O 1998 *Phys. Rev. Lett.* **81** 11.

[13] Le Berre M, Ressayre E, Tallet A, Pomeau Y, and Di Menza L 2002 *Phys. Rev. E.* **66** 026203.
[14] Bordeu I, Clerc M G, Lefever R, and Tlidi M 2015 *Communications in Nonlinear Science and Numerical Simulation* (to be published).
[15] Swift J and Hohenberg P C 1977 *Phys. Rev. A* **15** 319.
[16] Tlidi M, Georgiou M, and Mandel P 1993 *Phys. Rev. A* **48** 4605.
[17] Tlidi M, Mandel P, and Lefever R 1994 *Phys. Rev. Lett.* **73** 640.
[18] Vladimirov A G, Lefever R, and Tlidi M 2011 *Phys. Rev. A* **84** 043848.
[19] Coullet P, Riera C, and Tresser C 2000 *Prog. Theor. Phys. Supp.* **139**.
[20] del Campo F, Haudin F, Rojas R G, Bortolozzo U, Clerc M G and Residori S 2012 *Phys. Rev. E* **86** 036201.
[21] Lefever R and Lejeune O 1997 *Bulletin of Mathematical Biology* **59**.
[22] Juergens N 2013 *Science*, **339**.
[23] Fernandez-Oto C, Tlidi C, Escaff D, and Clerc M G 2014 *Philosophical Transactions of the Royal Society A: Mathematical, Physical and Engineering Sciences* **372**.
[24] Lefever R and Lejeune O 1997 *Bulletin of Mathematical biology* **59** 263.
[25] Lejeune O and Tlidi M 1999 *Journal of Vegetation Science* **10** 201.
[26] Martínez-García R, Calabrese J M, Hernandez-Garcia E, Lopez C 2013 *Geophysical Research Letters* **40** 6143.
[27] Lejeune O, Tlidi M, and Couteron P 2002 *Phys. Rev. E* **66**, 010901.
[28] Lee K J and Swinney H L 1995 *Phys. Rev. E* **51** 3.
[29] Koga S and Kuramoto Y 1980 *Progress of Theoretical Physics*, **63** 1.
[30] Vanag V K and Epstein I R 2007 *Chaos: An Interdisciplinary Journal of Nonlinear Science* **17** 3.
[31] Pearson J E 1993 *Science*, **261** 5118.
[32] Lee K J, McCormick W D, Ouyang Q, and Swinney H L 1993 *Science* **261** 5118.
[33] Mazin W, Rasmussen K E, Mosekilde E, Borckmans P, and Dewel G 1996 *Mathematics and Computers in Simulation* **40** 3.
[34] Sel'Kov E E 1968 *European Journal of Biochemistry* **4** 1.
[35] Gray P, Scott S K 1985 *The Journal of Physical Chemistry* **89** 1.
[36] Nishiura Y and Ueyama D 2001 *Physica D: Nonlinear Phenomena* **150** 3.
[37] Gray P and Scott S K 1983 *Chemical Engineering Science* **38** 1.
[38] Gray P and Scott S K 1984 *Chemical Engineering Science* **39** 6.
[39] Doelman A, Gardner R A, and Kaper T J 1998 *Physica D: Nonlinear Phenomena* **122** 1.
[40] Hale J K, Peletier L A, and Troy W C 2000 *SIAM Journal on Applied Mathematics* **61** 1.
[41] Wei J 2001 *Physica D: Nonlinear Phenomena* **148** 1.
[42] Muratov C B and Osipov V V 2002 *SIAM Journal on Applied Mathematics* **62** 5.

Appendix D

This appendix is a copy of the manuscript entitled: **Self-replication of localized vegetations patches in scarce environments.**

In preparation for being submitted to the *Physical Review X.*

This work will show the results presented in Chapter 6.

Self-replication of localized vegetation patches in scarce environments

I. Bordeu [*], **M. Tlidi** [†], **P. Couteron** [‡], **R. Lefever** [†] and **M. G. Clerc** [§]

[*]Departamento de Física, Facultad de Ciencias, Universidad de Chile, Santiago, Chile,[†]Faculté des Sciences, Université Libre de Bruxelles (ULB), CP 231, Campus Plaine, 1050 Bruxelles, Belgium,[‡]IRD, UMR AMAP, c/o Cirad, 34000 Montpellier, France, and [§]Departamento de Física, FCFM, Universidad de Chile, Casilla 487-3, Santiago, Chile

Submitted to Proceedings of the National Academy of Sciences of the United States of America

Desertification and the loss of fertile soil is a worldwide problem for both ecology and economy. Our ability to understand how vegetation manages to survive in arid and semiarid ecosystems can help in the development of future strategies to preserve or make use of scarce resources soil. In this article, we study a robust phenomena observed in semi-arid ecosystems, by which localized vegetation patches split in a process called self-replication. By observation of real ecosystems and comparing with theoretical and numerical analysis we show an underlying process of self-organization leading to pattern formation mediated by the self-replication process.

Vegetation | pattern formation | competition and facilitation | nonlinear dynamics

Abbreviations: NND, nearest neighbor distance

In arid and semi-arid landscapes of the African, American, Asian and Australian continents, it is common to encounter a non-uniform vegetation cover which exhibits large spatial scale structures, generically called vegetation patterns [1, 2]. These landscapes are characterized by either water limited resources and/or nutrient-poor territories. In the former case, the potential evapo-transpiration of the plants exceeds the water supply provided by rainfalls. At the level of individual plant, the water scarcity provokes an hydric stress that affects both the plants survival capacity and the plant growth. At the community level, this hydric stress promotes clustering behavior which induces spatial landscapes fragmentation. It is now generally admitted that this adaptation to hydric stress involves a symmetry-breaking modulational instability leading to the establishment of a stable spatial periodic pattern [3]-[23].

Vegetation patterns are not always periodic. The spatial distribution of vegetation cover, may consists of isolated or randomly distributed patches or gaps. Such irregular patterns can involve groves within grasslands [24, 25] or spots of bare soil within a grass matrix [26]. They consist of patches which are either isolated or in the form by clusters of patches . In both cases, such patterns have been interpreted as localized structures [24, 26, 8, 25] . A well documented example is the so-called fairy circles. They consist of circular areas devoid of vegetation embedded in an herbaceous vegetation. The aperiodic patterning phenomenon is not specific to peculiar soils or plants. Localized vegetation patches or gaps may develop on soil ranging from sandy and silty to clayey and the nature of vegetation may consist of grasses, shrubs and trees. The surface of vegetation patch can vary from small clumps of grasses (0.5-2 m^2) to large groves of mulga (Acacia aneura) trees (100-1000 m^2), such as those observed in central Australia [27]. On the other hand, the formation of localized pattern is an important issue not only in plant ecology context and environment science but also it is a multidisciplinary area of research involving physics, chemistry and mathematics [32].

Localized vegetation patches may exhibit a curvature instability that leads to a splitting of the patch into two new patches. An example of such behavior is shown in Fig. 1. This intriguing phenomenon often called spot-replication or fingering is well documented issue in the context of magnetic fluids [33], liquid crystals [34, 35], Chemical systems [36]-[47], in plant ecology [48], material science [49, 50], granular fluid systems [51, 52], and nonlinear optics [53]. The fingering instability of planar fronts leading to the formation of labyrinth structures has been reported by Hagberg et al. [54].

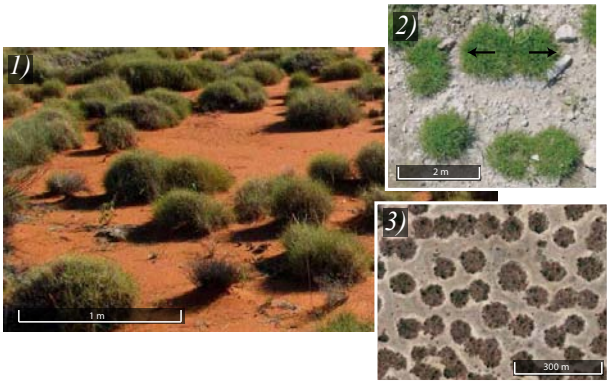

Fig. 1. (Color online) Localized patch instability. 1) Spinifex grassland, Yakabindi station, Western Australia (courtesy of Villis and Magi Nams). 2) Patterns of P. bulbosa observed in the Northern Negev [48]. 3) Satellite image showing localized vegetation patches, Zambia (Google Earth).

We investigate here the self-replication mechanism in the case of natural vegetation ecosystems. We show that this phe-

Significance

The stability of localized vegetation patches in semi-arid and arid landscapes is studied. Our analysis reveals that when the size of a single or more patches exceeds some critical size, an elliptical deformation affecting the circular shape of localized patches may occur. Splitting of the patches follows this curvature instability. Spots replicate themselves until they occupy the whole space available in a strictly isotropic environmental condition.

Reserved for Publication Footnotes

nomena is robust as it is observes in a wide range of species and size scales. We consider a general interaction-redistribution model, where numerical simulations and analytical analysis show that there exist a critical value of the level of the aridity under which a single circular patch grows up to a maximal diameter, the curvature instability leads to an elliptical deformation followed by patch multiplication. This process continue in time until the system reaches a self-organized vegetation pattern in an hexagonal form. Afterwards, we address the spatial organization problem and show how self-replication mediates the spatial distribution and propagation of the vegetation.

Field observations of self-replication

Location. Andes highlands are semi-arid ecosystems with a low amount of available resources. In particular, the Catamarca region in NW-Argentina (-23.436253°, -65.976767° at 3424 m a.s.l.), the average annual rainfall reaches 369 mm (source CRU CL 2.0), with a maximum in January of 71 mm and a minimum in July of 6 mm, temperature varies from warm in the day to sub-zero in the night. Here, it is well known that *Festuca orthophylla* which produces tall, evergreen tussocks dominates the landscape over extended areas and periods of time at elevations between 3225 and 4860 m a.s.l [55, 56].

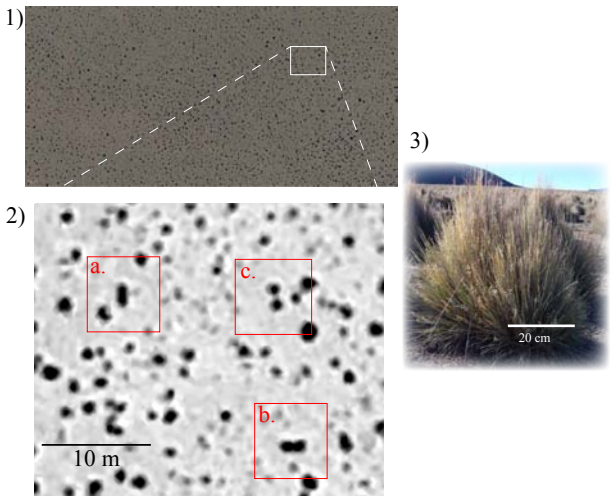

Fig. 2. Study site in the Catamarca region, dark spots correspond to *Festuca orthophylla* tussocks. 1) Satellite image showing localized vegetation patches (Google Earth) in the Catamarca region, Argentina. 2) Zoom of the region under study. 3) Average size tussocks of Festuca orthohylla in the Sajama National Park in the Bolivian Altiplano [56].

This specie is present in a variety of cold climates, adapting to diverse rainfall and soil moisture conditions. Festuca tussock arrange in circular shape compact structures composed by thousands of tightly packed tillers. The size of the tussocks depends on the resources available and weather conditions of their location, for instance, in western Bolivia they can reach 1.6 m [56]. An important characteristic of Festuca is their shallow rooting system, which has been reported to cover an area 6-fold the area of the above ground canopy [56]. This quality allows each plant to have access to the resources in a total area equivalent to 6-fold the area of the projected canopy, which is well known to be the most important mechanism to capture resources in highlands [56, 58]. This root distribution also allows tussock-tussock competition for resources, this will be important later on for understanding the spatial organization of the tussocks.

This site, was selected in order to have a minimal slope, and no topographic perturbations such as mountains, canyons, river or highways. The image obtained from Google Earth consists on a 4800x3562 pixels image, which corresponded to an area of 109.4 km^2 (384m x 285m), see Fig. 2.1.

Festuca structures are easily recognizable in the images for their high light absorption (they appear as black spots). As mentioned previously Festuca organizes in tightly packed structures of circular shape. An example of isolated circular patch is shown in Fig. 2.3. However, there is an important number of structure that have lost their circular shape. This modulational instability is the mechanism by which a tussock deform into an elliptical shape and consequently splits into two independent tussocks, we term this process self-splitting (see Fig. 2.2). This process is common to a wide range of species and scales, as observed in Fig. 1, where self-replications can be observed for structures in the scale of meters to hundreds of meters.

Spatial distribution analysis. The field image (Fig. 2.1) was used to study the spatial distribution of the tussocks. Detection of patches was performed through filtering, noise reduction and contrast enhancement of the image. Objects touching the border of the image were removed as they may not be completely observed, thus, they could introduce erroneous measurements to the analysis. The size of the structures that can be detected is lower-bounded by the satellite spatial resolution, nevertheless, we can hypothesize that the spatial distribution will be dominated by the bigger tussocks as a consequence of their fully developed shallow root systems.

After the detection of the patches, the boundaries of each object and their properties (area, centroid position, perimeter and equivalent diameter) can be precisely computed. The relation of meters per pixel is extracted directly from the image (20 m/250 pixels). A total of 3204 structures where detected. The first analysis, corresponded to detailed characterization of small distance properties such as nearest neighbor distance (NND), area covered and equivalent radius of each structure, this radius is calculated by comparing the area of the structure with that of a circle of that equivalent radius. The nearest neighbor distance is computed as the minimal boundary-to-boundary distance, this will allow us to extract some conclusions on the NND versus root sphere size. Canopy area and radius will be useful in understanding the underlying pattern emerging from redistribution and competition for resources. To expose the emergent spatial order in tussocks distribution, spatial Fourier analysis was performed in order to determine a characteristic wave number, circular integration was performed for a better presentation of the results. For the effect of Fourier analysis, a square sub-figure was selected from the original one. Finally, we have computed the Voronoi tessellation for the centres of the structures. This analysis, suitable for studying the regularity of a pattern has been used previously in aerial analysis to address pattern formation in vegetation structures [59]. For both NND and Voronoi cell computation, a subset of structures where selected such that they where far enough from the images border to avoid error induced from non visible structures.

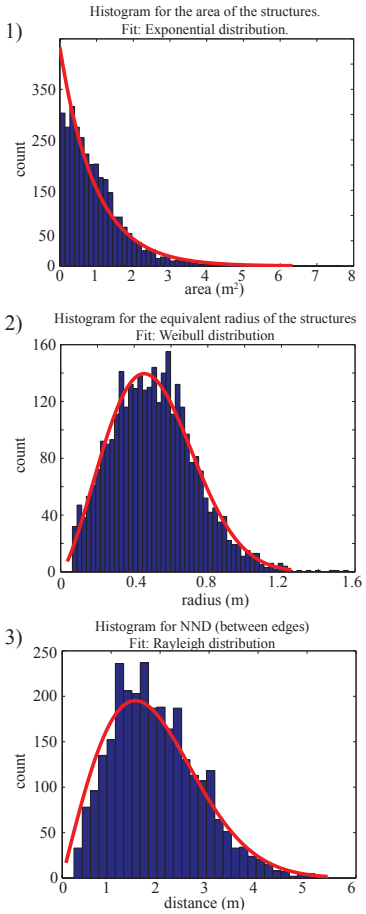

Fig. 3. Histograms for the 1) areas and 2) equivalent radius of the structures and 3) nearest neighbour distance between them.

Nearest neighbor distance and structure properties. From the image analysis of the aerial image from the Catamarca region in NW-Argentina a total area of 109.4 km^2 (384m x 285m) was studied. Structures found in the analysis ranged from an area of 0.012 m^2 to maximum area of 6.25 m^2 with a mean of 0.95±0.79 m^2 (see Fig. 3.1). By visual inspection, we have noticed that bigger structures are most probably evolving clusters of structures. The average equivalent radius was found to be 0.50±0.22 m as can be seen in Fig. 3.2. For calculating the minimal distance between the objects boundaries, only structures which are far enough from the image's border are considered, as the objects not captured in the image could be closer to these structures than the other observable ones. By this consideration, distances between 2837 objects are used. The distance between objects vary from 0.25 m to 4.63 m, and averaged a distance of 1.83±0.77 m (see Fig. 3.3).

Considering the average size and NND, and given that the distance between tussock is set under the constrain that the root spheres do not overlap, we can estimate the projected root sphere size of an average tussock as the half of the NND, this results in a root sphere of 1.4 m radius and 6.3 m^2 area, which corresponds to an area of 6.7-fold the area of the average structure. This is in agreement with previous field observations [57].

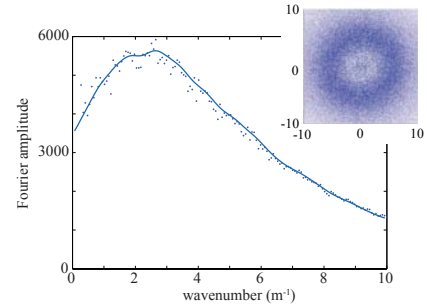

Fig. 4. Circular integration for spatial Fourier transform.

Fourier analysis. For the spatial Fourier analysis, we considered a square sub-figure of the original. This figure contained 1510 structures. The spatial Fourier transform is extensively used by pattern formation community to evaluate the degree of order. Pronounced peaks in the 2D Fourier amplitude indicate not only the existence of a characteristic length in the system but also a preferred spatial direction for the formation of the pattern.

From our spatial Fourier analysis we are unable to detect pronounced peak in the spectrum, indicating that there in no preferred direction for a pattern to form. However, in the circular integration of the spectrum, we observe a maximum wavenumber at k=2.4 m^{-1} (see Fig. 4), this is the first sign that the system is arranging in such a way that a characteristic length emerges ($L_c = 2\Pi$ /k = 2.6 m). As one would expect this characteristic length y related to the interaction between tussocks, no-overlap (between tussock root spheres) is achieved in average if the distance between the centres of the structures is at least 2.4 m according to estimations made in the previous section from the histogram analysis. Root competition between plants generates a minimal distance between tussocks.

Voronoi cells characterization. One of the problems of detecting patterns in natural ecosystems is the existence of high scale perturbations such as terrain inhomogeneities, weather conditions, wind, animal presence. All this external noise, alters the interaction between tussock therefore, mangles their ability to form a regular pattern. With no regular pattern, the task

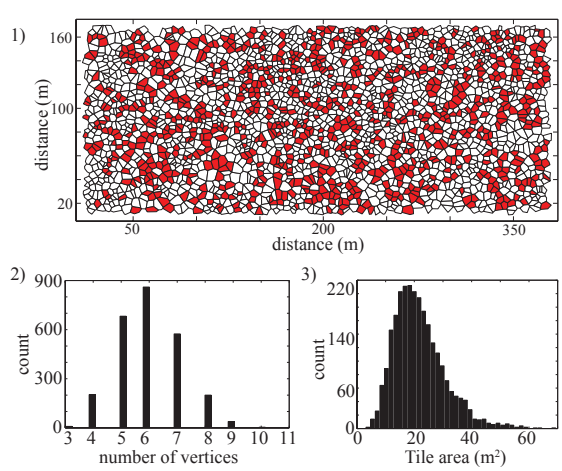

Fig. 5. Voronoi cell tessellation (top) 6-sided tiles are painted red. Histograms (bottom) for number of vertices in each cell (left), and tile area (right).

of finding some type of unitary cell in the tussoks arrangement can be facilitated by the introduction of the Voronoi tessellation [60]. Considering the centre of a structures, the Voronoi cell associated with that structure will correspond to all the points that are closer to its centre than to any other centre (see Fig. .1). In this sense, the Voronoi tessellation gives us information of the most probable cell arrangement. As it is observed (Fig. .2) the most probable vertex number is 6, which drive us to conjecture in a underlying tendency of Festuca tussocks to arrange in hexagons, this is reinforces by observing that 6-sided cells are clearly not randomly distributed but rather cluster in groups. Important data can also be extracted from the tile area (Fig. .3), each tile represent the amount of land that is closer to a certain tussock than to any other, thus the nutrients present in that portion of soil will be more accessible for the center tussock. The average tile size is 21.8 m^2, which corresponds to equivalent radius of 2.63 m, almost twice the radius estimated for the root sphere. This means that even when considering nearest neighbors, roots seem to determine the minimum distance, in a large scale, tussock disperse through the terrain. This can be understood as an exponential decay of the interaction between tussocks, where depending on the amount of space available, they will spread or tighten provided that the root spheres do not overlap.

Model equation for vegetation dynamics

Pattern formation in vegetated environments has been extensively studied both experimentally and theoretically. It is well known that competition for resources such as water leads to self-organization phenomenon. This process leads to the formation of a wide range of patterns that depends on the characteristics of both the environment and through root spatial underground distribution.

Several models describing vegetation patterns and self-organization in arid and semiarid landscapes have been proposed during last two decades. They can be classified into three types. The first approach often called a generic interaction-redistribution models. It is based on the relationship between the structure of individual plants and the facilitation-competition interactions existing within plant communities [3]-[12]. The second approach is based on the reaction-diffusion type of models. It takes into account of the influence of water transport by below ground diffusion and/or above ground run-off [13]-[19]. The third approach focuses on the role of environmental randomness as a source of noise induced symmetry breaking transitions [20, 21, 23].

In particular, the formation of localized structures in vegetation, also called localized vegetation patches has been studied in the case of poor resources, isotropic and homogeneous environment via a weak gradient approximation of the generalized logistic equation that described the non-local interaction between plants, a non-variational equation for the phytomass density $\rho(\boldsymbol{r}, t)$ was derived in [24]

$$\partial_t \rho = -\rho\left(\eta - \kappa\rho + \rho^2\right) + (\Delta - \Gamma\rho)\nabla^2\rho - \alpha\rho\nabla^4\rho, \qquad [1]$$

where $\boldsymbol{r}$ and t are the spatial coordinates and time, respectively. This equation contains three positive defined control parameters: η that account for the decrease-to-growth rate ratio; κ is the facilitation-to-competition susceptibility ratio; Δ is proportional to the square root of the facilitation-to-competition range ratio. The parameters Γ and α are the nonlinear diffusion coefficients. The real order parameter equation (1) constitutes the simplest model of spatial dynamics in which competitive interactions between individuals occur locally. An important feature of this equation is the presence of nonlinear diffusion terms $u\nabla^2 u$ and $u\nabla^4 u$ that render it non-gradient or nonvariational. These nonvariational terms are imputable to the dispersion process. If the dispersion is negligible then equation (1) is similar to the variational Swift-Hohenberg that is regularly derived in spatially extended systems. In that case, the coefficients of $\nabla^2 u$ and $\nabla^4 u$ are both independent of the biomass density.

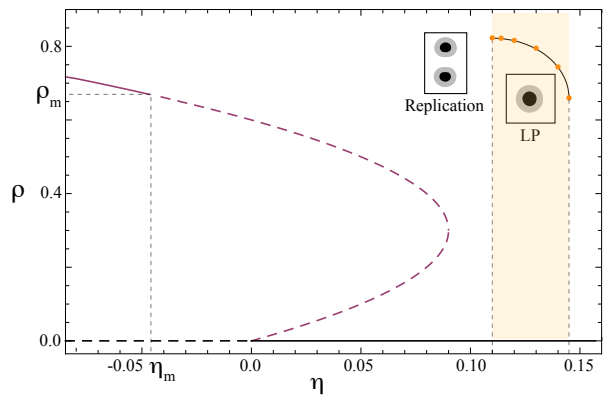

Fig. 6. (Color online) Bifurcation diagram of homogeneous plant population states (purple and black), dashed lines indicate unstable regime, and curve of stability of localized structures. The darkened area accounts for the region where localized patches (LP) are observed.

The homogeneous steady states; ρ_s; solutions of Eq. (1) are (i) no plant state, $\rho_s^0 = 0$, which corresponds to a territory devoid of vegetation and (ii) an homogeneous plant population $\rho_{s\pm} = (\kappa \pm \sqrt{\kappa^2 - 4\eta})/2$ where at each point of the territory, the vegetation production and death are exactly balanced. They should be real and positive. Two situations must be distinguished according to the sign of κ. When $\kappa \leq 0$, only the homogeneous steady state ρ_{s+}, defines the biomass density, for $\eta < 0$. It decreases monotonously with μ and vanishes at $\eta = 0$. When $\kappa > 0$, the physical part of homogeneous branch of solution extends up to the limit point $\rho_L = \kappa/2$ and $\eta_L = \kappa^2/4$. In the range $0 < \eta < \eta_L$, the biomass density exhibits a bistable behaviour: the stable homogeneous branches of solutions ρ_s^0 and ρ_{s+} coexist with the intermediate unstable branch ρ_{s-} as shown in Fig. 6. The former solution is always unstable even in the presence of homogeneous fluctuations.

The upper homogeneous state ρ_{s+} undergoes a modulational instability characterized by an intrinsic wavelength

$$\Lambda_m = 2\pi\sqrt{2\alpha}/\sqrt{\Gamma/\alpha - \Delta/\rho_m} \qquad [2]$$

which measure the distance between two maxima or minima of the plant distribution. The threshold associated with the modulational instability is solution of the following cubic equation:

$$(2\Gamma\rho_m - \Delta)^2 = 4\alpha\rho_m^2(2\rho_m - k) \qquad [3]$$

There exist more than one threshold associated with the modulational instability. In the following, we focus on parameter regime where the uniform plant distribution exhibit bistability ($\kappa > 0$) and a portion of this state becomes unstable with respect to the Turing bifurcation ($\eta_m < \eta < \eta_L$) as shown in Fig. 6. In this parameter range, any small fluctuation around the uniform plant distribution ρ_{s+} will trigger spontaneously the evolution of the system towards stationary,

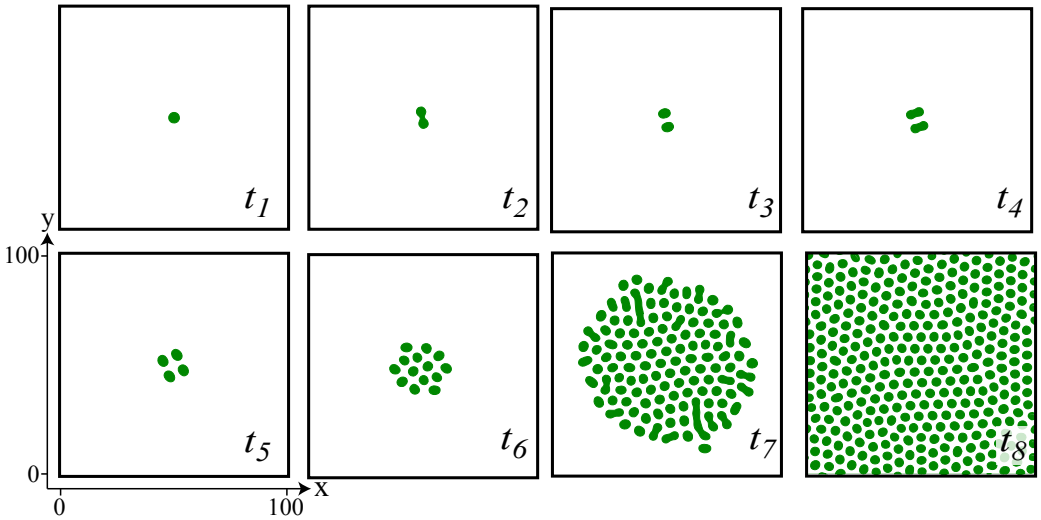

Fig. 7. (Color online) Localized patch self-replication of the vegetation model Eq. (1) for $\eta = 0.1$, $\kappa = 0.6$, $\Delta = 0.02$ $\Gamma = 0.5$, and $\alpha = 0.125$, integration grid 200×200. Temporal evolution is from left to right panels, and from top to bottom ones, $t_1 < t_2 < t_3, \cdots$. The localized patch suffers a curvature instability subsequently accompanied by the emergence of two spots. In turn these spots suffer a similar instability thus generating more spots, which begin to invade the system generating the emergence of a hexagonal pattern with several defects.

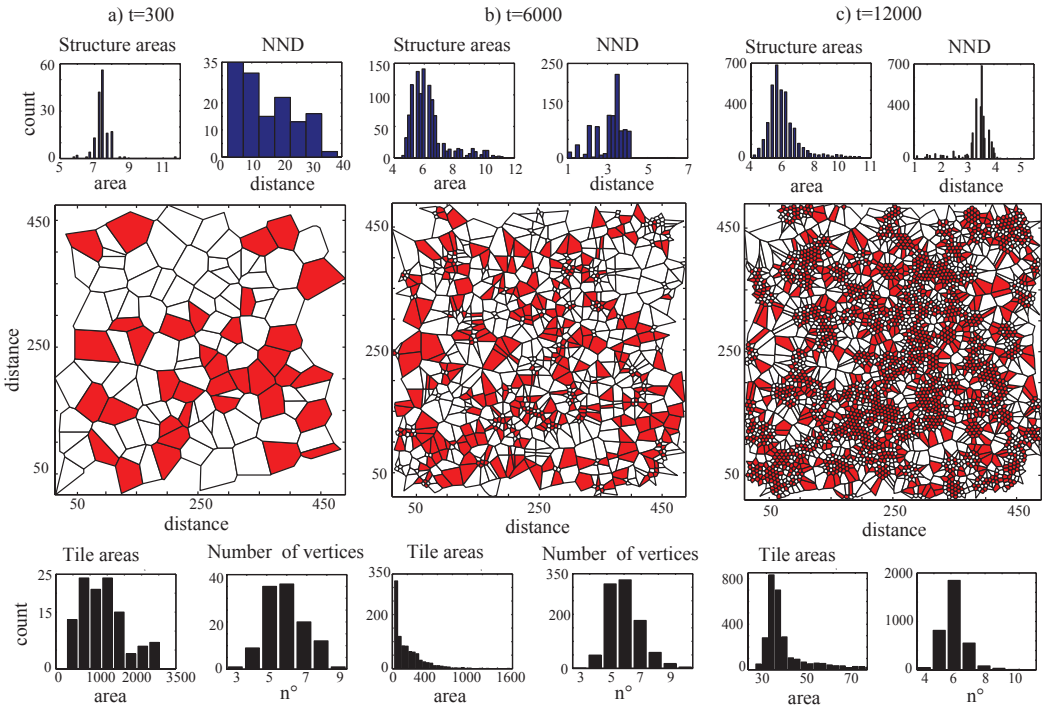

Fig. 8. Numerical simulations of non-variational phytomass model (1) with 155 randomly distributed localized patches as initial conditions, with $\eta = 0.1$, $\kappa = 0.6$, $\Delta = 0.02$ $\Gamma = 0.5$, and $\alpha = 0.125$, integration grid of 1000×1000. At different evolution times, the Voronoi cell tessellation, histograms for number of vertices in each cell, tile area, nearest neighbor distance, and structure areas are analyzed.

spatially periodic distributions of the biomass density which will invade the whole territory. A detailed nonlinear analysis of two-dimensional periodic vegetation patterns such as stripes (often called tiger bush), and hexagons consisting of either sparsely populated or bare areas alternate with dense vegetations patches have been reported in [4].

Field observation vs model

When increasing the aridity parameter η, the structures that appear first are gaps. They consist of spots of spare vegetation. The region where these localized patches are observed is depicted in Fig. 6. They are stable until they lose their stability towards the formation of localized patches. When decreasing aridity, a single patch exhibits an elliptically deformation followed by splitting as shown in Fig. 7. This self-replicating process continues until the system is entirely occupied by spots. Only spots which have available space around them are able to replicate because of this, only spots located in the edges can replicate. In the real ecosystem available space can be generated by the death of a plant by natural or external perturbations (animals, fires) this is the reason we can observe self-replication throughout all the territory analyzed previously.

The pattern obtained from the replication of a single spot is an hexagonal configuration, defects observed are induced by the boundary conditions, nevertheless, after a sufficiently long simulation time, the system arrives to a regular hexagonal pattern (Fig. 7). This regularity is not observed in the arrangement of Festuca tussocks observed in Fig. 2 as vegetation in a real ecosystem is not nucleated by a single spot but rather developed by the seed spreading by wind and animals thus generating multiple tussocks in different locations, each with the possibility of splitting to spread through the terrain.

To numerically test the effect of seed spreading, we have studied the evolution of the model with the initial condition of 155 randomly distributed spots (cf. Fig. 8.a), the aridity level allows each of the spots to self-replicate. With temporal evolution, communities of spots interact as the replicating process continues (see Fig. 8.b). By observing the evolution of these spots we can show that the self-replication process favors a spatial organization similar to the field observation. Initially, as seen in Fig. 8, the system has no particular order, histograms do not show any clear trend, however, further evolving in time, (t=6000) self-replication has generated 1060 spots, for which characteristic values emerge for the areas of the structures and NND, and the number of vertices histogram behave as observed for the Festuca tussocks. At time t=12000 the structure count is 3641, their areas and NND show a clear maximum value indicating an emergent ordering, the process of self-replication favors a dispersion of the structures and tile areas from the mean, as the observed in the real ecosystem. In this line, the process of self-replication allows the system to spatially organize.

Conclusions

We have studied the self-splitting phenomenon through a vegetation point of view. Through observations made by means of remote sensing analysis of the Andes semi-arid ecosystem we have localized Festuca tussocks which by a modulational instability deform from heir circular shape to an elliptical shape, process after which the tussocks split into two new structures, we have observed this process in a variety of species and size scales. By statistical analysis we have encounter characteristic distributions which are signatures of an underlying self-organization process. Though a general interaction-redistribution model we show the existence of self-replication and the mechanism by which this phenomena leads to an extended pattern. Comparison between numerical and field observations indicate intriguing similarities in the distribution of areas and distance between structures. Self-replication in vegetation give new lights on the way plants propagate and populate the semi-arid terrains.

ACKNOWLEDGMENTS. M.G.C. thanks the financial support of FONDECYT project 1150507. I.B. thanks the support from CONICYT, Beca de Magister Nacional and the Departamento de Postgrado y Postítulo of the Vicerrectoria de Asuntos Acadmicos, Universidad de Chile. M.T. received support from the Fonds National de la Recherche Scientifique (Belgium).

1. Greig-Smith P (1979) Pattern in vegetation. The Journal of Ecology 755-779.
2. Levin SA (1992) The problem of pattern and scale in ecology: the Robert H. MacArthur award lecture. Ecology 73(6):1943-1967.
3. Lefever R, Lejeune O (1997) On the origin of tiger bush. Bulletin of Mathematical Biology 59(2):263-294.
4. Lejeune O, Tlidi M (1999) A model for the explanation of vegetation stripes (tiger bush). Journal of Vegetation science 10(2):201-208.
5. Gilad E, Von Hardenberg J, Provenzale A, Shachak M, Meron E (2004) Ecosystem engineers: from pattern formation to habitat creation. Physical Review Letters 93(9):098105.
6. Barbier N, Couteron P, Lefever R, Deblauwe V, Lejeune O (2008) Spatial decoupling of facilitation and competition at the origin of gapped vegetation patterns. Ecology 89(6):1521-1531.
7. Lefever R, Barbier N, Couteron P, Lejeune O (2009) Deeply gapped vegetation patterns: on crown/root allometry, criticality and desertification. Journal of Theoretical Biology 261(2):194-209.
8. Couteron P, Anthelme F, Clerc MG, Escaff, D, Fernandez-Oto C, Tlidi M (2014) Plant clonal morphologies and spatial patterns as self-organized responses to resource-limited environments. Philosophical Transactions of the Royal Society A: Mathematical, Physical and Engineering Sciences 372(2027):20140102.
9. Grube S, (2002) The fairy circles of Kaokoland (Northwest Namibia) is the harvester termite Hodotermes mossambicus the prime causal factor in circle formation?. Basic and Applied Ecology 3(4):367-370.
10. van Rooyen MW, Theron GK, van Rooyen N, Jankowitz WJ, Matthews WS (2004) Mysterious circles in the Namib Desert: review of hypotheses on their origin. Journal of Arid Environments 57(4):467-485.
11. Lefever R, Turner JW (2012) A quantitative theory of vegetation patterns based on plant structure and the non-local FKPP equation. Comptes Rendus Mcanique 340(11):818-828.
12. Martínez-García R, Calabrese JM, Hernández-García E, López C (2013) Vegetation pattern formation in semiarid systems without facilitative mechanisms. Geophysical Research Letters 40(23):6143-6147.
13. Klausmeier CA (1999) Regular and irregular patterns in semiarid vegetation. Science 284(5421):1826-1828.
14. Von Hardenberg J, Meron E, Shachak M, Zarmi Y (2001) Diversity of vegetation patterns and desertification. Physical Review Letters 87(19):198101.
15. HilleRisLambers R, Rietkerk M, van den Bosch F, Prins HH, de Kroon H (2001) Vegetation pattern formation in semi-arid grazing systems. Ecology 82(1):50-61.
16. Okayasu T, Aizawa Y (2001) Systematic analysis of periodic vegetation patterns. Progress of Theoretical Physics 106(4):705-720.
17. Sherratt, JA (2005). An analysis of vegetation stripe formation in semi-arid landscapes. Journal of mathematical biology 51(2):183-197.
18. Wang W, Liu Q-X, Jin Z (2007) Spatiotemporal complexity of a ratio-dependent predator-prey system. Physical Review E 75(5):051913.
19. Kéfi S, Rietkerk M, van Baalen M, Loreau M (2007) Local facilitation, bistability and transitions in arid ecosystems. Theoretical Population Biology 71(3):367-379.
20. D'Odorico P, Laio F, Ridolfi L (2006) Patterns as indicators of productivity enhancement by facilitation and competition in dryland vegetation. Journal of Geophysical Research: Biogeosciences 111(G3):20052012.
21. D'Odorico P, Laio F, Porporato A, Ridolfi L, Barbier N (2007) Noise-induced vegetation patterns in fireprone savannas. Journal of Geophysical Research: Biogeosciences 112(G2):20052012.
22. Borgogno F, D'Odorico P, Laio F, Ridolfi L (2009) Mathematical models of vegetation pattern formation in ecohydrology. Reviews of Geophysics 47(1).
23. Ridolfi L, D'Odorico P, Laio F (2011) Noise-induced phenomena in the environmental sciences. Cambridge University Press.
24. Lejeune O, Tlidi M, Couteron P (2002) Localized vegetation patches: a self-organized response to resource scarcity. Physical Review E 66(1):010901.
25. Escaff D, Fernandez-Oto C, Clerc MG, and Tlidi M, (2015) Localized vegetation patterns, fairy circles, and localized patches in arid landscapes. Physical Review E 91(2):022924.
26. Tlidi M, Lefever R, Vladimirov A (2008) On vegetation clustering, localized bare soil spots and fairy circles. Lect. Notes. Phys. 751:381.
27. Dunkerley DL (2002) Infiltration rates and soil moisture in a groved mulga community near Alice Springs, arid central Australia: evidence for complex internal rainwater redistribution in a runoffrunon landscape. Journal of Arid Environments 51(2):199-219.
28. Rietkerk M, Dekker SC, de Ruiter PC, van de Koppel J (2004) Self-organized patchiness and catastrophic shifts in ecosystems. Science 305(5692):1926-1929.

29. Meron E, Gilad E, von Hardenberg J, Shachak M, Zarmi Y (2004) Vegetation patterns along a rainfall gradient. Chaos, Solitons & Fractals 19(2):367-376.
30. Meron E, Yizhaq H, Gilad E (2007) Localized structures in dryland vegetation: forms and functions. Chaos: An Interdisciplinary Journal of Nonlinear Science 17(3):037109.
31. Sheffer E, Yizhaq H, Shachak M, Meron E (2011) Mechanisms of vegetation-ring formation in water-limited systems. Journal of theoretical biology 273(1):138-146.
32. Tlidi M, Staliunas K, Panajotov K, Vladimiorv AG, Clerc MG (2014) Localized structures in dissipative media: From Optics to Plant Ecology. Phil. Trans. R. Soc. A 372(2027):20140101.
33. Dickstein AJ, Erramilli S, Goldstein RE, Jackson DP, Langer SA (1993) Labyrinthine pattern formation in magnetic fluids. Science 261(5124):1012-1015.
34. Ribiere P, Oswald P (1990) Nucleation and growth of cholesteric fingers under electric field. Journal de Physique 51(16):1703-1720.
35. Oswald P, Baudry J, Pirkl S (2000) Static and dynamic properties of cholesteric fingers in electric field. Physics Reports 337(1):67-96.
36. Pearson JE (1993) Complex patterns in a simple system. Science 261(5118):189-192.
37. Lee KJ, McCormick WD, Pearson JE, Swinney HL (1994) Experimental observation of self-replicating spots in a reaction-diffusion system. Nature 369(6477):215-218.
38. Muñuzuri AP, Pérez-Villar V, Markus M (1997) Splitting of autowaves in an active medium. Physical review letters 79(10):1941.
39. Kaminaga A, Vanag VK, Epstein IR (2006) A reactiondiffusion memory device. Angewandte Chemie International Edition 45(19):3087-3089.
40. Kaminaga A, Vanag VK, Epstein IR (2005) " Black spots" in a surfactant-rich Belousov-Zhabotinsky reaction dispersed in a water-in-oil microemulsion system. Journal of Chemical Physics 122(17):174706.
41. Kolokolnikov T, Tlidi M (2007) Spot deformation and replication in the two-dimensional belousov-zhabotinski reaction in a water-in-oil microemulsion. Physical review letters 98(18):188303.
42. Davies PW, Blanchedeau P, Dulos E, De Kepper P (1998) Dividing blobs, chemical flowers, and patterned islands in a reaction-diffusion system. The Journal of Physical Chemistry A 102(43):8236-8244.
43. Muratov CB, Osipov VV (1996) General theory of instabilities for patterns with sharp interfaces in reaction-diffusion systems. Physical Review E 53(4):3101; Muratov CB, Osipov VV (1996) Scenarios of domain pattern formation in a reaction-diffusion system. Physical Review E 54(5):4860; Muratov CB (2002) Theory of domain patterns in systems with long-range interactions of Coulomb type. Physical Review E 66(6):066108.
44. Monine M, Pismen L, Br M, Or-Guil M (2002) Modeling triangular titration fronts in the O2+ H2 reaction on a catalytic Rh (111) surface. The Journal of chemical physics 117(9):4473-4478.
45. Schaak A, Imbihl R (1998) Triangular-shaped reaction fronts in a catalytic surface reaction. Chemical physics letters 283(5):386-390.
46. Hayase Y, Ohta T (1998) Sierpinski gasket in a reaction-diffusion system. Physical review letters 81(8):1726.
47. Hayase Y, Ohta T (2000) Self-replicating pulses and Sierpinski gaskets in excitable media. Physical Review E 62(5):5998.
48. Meron E, Gilad E, von Hardenberg J, Shachak M, Zarmi Y (2004) Vegetation patterns along a rainfall gradient. Chaos, Solitons & Fractals 19(2):367-376.
49. Ren X, Wei J (2003) On the spectra of three-dimensional lamellar solutions of the diblock copolymer problem. SIAM journal on mathematical analysis 35(1):1-32.
50. Nishiura Y, Suzuki H (2005) Higher dimensional SLEP equation and applications to morphological stability in polymer problems. SIAM journal on mathematical analysis 36(3):916-966.
51. Sandnes B, Knudsen HA, Mly KJ, Flekky EG (2007) Labyrinth patterns in confined granular-fluid systems. Physical review letters 99(3):038001.
52. Sandnes B, Flekky EG, Knudsen HA, Mly KJ, See H (2011) Patterns and flow in frictional fluid dynamics. Nature communications 2:288.
53. Tlidi M, Vladimirov AG, Mandel P (2002) Curvature instability in passive diffractive resonators. Physical review letters 89(23):233901.
54. Hagberg A, Yochelis A, Yizhaq H, Elphick C, Pismen L, Meron E (2006) Linear and nonlinear front instabilities in bistable systems. Physica D: Nonlinear Phenomena 217(2):186-192.
55. Ospina González JC, Aliscioni SS, Denham SS (2013) Estudios taxonómicos en el género Festuca L.(Poaceae) de Argentina y Chile. Gayana. Botánica 70(1):01-15.
56. Monteiro JAF (2012) Functional morphology and productivity of a Tussock grassland in the Bolivian Altiplano (Doctoral dissertation, University of Basel).
57. Monteiro JAF, Hiltbrunner E, Krner C (2011) Functional morphology and microclimate of Festuca orthophylla, the dominant tall tussock grass in the Andean Altiplano. Flora-Morphology, Distribution, Functional Ecology of Plants 206(4):387-396.
58. Geyger E (1985) Untersuchungen zum Wasserhaushalt der Vegetation im nordargentinischen Andenhochland (Doctoral dissertation, PhD Thesis, Universitt Gttingen, Gttingen, Germany).
59. Getzin S, Wiegand K, Wiegand T, Yizhaq H, von Hardenberg J, Meron E (2015) Adopting a spatially explicit perspective to study the mysterious fairy circles of Namibia. Ecography 38(1):1-11.
60. Aurenhammer F (1991) Voronoi diagramsa survey of a fundamental geometric data structure. ACM Computing Surveys (CSUR) 23(3):345-405.